DOE/ET/13547-T1

HOT CORROSIVITY OF COAL GASIFICATION PRODUCTS ON GAS TURBINE ALLOYS

Summary Report, April 15, 1978—November 15, 1979

By
G. H. Meier
E. A. Gulbransen

Work Performed Under Contract AC01-79ET13547

University of Pittsburgh
Dept. of Metallurgical and Materials Engineering
Pittsburgh, Pennsylvania

U. S. DEPARTMENT OF ENERGY

DISCLAIMER

DISCLAIMER

Available from the National Technical Information Service, U. S. Department of Commerce, Springfield, Virginia 22161.

Price: Paper Copy $9.00
Microfiche $3.50

DOE/ET/13547-T1
Distribution Category UC-90h

HOT CORROSIVITY OF COAL GASIFICATION PRODUCTS ON GAS TURBINE ALLOYS

Summary Report for Period

15 April 1978 through 15 November 1979

G. H. Meier and E. A. Gulbransen

Department of Metallurgical and Materials Engineering
University of Pittsburgh
Pittsburgh, Pennsylvania 15261

PREPARED FOR THE UNITED STATES
DEPARTMENT OF ENERGY

Under Contract No. DE AC01 79 ET 13547

Table of Contents

1.0 Objective

The object of this program is to develop information about the hot corrosion of gas turbine alloys in the environment likely to be found when a gas turbine is operated on low Btu gas produced from coal in a fluidized bed gasifier.

The program is designed to determine the mechanisms of attack and the major factors which influence the kinetics of hot corrosion in these environments.

The program deals with selected existing gas turbine alloys and a few simple alloys of potential gas turbine alloy composition. The alloys have been selected to be representative of several different metallurgical types which may exhibit different hot corrosion behavior.

This study is intended to serve the dual purpose of developing a fundamental understanding of hot corrosion processes and of providing data essential in the design and selection of alloys for use in turbines using gasified coal as fuel.

2.0 Introduction

The accelerated oxidation of Ni and Co alloys in aircraft and marine turbines due to the condensation of Na_2SO_4 on blades and vanes has been well documented and extensively investigated.[1-3] The severity of this type of attack, termed hot corrosion, has been shown to be very sensitive to a number of variables including deposit compositions, atmosphere, temperature and temperature cycling, erosion, alloy composition, and alloy microstructure. Similar corrosion is to be expected in turbines fueled by coal conversion products but the process is likely to be considerably more complex due to the wider range of deposit compositions which may form from contaminants in the fuel. Low BTU coal gas, for example, may contain HCl, NaCl, NaOH, KCl, KOH, Na, K, H_2S, and SO_2. Upon

combustion in the gas turbine H_2S will be oxidized to SO_2 and SO_2 may react to form SO_3. The NaCl and KCl will dissociate and react to form Na_2SO_4 and K_2SO_4. The conversion of gaseous or finely particulate NaCl or KCl is observed to occur extremely rapidly in the presence of SO_2[4,5]. However, large particles of chlorides, which could occur by dislodgement from the compressor, may survive their transit through the combustion chamber. Therefore, one must consider the possibilty of deposition of Na_2SO_4 and K_2SO_4 on the turbine components either by condensation from the vapor or impaction of droplets and that the deposits may be contaminated with chlorides. A study at General Electric [6] has indicated the following results regarding alkali conversion during fuel combustion.

(i) Most of the Na contained in the fuel is unlocked during combustion;

(ii) Only a small proportion of the K is unlocked;

(iii) Deposits on turbine components will likely be Na_2SO_4-K_2SO_4 mixtures.

The last point is consistent with the thermodynamics of the Na-S-O and K-S-O systems as seen from the condensed phase stability diagrams[7] in Figures 1 and 2. At oxygen pressures on the order of one atmosphere the sulfates are stable even at low sulfur pressures.

The difference in melting points of Na_2SO_4 (1157K) and K_2SO_4 (1342K) indicates less liklihood of forming liquid deposits of K_2SO_4 at the temperatures of turbine operation (1000-1400K). However, a eutectic exists in the Na_2SO_4-K_2SO_4 system at 20 mole percent K_2SO_4 and a temperature of 1150K and potassium pyrosulfate is stable in K_2SO_4 at low pressures of SO_3 at low temperatures (650 - 750K) resulting in liquid phases[9]. Also it is observed that $CoSO_4$ produced by reaction of Co-alloys with SO_3 forms low melting solutions with Na_2SO_4

at temperatures as low as 873K.[3] Therefore, it is clear that liquid deposits containing both K_2SO_4 and Na_2SO_4 are of potential interest over the entire operating temperature range of gas turbines.

The presence of Pb, Mo, and V as contaminants may alter the chemistry of deposits and, therefore, influence the corrosion process. All three have been shown to produce detrimental effects in the Na_2SO_4 induced hot corrosion of some alloys. The presence of Mg and Ca in the coal and the use of dolomite and limestone for S removal presents the possibility of $MgSO_4$ and $CaSO_4$ being present in deposits on turbine components. The stability diagrams[7] in Figures 3 and 4 show that these sulfates are stable over most of the sulfur and oxygen potentials likely to obtain in turbines. The presence of $MgSO_4$ may be particularly important since it forms low melting mixtures with Na_2SO_4 which are apparently quite corrosive. There is also a high probability of Si being contained in the deposits either as SiO_2 or silicates.

Once a deposit has formed on an alloy surface the extent to which it affects the corrosion resistance of the alloy will depend on whether or not the deposit melts, how adherent it is, and the extent to which it wets the surface. A liquid deposit is generally necessary for severe hot corrosion to occur although some examples exist where dense, thick solid deposits have, apparently, resulted in considerable corrosion. The relationship of adhesion and wetting to hot corrosion has not been studied. Furthermore, the factors which affect the adhesion and wetting behavior of sulfates on metal or oxide surfaces have not been extensively investigated. However, considerable work on the surface tension and wetting behavior of alkali metal carbonates is available in the Russian literature.[10-12] This work has shown that the adhesion and wetting is, of course, affected by the surface tension of the liquid with the

contact angle increasing with increasing surface tension. The surface tension was, in turn, influenced by the molecular structure and composition of the liquid and the temperature. It was found that surface tension increased with increasing binding energy and decreasing cation radius for the carbonates of Li, Na, K, and Cs. A similar trend was reported for the sulfates of the same metals.[10] Additives such as oxides were found to decrease the surface tension of the carbonates if their effective cationic dipole moment was lower than that for the cation of the carbonate. The atmosphere was found to have little effect on the surface tension. The tendency of a given liquid to wet a surface was found to depend on the nature of the substrate; its composition, crystal structure, roughness, etc. The tendency of the liquid salt to wet the surface of an alloy is quite important to its hot corrosion behavior in that it will affect the adhesion of the deposit and, for a given loading of salt, will determine the local deposit thickness. Increased salt thickness has been found to affect the rate of hot corrosion and, depending on the particular mechanism, may accelerate or retard the reaction.[3]

Once the alloy surface has been partially or completely wet by the molten salt conditions for severe corrosion may develop. The hot corrosion of virtually all susceptible alloys is observed to occur in two stages: an initiation stage during which the rate of corrosion is slow and a propogation stage in which rapid, often catastrophic corrosion occurs. During the initiation stage the alloy is being altered to make it susceptible to rapid attack. This alteration may include depletion of the element responsible for forming the protective scale (usually Al or Cr), formation of sulfides in the alloy due to sulfur penetration through the scale, dissolution of oxides into the salt, and development

of growth stresses in the scale. This alteration also can result in shifts in salt composition toward more corrosive conditions. The length of the initiation stage varies from seconds to thousands of hours depending on a large number of variables including alloy composition, alloy microstructure, salt composition, atmosphere, temperature, extent of thermal cycling, salt thickness, specimen geometry, and presence or absence of erosive conditions. In many cases the end of the initiation stage follows the local penetration of the salt through the scale and subsequent spreading along the scale/alloy interface. This situation in which the salt reaches sites of low oxygen activity and is in contact with an alloy depleted in Al or Cr generally leads to the rapid propogation stage. Propogation occurs by one or more of the following mechanisms:[3]

(i) Basic fluxing in which the scale is degraded by reaction with oxide ions in the salt,

(ii) Acidic fluxing in which the scales is degraded by donating oxide ions to the salt, and

(iii) Sulfidation which involves intense sulfidation of the alloy and subsequent oxidation of the sulfides to produce a thick, non-protective oxide.

This report describes the results of a laboratory study of the major steps in the chronology of hot corrosion of Ni-, Co-, and Fe-base alloys under the influence of deposits likely to form when coal conversion products are used as fuels. These steps involve the melting and wetting behavior of sulfate deposits, the initiation of rapid hot corrosion, and the propogation of the attack. The effects of alloy composition and microstructure, salt composition, temperature, atmosphere composition and thermal cycling on these phenomena have been observed.

3.0 Experimental Procedure

The metals and alloys studied include pure Ni and Co, a number of simple Ni- and Co-base alloys containing Cr, Al, Ti, and various refractory metals, and the commercial alloys IN-738, B-1900, Ni-50Cr, and FSX-414. In addition a number of alloys of typical coating compositions such as Ni-Cr-Al, Co-Cr-Al, and Fe-Cr-Al were studied. The laboratory alloys were tungsten arc melted under an argon atmosphere, remelted several times, and most were drop cast into a water cooled copper chill. The alloys were homogenized for 72 hours in evacuated quartz capsules at 1050°C. The commercial alloys were given conventional heat treatments for the individual alloys.

Oxidation coupons were cut from the alloys, polished through 600 grit silicon carbide and cleaned ultrasonically. The salt coatings were applied by spraying with their aqueous solutions while the coupons were heated using a hot plate and a heat lamp. Coating weights were generally 1 mg/cm^2. A limited number of experiments were made with heavier coatings.

A continuous reading Cahn microbalance and an invar beam balance were used to record weight changes between 750° and 1000°C at 1 atmosphere of slowly flowing oxygen. The reaction was initiated by raising a preheated furnace around a quartz tube in which the specimen was supported with oxygen flowing. The furnace was raised in a time period of 10 seconds. At 900°C the system and specimen came to thermal equilibrium in less than one minute. Gases were doped with SO_3 by using O_2 - SO_2 mixtures or by passing O_2 through a permeation tube apparatus to introduce small amounts of SO_2 and passing the gas over a Pt catalyst to establish the SO_2/SO_3 equilibrium. In some experiments the gas was doped with NaCl vapor by passing it over a boat of NaCl held at the temperature

to give the desired vapor pressure.

Oxidized specimens were studied using optical and scanning electron metallography, x-ray diffraction, and microprobe techniques. The melting and wetting of deposited salts was observed using a hot stage microscope.

4.0 Results and Discussion

4.1 Wetting and Surface Tension Effects

Many of the steps in the hot corrosion process depend on the ability of a molten salt to wet the surface of a component. These include the deposition and re-evaporation of the salt, the adhesion of the deposit to the surface, the distribution of the salt over the surface, and the ability of the salt to penetrate through cracks or other defects in an oxide scale. The distribution of the salt on the surface is of particular importance since it will determine the local deposit thickness for a given total loading on the surface, i.e. a salt which only partially wets the surface will result in some regions bearing salt deposits thicker than predicted for the nominal loading. It is recognized that salt thickness has a strong influence on the rate of hot corrosion with thicker deposits being more detrimental for some mechanisms and less so for others. With this background the wetting behavior of Na_2SO_4 on a number of metals and alloys, both bare and preoxidized, was observed using hot stage optical microscopy and scanning electron microscopy.

Figure 5a shows the behavior of a 1 mg/cm^2 coating of Na_2SO_4 applied to a bare Fe-18Cr-6Al alloy and heated in air for 2 hours at 900°C. The salt has wet most of the surface which is shown by the EDAX spectrum in Figure 5b to contain significant amounts of Fe, Cr, and Al oxides. The spectrum for the salt shows Na and S from the salt and small amounts of Fe, Cr, and Al which are likely present in the scale

under the salt. Figure 6a shows the contrasting behavior of Na_2SO_4 in a Co-18Cr-6Al alloy exposed under the same conditions. The salt has not wet the surface but has formed a cellular structure which consists of Co, Cr, and Al oxides.

The difference in wetting of FeCr-Al and CoCrAl alloys, both of which are nominally Al_2O_3-formers, suggests the transient oxides which form on heating affect the wetting behavior. Therefore, the same two alloys were preoxidized in air at 900°C for 30 minutes to produce an Al-rich oxide before application of Na_2SO_4. As seen in Figure 7, subsequent heating in air at 900°C for 30 minutes produces similar spreading of the salt as the crystals melt.

In order to further ascertain the effects of transient oxidation products on salt wetting specimens of pure Fe, Co, and Ni were preoxidized for 30 minutes at 900°C and then exposed in air at 900°C for 30 minutes with a Na_2SO_4 coating. Figure 8a shows the surface of the preoxidized Fe and Figure 8b shows the surface after exposure with Na_2SO_4. It appears the salt is spreading over the surface but the considerable roughness makes comparison with the Fe-Cr-Al alloy difficult. Figure 9a shows the surface of preoxidized Co indicating a fine-grained layer of Co_3O_4 overlaying CoO. Figure 9b shows that preoxidized specimens after exposure with Na_2SO_4 showing only massive CoO and the complete absence of Na_2SO_4 which has penetrated into the scale. (The penetration will be discussed more fully in a subsequent section.) Therefore, little can be said about the tendency of Na_2SO_4 to wet Co oxides. Similar results were obtained for pure Ni as seen in Figure 10. The preoxidized specimen exposed with Na_2SO_4 shows a bulged, cracked scale through which the Na_2SO_4 has penetrated.

A number of Cr_2O_3 forming alloys were also investigated with regard to the wetting behavior of Na_2SO_4. Figure 11a shows the surface of pure Cr after 30 minutes in air at 900°C with a coating of Na_2SO_4 showing platelets of Cr_2O_3 protruding through a uniform layer of salt. Figure 11b shows a Co-20Ni-27Cr alloy exposed under the same conditions. The salt has spread rather uniformly but the Cr_2O_3 platelets are absent, presumably because a considerable amount of spinel $CoCr_2O_4$ forms in the early stages of oxidation of this alloy. Figure 12 shows the behavior of Na_2SO_4 in Ni-20Cr and Ni-50Cr alloys. The salt on the Ni-20Cr, which forms considerable amounts of NiO and $NiCr_2O_4$ as transient products, has penetrated down into the scale in numerous locations and is hardly visible, Figure 12a. The appearance of the Ni-50Cr, Figure 12b, which forms a Cr_2O_3 scale almost immediately, is identical to that of pure Cr, Figure 11a, with Cr_2O_3 platelets protruding through a rather uniform layer of Na_2SO_4.

The above results indicate that the wetting behavior of Na_2SO_4 on various alloys depends on the nature of the oxide scale. This is probably due to differences in surface roughness and different values of the interfacial free energies for the oxide/gas and oxide/salt interfaces. In addition the dissolution of components of the scale into the salt can change the value of the interfacial free energy for the salt/gas interface. To evaluate the latter possibility contact angle measurements for Na_2SO_4 on various substrates have been started and the effects of various additives to the Na_2SO_4 are being observed. Figure 13 shows a pellet of pure Na_2SO_4 after melting on Pt at 900°C with a contact angle of 16.5° being obtained. Attempts to measure the contact angles on preoxidized metals and alloys have proved difficult because of the tendency of the salt to rapidly react with the scales so that a constant

angle is not obtained. The measurements will be continued on plates of the pure oxides such as Al_2O_3, etc.

No results are available yet for the effects on surface tension of various contaminants which could come from the scales or turbine atmosphere but existing studies from the literature indicate these effects may be substantial. Figure 14, taken from the work of Moiseev and Stepanov[12], shows the effect of various additives on the surface tension of molten Li_2CO_3 at 765°C. The analysis of these results is not completely clear. Moiseev and Stepanov were able to correlate much of the surface tension effects with the relative dipole moments of the cations introduced, cations with small dipole moments decreasing the surface tension. Similar effects are likely in sulfate melts.

Thus, while only qualitative results have been obtained, it is felt that the effects of contaminants on the surface tensions and wetting behavior of sulfates on oxidized alloys may be significant in expanding the understanding of the hot corrosion process. This understanding may then lead to additives for producing desirable surface properties for minimization of attack. To this end apparatus is presently being constructed to allow contact angle measurements and observations of wetting to be made under controlled atmospheres.

4.2 Hot Corrosion of Pure Ni

Accelerated oxidation of Na_2SO_4-coated Ni at temperatures above the melting point of Na_2SO_4 has been reported by several investigators. Goebel and Pettit[13] found that coating of pure Ni with Na_2SO_4 increased the oxidation rate and proposed that the formation of NiO reduces the local oxygen pressure in the salt and incerases the sulfur potential. Sulfur diffuses through the normally protective NiO scale causing the sulfate layer above it to become enriched in oxide ions (i.e. the Na_2O

activity increases). The oxide ions, in turn, react with NiO to form nickelate ions ($NiO_2^=$) which are sufficiently soluble in the sulfate melt to destroy the protective NiO layer (Basic Fluxing). This results in the deposition of a porous, non protective scale near the salt/gas interface where the oxygen potential is higher.

Another model, proposed by Reising and Krause[14] treats the molten salt as a pseudo scale which permits the simultaneous diffusion of oxygen from the air to the metal surface and of metal cations from the surface to the salt-gas interface. A porous metal oxide corrosion product forms on the surface and absorbs some of the melt as it is formed. Eventually all of the salt becomes trapped in the scale and rapid corrosion ceases allowing a protective nickel oxide scale to form. The present study involves the effect of salt composition, gas composition, and temperature on the hot corrosion of Ni.

The effect of salt composition on the hot corrosion of Ni at 900°C is illustrated in Figure 15. The rate of oxidation with a 1 mg/cm^2 salt coating is seen to be accelerated over that for uncoated Ni for a short time and then reaches a plateau. The salt additives which lower the Na_2O activity in the salt result in the cessation of rapid corrosion at smaller weight increases as seen by comparison with the following activities obtained from electrochemical measurements and/or thermochemical calculations.

Salt	log a Na_2O
Na_2SO_4	-12.1
Na_2SO_4 + 20 mole % K_2SO_4	-11.6
Na_2SO_4 + SiO_2	-13.1
Na_2SO_4 + MoO_3	-13.9
Na_2SO_4 + TiO_2	-15.7

The addition of MoO_3 to the salt, which also decreases the Na_2O activity, is an exception to the above, apparently, because of the formation of $NiMoO_4$ as a reaction product.

In an attempt to observe the progression of hot corrosion of Ni Na_2SO_4-coated specimens were oxidized in the microbalance and interrupted at different times. Figure 16 shows the surface of a specimen oxidized at 890°C for 10 seconds corresponding to a weight increase of 0.2 mg/cm^2. These micrographs show surface cracks in the oxide and the salt flowing into them. The pH of the salt remaining on the surface was tested with moistened test paper and found to be approximately 9 indicating the salt had become basic immediately upon melting. Figure 17a shows the surface of the same specimen at low magnification indicating nodule formation under the salt. Figures 17b and c show the same surface from which the salt has been washed with distilled water. The scale is seen to replicate the polishing scratches from the metal indicating it is the first oxide formed. Surface cracks are seen to link the nodules and a large amount of porous nickel oxide fills the nodules.

Figure 18 shows cross sections of the above specimen at various locations where sulfides have formed in the metal even at this short exposure time. Importantly, the oxide appears to have become discontinuous in these regions. Figure 19 is a cross section of one of the nodules on this specimen showing the porous NiO permeated with Na_2SO_4 and a mixture of Na_2SO_4, NiO, and NiS at the scale/metal interface. The honeycomb-like structure of the oxide suggests a repetitive sulfidation-oxidation sequence.

Figure 20 is the surface of a specimen exposed for 30 seconds corresponding to a weight increase of 2 mg/cm^2. The polishing marks are still evident but the micrographs and EDAX spectrum show that virtually

all the Na_2SO_4 is gone from the surface. Figure 21 is a cross section of this scale showing the presence of a honeycomb-like NiO scale permeated with Na_2SO_4 under the thin, first-formed oxide.

Figure 22 is a cross section of the porous scale on a specimen exposed for 180 minutes ie after the rapid reaction has ceased. An additional feature of this microstructure is the formation of sulfide and oxide along metal grain boundaries.

Based on the above results the following model, shown schematically in Figure 23, is proposed to describe the hot corrosion of Ni by molten Na_2SO_4. A thin NiO scale forms on heating and is covered by the Na_2SO_4 as it melts. The continued formation of oxide rapidly lowers the p_{O_2} in the salt, as originally proposed by Goebel and Pettit[13], and the sulfur potential increases leading to transport through the thin oxide and sulfide formation at the scale/metal interface, Figure 23a. The nature of the sulfur transport has not been verified but the fact that sulfides are observed in times as short as 10 seconds at 900°C suggests that transport is not by lattice diffusion of sulfur ions through the NiO. Wagner et al[15] found the diffusivity of S in NiO to be on the order of 10^{-14} - 10^{-12} cm^2/sec depending on the oxygen partial pressure. If a value of 10^{-13} cm^2/sec is chosen the diffusion distance in 10 seconds at 900°c is on the order of 10^{-6} cm which is small compared to the thickness of the initial NiO scale. Therefore, it appears a more likely mechanism is transport by SO_2 molecules penetrating through such defects in the scale as microcracks as was found by Wooton and Birks[16] for oxidation of Ni in Ar-SO_2 mixtures. The source of the SO_2 is the dissociation of the sulfate

$$SO_4^{=} \rightarrow SO_2(g) + \frac{1}{2} O_2(g) + O = \quad (1)$$

Also, as seen from Equation 1, as SO_2 and O_2 are consumed the oxide ion

activity in the salt will increase to maintain equilibrium resulting in the salt becoming more basic. This is consistent with the pH measurements in the present study. The increase in basicity will be greatest over the areas where the sulfides form, i.e. where SO_2 is consumed most rapidly and in these regions the NiO scale will react to form soluble nickelate ions in the melt, Figure 23b, which will diffuse to the salt/gas interface where the oxide ion concentration is low and will reprecipitate as NiO. The dissolution of the scale then allows the salt to penetrate it and spread along the scale/metal interface, Figure 23c, lifting and cracking the scale. This cracking may actually be initiated by the formation of a Ni-S liquid phase at the scale metal interface with a greater molar volume than that of the nickel. The cracking of the scale also allows oxygen penetration which oxidizes the sulfides freeing sulfur to penetrate further into the metal. The repetition of this process produces the porous, honeycomb-like NiO scale, Figure 23d, and results in diffusion of sulfur and, subsequently, oxygen along the grain boundaries of the metal, Figure 23e. Eventaully as Na_2SO_4 is trapped in the porous scale the rapid reaction ceases and a dense, protective NiO layer forms.

The results of hot corrosion of Ni with various additives is also consistent with the proposed model (with the exception of MoO_3 which will be discussed separately). For example, the addition of K_2SO_4 into Na_2SO_4 increases the basicity of the salt and, as seen from Figure 15, increases the total weight gain. The initiation of the reaction sequence is also more rapid with K_2SO_4 additions, as seen from Figure 24, where after 10 seconds all of the salt has penetrated beneath the scale and the scale degradation is similar to that produced in times of 30 seconds or longer by pure Na_2SO_4. The more rapid initial attack is

likely influenced by the slightly lower melting point of the K_2SO_4 doped salt as well as its increased basicity.

On the other hand, the addition of TiO_2 into Na_2SO_4 which decreases the basicity slows the reaction dramatically. The kinetics of the initial reaction rate may be described as parabolic instead of linear as for pure Na_2SO_4. Figures 25 a and b show the surface of a Na_2SO_4 + TiO_2 coated nickel specimen, which was subjected to the same treatment as described before for pure Na_2SO_4 and Na_2SO_4 + K_2SO_4. It can be seen that even though the salt has melted the attack of the surface is not as severe as in the above cases. No severe surface cracks have been observed in this specimen except for a few holes as indicated by arrows at A and B. The white particles left on the surface are undissolved sodium titanite. Figures 26 a and b show the scale of this specimen. It is clear sulfides have formed at the scale-metal interface and the scale has become discontinuous at this location. Figure 25 c and d also show the surface of the nickel specimen coated with 1 mg/cm^2 Na_2SO_4 + TiO_2 and oxidized at 900°C for 15 minutes. The rupture of the scale is apparent. A cross section of this specimen is illustrated in Figure 26 c and d which is similar to that in pure Na_2SO_4. Similar results are obtained for Ni coated with Na_2SO_4 + SiO_2.

The addition of MoO_3 also decreases the basicity of Na_2SO_4 but it results in a rapid, parabolic reaction rate which produces larger weight gains than any other salt studied, Figure 15. The scale morphology produced is illustrated in Figure 27. There is little sulfidation evident even along grain boundaries. The following model, shown schematically in Figure 28, is offered to explain the effect of MoO_3. It has been proposed that SO_3 is more mobile than oxygen in Na_2SO_4 and therefore provides most of the oxygen transport[17]. W. C. Fang and D. A. Shores

have determined the diffusion coefficient of SO_3 (as $S_2O_7^{=}$) in Na_2SO_4 by cathodic reduction of the $S_2O_7^{=}$ ion on a platinum electrode. A value of 10^{-4} cm^2/sec was obtained at 900°C as compared to a value of 10^{-5} cm^2/sec for oxygen in Na_2SO_4 at 1000°C. When MoO_3 is added to Na_2SO_4 the formation of $MoO_4^{=}$ ions may provide easier transport in the melt. The following reaction may then occur at the metal-salt interface,

$$Ni \rightarrow Ni^{++} + 2\ e \tag{2}$$

$$MoO_4^{=} + 2\ e \rightarrow MoO_4^{4-} \tag{3}$$

Ni^{++} and MoO_4^{4-} will be transported to the salt/gas interface through the molten salt, and at this interface the following reaction may occur

$$MoO_4^{4-} + \frac{1}{2}O_2 \rightarrow MoO_4^{=} + O^{=} \tag{4}$$

$$Ni^{++} + O^{=} \rightarrow NiO \tag{5}$$

In other words, the presence of $MoO_4^{=}$ ions in the salt will change the transport mechanism and increase the rate of oxide formation. In addition the presence of the $MoO_4^{=}$ may increase the solubility of NiO in the salt preventing a protective layer from ever forming. In fact, the X-ray diffraction results show the presence of $NiMoO_4$ in MoO_3-saturated Na_2SO_4 coatings on oxidized specimens. Reising[18] and Stringer, et. al.[19] also noticed the addition of Na_2MoO_4 into Na_2SO_4, which should not change the acidity of the salt, results in an accelerated reaction for nickel and nickel alloys.

An additional interesting aspect of Figure 15 is that pure K_2SO_4 results in accelerated corrosion of Ni at 900°C even though this temperature is well below the melting point of K_2SO_4 (1069°C). Figures 29 a and b show the surface of Ni coated with 1 mg/cm^2 and oxidized at 900°C for 40 minutes. There is no evidence of melting but many of the salt particles have sintered together. Figures 30 a and b are cross-sections of the scale which, with the corresponding EDAX spectrum, give evidence

of a potassium-containing liquid phase having formed and been incorporated into the scale. Figure 31 a shows a specimen oxidized under the same conditions for 3 hours. A thick, porous NiO scale has formed containing small nickel sulfides. Figure 31b shows the scale on a specimen exposed at 977°C for 48 hours. Sulfide formation at the scale/metal interface is evident.

The mechanism by which K_2SO_4 accelerates the corrosion of Ni is not yet clear but microstructures such as Figure 30 b strongly suggest some melting has occurred. This may be due to reaction between NiO and K_2SO_4 to produce $NiSO_4$ at a low activity which may form a low melting solution with K_2SO_4. Unfortunately thermodynamic data are not available for confirmation of this possibility.

Figure 32 presents the rate of oxidation of nickel coated with various salts in argon in which the oxygen partial pressure is approximately 10^{-3} atm. The rate of reaction is very slow and practically all specimens lose weight due to Na_2SO_4 evaporation except in the case when MoO_3 is added to Na_2SO_4. Figure 33 a and b show the surface of nickel which was coated with Na_2SO_4 (1 mg/cm^2) and oxidized in an Ar atmosphere at 900°C for 40 minutes. The salt has melted and spread over the surface and fine grains of oxide have formed under the salt. A cross section of this scale is shown in Figure 33c. The outer bright portion is Na_2SO_4. Nickel oxide has formed under this melt. Energy dispersive X-ray analysis shows small amounts of nickel oxide dissolved into the Na_2SO_4. No sulfides have been detected at the scale-metal interface. Figure 34 shows the scale of nickel coated with MoO_3 modified salt and oxidized in argon for 3 hours at 900°C. A fine equiaxed oxide formed at the scale-metal interface. Sulfides have formed along grain boundaries and the scale-metal interface is irregular.

The slow oxidation of the specimens in argon is consistent with the mechanism described previously and illustrated in Figure 23. However, in the low p_{O_2} atmosphere significant reprecipitation of NiO at the salt/gas interface does not occur to free up oxide ions to further degrade the scale. Therefore, penetration of the salt through the scale does not occur. The exception to this mechanism is again the corrosion of Ni in MoO_3-containing Na_2SO_4. This mechanism is not completely understood but the accelerating effect of MoO_3 may be due to direct degradation of the thin NiO scale by formation of soluble $NiMoO_4$.

The above results and the proposed mechanisms for the hot corrosion of Ni indicate a strong importance of salt acidity. To test this concept Na_2SO_4-coated nickel specimens were exposed in oxygen atmospheres containing various amounts of SO_2. Figure 35 shows the effect of atmosphere composition on the kinetics of hot corrosion. The SO_2-containing gases were passed over a Pt catalyst to establish the equilibrium SO_2/SO_3 ratio and correspond to log a_{Na_2O} between -12 and -14.5. Clearly the addition of SO_3 to the atmosphere has decreased the rate of oxidation more effectively than the addition of compounds such as TiO_2 to the salt even though the additives produce a much lower a_{Na_2O}. This suggests that the additives do not dissolve rapidly enough in the short time before the rate plateau is reached (usually several minutes) to come to equilibrium whereas the thin Na_2SO_4 film apparently equilibrates rapidly with SO_3 in the gas. Figure 36 allows comparison of the scales formed with and without SO_3 in the atmosphere. The presence of SO_3 in the atmosphere results in a thinner scale and the absence of the cellular scale morphology.

Figure 37 shows the rate of oxidation of Ni at 750° with and without Na_2SO_4 coating. The presence of solid Na_2SO_4 (Tmp = 884°C) is seen to markedly accelerate the rate of oxidation both in the presence and absence

of SO_3 in the gas. This behavior is similar to that observed for K_2SO_4-coated Ni at 900° (Figure 15) where the rate of oxidation was accelerated even though the temperature was below the melting point of K_2SO_4 (1069°C). Figures 38 a and b compare the scales on Ni after simple oxidation and hot corrosion at 750°C. The scale on the salt coated specimen is thicker but not porous or cellular as it is at higher temperatures. The effect of Na_2SO_4 at 750°C is not clear at this point. It is possible that sulfur dissolved in the NiO results in more rapid scale growth. However, it appears there is direct interaction between the salt and scale. Figures 38 c and d show the Na_2SO_4 on the surface of Ni may have started to melt. This is somewhat surprising because in the case of pure O_2 no low-melting constituents such as a $NiSO_4$-Na_2SO_4 eutectic should form, but, as discussed for K_2SO_4-coated specimens, $NiSO_4$ at activities much less than unity may be formed.

4.3 Hot Corrosion of Pure Cobalt

The effect of salt composition on the hot corrosion of pure Co at 900°C is illustrated in Figure 39. All of the Na_2SO_4- based coatings slow the rate of oxidation relative to uncoated Co and the various additives to the salt have little effect on the rates. Goebel and Pettit[20] and Johnson, et. al.[21] also observed that coatings of pure Na_2SO_4 slowed the rate of oxidation of Co. This behavior was explained as being due to the rapid rate of growth of CoO, which produced a thick layer of oxide before the salt melted. The Na_2SO_4 was then unable to penetrate the thick scale and behaved as an extra protective layer. A coating of K_2SO_4 which remains solid at 900°C is seen to have no effect on the oxidation rate of Co since the coating does not restrict the access of oxygen to the specimen surface. Figure 40 shows the scales formed on selected specimens of pure Co at 900°C. Even though the salts do not

accelerate the oxidation of cobalt they do result in the scale becoming non-uniform compared to uncoated Co, Figure 40a, and sulfur penetration through the scale produces sulfides at the scale/metal interface and on metal grain boundaries. These results indicate the same hot corrosion processes occur for Co as those described in the previous section for Ni but the faster growth rate of CoO prevents their effects from being seen in the oxidation rates.

Figure 41 shows the rate of oxidation of Co at 750°C in O_2 and O_2 + 1000 ppm SO_2 (equilibrated to equilibrium P_{SO_2}/P_{SO_3})with and without Na_2SO_4, coatings. The presence of the salt decerases the rate in both atmospheres. Figure 42 shows the scales formed on selected specimens indicating that the salt results in scale non-uniformity even though it decreases the overall growth rate. The micrograph and corresponding sulfur map of Figures 42 c and d indicate that the scale grows thicker in regions which are penetrated by sulfur to form sulfides at the scale/metal interface. Whether this is due to a sulfur doping effect or the formation of sulfide short-circuit paths through the scale is not yet clear. Figure 43 shows the outer surface of scales formed in the presence (b,c,d) and absence (a) of Na_2SO_4 at 750°C. There is a clear difference in the scale morphology between coated and uncoated specimens and a strong indication of interaction between the salt and scale. As in the case of Ni the salt gives indications of melting in some areas even though no low melting phases should form. In order to investigate this phenomenon Na_2SO_4 coatings were sprayed on both platinum and cobalt coupons and heated in a hot stage microscope. Figure 44 shows the Na_2SO_4 on platinum before heating, after heating to 750°C, and after heating to 900°C. It is clear that little change in the Na_2SO_4 crystals occurs on heating to 750°C and that complete melting has occurred at 900°C.

Figure 45 shows the same sequence for Na_2SO_4 on cobalt. Here there is evidence of melting of the salt even at 750°C. As discussed for Ni, the most likely explanation of this effect is that the SO_3 pressure generated by the Na_2SO_4 is high enough to allow $CoSO_4$ formation by interaction between the salt and scale. Although pure $CoSO_4$ would not be stable under these conditions $CoSO_4$ dissolved in Na_2SO_4 may be stable and may lead to a lowering of the melting point. This phenomenon must be investigated further as it has important implications regarding the mechanisms of hot corrosion at low temperatures (700-800°C).

An additional feature of the hot corrosion of cobalt at 750°C are the bulges which form in the scale such as those shown in Figure 42. These bulges are found to occur between an outer Co_3O_4 layer and an inner CoO layer. The origin of this effect is not clear but is apparently associated with the presence of sulfur rather than a condensed salt since, as seen in Figure 46, these bulges form in the absence of Na_2SO_4 when SO_2 is present in the oxidizing gas.

4.4 Hot Corrosion of Nickel-Base Alloys

4.4.1 Simple Binary and Ternary Alloys

The hot corrosion of simple Ni-Al, Ni-Cr, and Ni-Cr-Al alloys which are the basis for most high temperature alloys has been studied to provide a baseline for interpreting the more complex behavior of commercial superalloys.

Figure 47 shows the effect of salt composition on the rates of oxidation of a Ni-6 wt% Al alloy. The shape of the weight change curves are qualitatively the same as those for pure Ni. However, the initial rapid reaction ceases at a smaller weight increase due to the formation of $NiAl_2O_4$ in the inner portions of the NiO scale and linking up of Al_2O_3 internal oxides at the scale/metal interface. A typical scale is

shown in Figure 48. The scale is rich in NiO and $NiAl_2O_4$ over an internally oxidized region of Al_2O_3 in essentially pure Ni.

Figure 49 shows the effect of salt chemistry on the rate of oxidation of Ni-16Cr alloys at 977°C. The initial rapid rate is due to basic fluxing of NiO formed during the transient period of reaction but the rate rapidly decreases due to Cr_2O_3 reacting with Na_2O in the salt[22,23] and to the formation of a Cr_2O_3 scale. After long times the rate is essentially the same as that for simple oxidation. The continued decrease in weight of the specimen coated with $Na_2SO_4 + K_2SO_4$ is due to evaporation of K_2SO_4 from the salt. The reaction of Ni-50 wt% Cr coated with the salts results in similar weight gains after long times but the initial rapid reaction is absent due to the absence of significant NiO formation during the transient oxidation period and the rapid formation of a Cr_2O_3scale.

Figure 50 shows the effect of salt chemistry on the rate of oxidation of Ni-10 wt% Cr-4 wt% Al at 900°C. The shape of the curves is qualitatively the same as that for Ni-6Al; however, the points at which the rapid basic fluxing ceases occur at smaller weight gains due to the effect of Cr_2O_3 dissolution in the salt decreasing the Na_2O activity[22,23]. The weight gains at which the rate decreases occur are in the same order for the various additives as was observed for Ni-6Al further reflecting the effects of the additives in decreasing the Na_2O activity.

The important observation from these experiments is that simple Ni alloys containing significant amounts of Al and/or Cr do not undergo severe hot corrosion in the temperature range 900-1000°C with any of the salts tested.

4.4.2 Commercial Alloys (B-1900, IN-738)

The significant difference between the oxidation and hot corrosion resistance of B-1900 has long been recognized and subject to extensive study[21,22,24-26]. The composition of this alloy is Ni-8Cr-6Al-6Mo-10Co-1.0Ti-4.3Ta-9.11C-0.15B-0.07Zr which is extremely susceptible to hot corrosion attack. Figure 51 shows the rate of oxidation of B-1900 at 950°C in the presence of a 1 mg/cm^2 Na_2SO_4 coating. (The rate of simple oxidation is too low to be observable on the scale of Figure 51.) After a short incubation time a rapidly accelerating weight gain occurs. The oxide scale formed on the specimens during the reaction was very porous and thick with a layered texture which peeled off on cooling to room temperature. X-ray diffraction analysis of the spalled scale indicated a large amount of NiO and a small amount of $NiMoO_4$ and spinel. X-ray analyses were also made of the oxide that remained on the specimen indicating a large amount of $NiMoO_4$ on the surface. Therefore, it is apparent the oxide peeled off just above a $NiMoO_4$ layer that was close to the alloy-oxide interface. The metallographic results from this region shown in Figure 52 indicate a region of Mo-rich phases restricted to a narrow zone between the outer porous scale and inner matrix. EDAX results indicate this layer contains Na, S, Ta, Mo, Ni, Cr and Al. It appears this region may be a solution of Na_2SO_4 and Na_2MoO_4 into which Al_2O_3, Cr_2O_3, NiO and Ta_2O_5 are dissolved. Beyond this zone the layered scale contains mainly NiO. Internal oxides at the metal-scale interface consist mainly of Cr and Al oxides. It is clear a continuous layer of Cr_2O_3 and Al_2O_3 is not developed on the alloy surface. Spherical chromium sulfide particles form in front of the internal oxide stringers.

The effect of salt composition on the hot corrosion of alloy B-1900 was also studied. Figure 51 also shows the rate of oxidation of B-1900

at 950°C with several salt coatings. Coating with 1 mg/cm^2 Na_2SO_4 + K_2SO_4 results in a sudden increase in reaction rate in the initial stage. Increasing the acidity of the salt by adding SiO_2 and TiO_2 decerases this initial oxidation rate. The addition of SiO_2 to the salt results in a short incubation period followed by rapid oxidation with the rate approximately equal to that for Na_2SO_4. The specimen coated with Na_2SO_4 + TiO_2 showed a considerably longer incubation time. Apparently, the increase in the acidity of the deposited salt results in the increase in the incubation period to breakaway for B-1900 by prevention of basic fluxing of the transient oxides during the initial stages of exposure.

The difference in hot corrosion behavior of B-1900 as compared with the simple Ni-Cr-Al alloys is due to the high refractory metal content of B-1900. The oxides of the refractory elements such as molybdenum, tungsten and vanadium will dissolve into the Na_2SO_4 forming molybdates, tungstates and vanadates and composition of the Na_2SO_4 will be displaced to a more acidic salt. The addition of the refractory element oxides into the salt will depend on the characteristics of the oxidation of the alloy. For some alloys the refractory elements are oxidized at the very beginning of the oxidation process, whereas for other selective oxidation of other elements results in longer exposure times before the refractory element oxides are available to the Na_2SO_4. In the hot corrosion of B-1900, it seems at the initial stage a basic fluxing reaction dominates. The refractory element concentration at this stage is not enough to cause an acidic reaction to occur. The reaction is similar to that for Ni-10Cr-4Al alloy. A continuous layer of Cr_2O_3 and Al_2O_3 will not be able to form on the surface, an oxygen gradient will be developed across the thin film of the salt, and as the result of this gradient in the oxygen pressure, the sulfur activity will increase and sulfides will form

on the surface. In turn the oxide ion content in the Na_2SO_4 will reach a point at which Al_2O_3 and Cr_2O_3 dissolve into Na_2SO_4 as anions. The aluminate and chromate ions diffuse away from the surface and decompose into Al_2O_3 and Cr_2O_3. However, unlike Ni-10Cr-4Al the oxides of molybdenum will also dissolve into the Na_2SO_4 forming molybdates. The increased acidity of the salt then results in acid fluxing of Al_2O_3 so that a protective scale never reforms and catastrophic degradation ensues.

The Cr_2O_3-forming alloy IN-738 (Ni-16Cr-3.4Al-3.4Ti-1.7Mo-2.6W-1.7Ta-8.5Co-0.9Cb-0.17C-0.2Mn-0.3Si-0.1Zr-0.01B) is generally thought to have superior hot corrosion resistance to alloys such as B-1900. However, IN-738 is also subject to severe corrosion as seen from Figure 53. The rate curves are characterized by an incubation period followed by a breakaway period during which the rate is markedly accelerated. It is clear that the time to breakaway is temperature sensitive being a minimum between 950 and 970°C. The nature of the breakaway phenomenon in alloys such as IN-738 is being studied in a separate NASA-funded program but a review of the results[27] are pertinent to the present discussion. Figure 54 shows several cross sections of an IN-738 specimen which was oxidized for 10 hours with a 1 mg/cm^2 coating of Na_2SO_4. These sections are taken successively from the specimen center to a corner but, since the breakaway begins at specimen corners, also show the chronology of protective scale breakdown. Figure 54a is at the region where a protective scale still exists. The morphology indicates the sulfur has penetrated through the outer scale of the oxide forming (Cr,Ti) sulfides beneath the subscale of needle-like Al_2O_3. The outer scale is Cr_2O_3 which is overlaid by a think layer of TiO_2. Figure 54b shows a region of the scale which has broken down. The internal oxidation zone is absent and a large amount of sulfides start to form. These are chromium

sulfides; no titanium is found in these sulfides. In other regions of the specimens (Figure 54c), a layer of (Cr,Al) sulfides form at the scale-metal interface. It is clear the internal Al_2O_3 has disappeared and the outer Cr_2O_3 scale is becoming thinner. A large amount of chromium sulfides were observed in the matrix, and the alloy near the surface is depleted of chromium. Figure 54d shows the actual scale breakdown. Locally the outer Cr_2O_3 becomes thicker and at the tip of the crack, Na, S, Cr, Ti, Ta, W and Mo were detected by EDAX. The sulfidation is extensive. Figure 54e shows the scale corresponding to the place where breakaway has already occurred. The outer scale, not shown, is greater than 70μm thick. The formation of sulfides along the grain boundaries lifts portions of the alloy into the scale. These are subsequently oxidized to form a layered NiO scale.

It has been observed that the actual scale breakdown occurs at sites where alloy carbides intersect the specimen surface and carbon-free model alloys have not been observed to undergo breakaway[27]. The model which has been proposed to explain the hot corrosion of IN-738 is shown schematically in Figure 55. Initially a thin, protective layer of Cr_2O_3 forms under the Na_2SO_4, Figure 55a. However, at the sites where alloy carbides, (Ti, Ta, Mo, W, Cb)C, intersect the surface there exists locally high concentrations of elements which when oxidized and coming in contact with the molten salt produce very acid conditions. This results in the local dissolution of the scale and the penetration of the salt to the scale/alloy interface, Figure 55b. Here, since the salt is partially isolated from the atmosphere, the p_{O_2} will decrease and the p_{S_2} will increase. This results in the Al_2O_3 internal oxides becoming an essentially continuous Al_2O_3 layer and an increase in the density of sulfides which contain primarily Cr and Ti, Figure 55c.

As this process continues the p_{S_2} continues to incerase and refractory metal oxides are concentrated in the salt. The increased p_{S_2} results in the formation of massive Cr-sulfides, which are less stable than the Cr-Ti sulfides, in alloy grain boundaries, Figure 55d, and the eventual incorporation of entire grains of metal, which are now essentially pure Ni, into the scale where they are oxidized to produce the layered NiO scale characteristic of breakaway corrosion, Figure 55e. Figure 56 shows the effect of salt composition on the hot corrosion of IN-738 at 977°C. The increased attack with increasingly more acid salts is consistent with the above model.

Table I summarizes the effect of salt composition on the hot corrosion of a number of Ni-base alloys at 977°C (1250K). Simple Cr_2O_3-forming alloys (Ni-20Cr, Ni-50Cr) are seen to show small weight changes and to be relatively insensitive to changes in salt composition. Those alloys which are susceptible to extensive hot corrosion are sensitive to salt composition. Salts which are solid at the reaction temperature, K_2SO_4 (T_{mp}=1342K) and $CaSO_4$ (T_{mp}=1673K) have little effect on the rates of oxidation except for pure Ni which is heavily oxidized in the presence of K_2SO_4.

In summary, the Ni-base alloys studied show hot corrosion behavior which is quite sensitive to alloy and salt composition. Binary Ni-Cr alloys show good resistance to all the salts studied but the addition of alloying elements to provide superalloy compositions such as IN-738 result in extremely rapid attack after an incubation period. The breakaway attack of this type of alloy appears to be related to the presence of carbides in the alloy. Alloy B-1900 shows rapid corrosion when coated with Na_2SO_4 with essentially no incubation time while coating with more

acid salts results in a short incubation period prior to breakaway. The poor corrosion resistance of the commercial alloys indicates that they may not be used in the uncoated condition.

4.5 Hot Corrosion of Cobalt-Base Alloys

Figure 57 presents the rates of oxidation at 900°C of Co-20 wt% Cr and Co-20 Cr into which has been added 20 wt% Ni or 5 wt% Ti. The presence of the salts is seen to accelrate oxidation, but not by a large amount. Of the salts shown the mixture Na_2SO_4 + 20% K_2SO_4 produces the most rapid corrosion. The reason for this is not clear; however, electrochemical cell measurements have indicated that this salt has the highest activity of Na_2O of any of the salts used suggesting that formation of sodium cobaltate or chromate may be involved with the enhanced corrosion. Figure 58 shows the scale formed on Co-20 Cr which was coated with 1 mg/cm^2 Na_2SO_4 + K_2SO_4 and reacted for 48 hours at 900°C. The outer scale is CoO containing a small amount of Co_3O_4, the inner scale is spinel $CoCr_2O_4$, and the particles in the alloy are chromium sulfide. This scale is typical of the salt-coated alloys and of the alloy reacted in simple oxidation except for the absence of sulfides in this case. Figure 57 also shows a marked decrease in the rate of oxidation and hot corrosion of Co-20Cr when 20 wt% Ni is added. This is the result of three factors. First, the outer scale on this alloy is a solid solution (CoO-NiO) which grows more slowly than the CoO on Co-20Cr. Secondly, the diffusivity of Cr is greater in the Co-20Ni alloy which results in a flux of Cr to the scale/metal interface sufficient to form Cr_2O_3 rather than $CoCr_2O_4$. Finally, the Ni, by stabilizing the fcc structure, avoids disruption of the scale due to the allotropic transformation in the Cr-depleted zone underlying the scale. This effect is clearly shown in Figure 59. The addition of 5% Ti to Co-20Cr is seen from

Figure 57 to decrease the rate of oxidation markedly. This is the result of formation of a continuous Cr_2O_3 scale on the Ti-containing alloy. However, the scales on all Ti-containing alloys were found to spall extensively on cooling.

Figure 60 shows the rate of oxidation of Co-27Cr and Co-27Cr-20Ni at 900°C both in simple oxidation and hot corrosion. The rates of oxidation are slower for Co-27Cr than Co-20Cr due to the formationof a Cr_2O_3-rich layer on the former and the presence of a salt coating has little effect on the rate. The addition of 20 wt% Ni to Co-27Cr further improves the oxidation and hot corrosion resistance, for the reasons described previously, giving the best oxidation properties of any simple Co-base alloy studied. Figure 61 shows the effect of deposit composition on the rate of oxidation of Co-27Cr at 977°C. The acceleration due to the presence of the salt coatings is slight except for Na_2SO_4 to which NaCl has been added. This result is general. All Cr_2O_3-forming Co-base alloys studied showed the most severe attack when chlorides were present in the salt. The influence of the chlorides was always to:

(i) increase specific weight gains at temperature;

(ii) increase the depth of internal oxidation and sulfidation;

(iii) increase the amount of scale spalling on cooling.

These observations are conveniently illustrated for the commercial alloy FSX-414 (Co-29.5Cr-7W-10Ni-2Fe-0.35C). Figure 62 shows the rate of oxidation of FSX-414 at 977°C with various salt coatings. Like Co-27Cr the rate is slow and relatively independent of salt composition except for the chloride-containing salt. The slight weight decreases observed with Na_2SO_4 and $Na_2SO_4 + K_2SO_4$ coatings are the result of salt evaporation. Even though the absolute weight gains produced by the salt containing NaCl are not catastrophic the useful thickness of the alloys

is rapidly degraded. This can be seen from Figure 63 which shows the penetration of chromium sulfide and oxide goes deep into the alloy, particularly along the grain boundary carbides. Such penetration is not observed in the absence of chlorides (Figure 64a). The alloy regions beneath the scale are also seen to contain a considerable number of voids suggesting the formation of a vapor phase. This has been observed by El-Dahshan, et. al.[28] for Co-Cr-C alloys and explained in terms of the penetration of Cr-carbide networks and their conversion to $CrCl_2$. The influence of chloride on the spalling characteristics of FSX-414 are illustrated in Figure 65. The spalling is minimal for simple oxidation and Na_2SO_4 coating but almost complete for the specimen coated with Na_2SO_4 + NaCl.

The smallest weight increases at 900°C for all Co-base alloys were observed for a Hf-modified CoCrAl coating alloy (Co-18Cr-6Al-1Hf) as illustrated in Figure 66. However, the alumina scale which forms spalls extensively when NaCl is present in the salt. More extensive investigation of coating alloys will be discussed in the next section.

The effects of Na_2SO_4 and NaCl on the 48 hour oxidation weight gains of a number of Co-base alloys at 900°C are summarized in Table II. Several of the alloys, particularly Co-20Ni-27Cr, Co-18Cr-6Al-1Hf, and FSX-414, are relatively unaffected by the deposition of pure Na_2SO_4 but the addition of 20% NaCl results in extensive scale spalling from all alloys with the exception of FSX-418 which is Y-modified FSX-414. All of the alloys were heavily attacked when coated with pure NaCl. However, this test is considered too severe since the quantity of chloride remaining in a turbine at this temperature will never be large. The final column of Table II includes the results for NaCl coating at 750°C. Again most of the alloys are rather heavily attacked.

In summary, a number of Co-base alloys (Co-20Ni-27Cr, Co-18Cr-6Al-1Hf, FSX-414 and similar alloys) have adequate hot corrosion resistance at temperatures of 900°C and above to most of the deposits likely to form in turbines running on gasified coal if the presence of chlorides can be minimized. In this latter case alloys containing extensive carbide networks will be heavily attacked. Most of these alloys, with the exception of FSX-414, must be considered only for coating applications because they lack high-tempereature strength.

4.6 Hot Corrosion of Coating Alloys

The results of the previous two sections indicate that coated alloys will be required for most or, perhaps, all of the components in turbines fired by coal conversion products. Therefore, studies of the hot corrosion behavior of potential coating alloys have been initiated. The alloys include systems based on Co-Cr and Co-Cr-Al which were shown in the previous sections have good hot corrosion resistance at temperatures on the order of 900°C and Fe-Cr-Al alloys.

4.6.1 Cobalt Base Coatings

Coatings based on the Co-Cr-Al system are now widely used in marine and aircraft turbines. They are known to have excellent hot corrosion resistance at normal turbine operation temperatures (900-1000°C). However, they are subject to severe degradation at lower temperatures (700-800°C) which can occur when the turbines are operating at low power or at particular locations on turbine components which normally fall into this temperature range[29]. This severe corrosion is often associated with high SO_3 pressures on the order of 10^{-4} atm. Therefore, studies of Co-Cr and Co-Cr-Al alloys at temp atures between 700 and 800°C and exposed to Na_2SO_4 coatings and gases containing SO_3 and/or NaCl have been undertaken.

TableIIIpresents the 48 hour weight changes of selected cobalt-base alloys exposed at 750°C in O_2 and in two different SO_3 pressures ($p_{SO_3} = 6 \times 10^{-4}$ atm and 6×10^{-3} atm). Simple oxidation tests without Na_2SO_4 were also done for comparison. Co-27Cr and Co-18Cr-6Al-1Hf were most extensively studied as representative of Cr_2O_3-forming and Al_2O_3-forming alloys.

The Co-27Cr alloy was not corroded in O_2 + 1000 ppm (SO_2 + SO_3) ($p_{SO_3} = 6 \times 10^{-4}$ atm). However, at higher SO_3 pressures, pitting type attack was observed. Figure 67 shows a SEM micrograph of Co-27Cr exposed in O_2 + 1%(SO_2 + SO_3) ($p_{SO_3} = 6 \times 10^{-3}$ atm) with 1 mg/cm^2 Na_2SO_4 at 750°C for 48 hours. The thick external scale was identified by X-ray diffraction as Co_3O_4 . Cobalt is depleted in the pitted region while chromium is enriched within the pit. Sulfur is enriched in the boundary layer between the pit and alloy. Beneath the sulfur-rich band, another layer of stringers are observed. This type of attack is particularly detrimental to coatings because of its localized nature which can result in severe degradation and even penetration of the coating even though the total change in weight is small as seen in Table III.

The same type of attack is even more prevalent in the Co-18Cr-6Al-1Hf alloy as seen in Figure 68 where pitting has occurred even at the lower SO_3 pressure of 6×10^{-4} atm. Again the pit is seen to be free of cobalt, which forms a scale over the top, and enriched in chromium. Aluminum and sulfur are concentrated at the attack front.

Considerable uncertainty still exists regarding the mechanisms of this form of corrosion despite several careful investigations. The corrosion morphology corresponding to low temperature hot corrosion has been well characterized on components removed from marine service[29,30].

The attack is primarily of a pitting type with the oxide in the pits enriched in Cr and Al in alternating layers and depleted in Co. A Co-rich oxide covers the pits. There is little or no sulfidation in the alloy and generally no depletion of β-CoAl below the oxide pit. Small amounts of water soluble Co have also been observed on corroded coatings. Barkalow and Pettit[29] were able to reproduce this morphology at 700°C by exposing CoCrAlY coatings with Na_2SO_4 deposits to oxygen containing SO_3 at pressures greater than 10^{-4} atm. The rate of degradation was found to be proportional to the SO_3 pressure and negligible on the absence of SO_3. These observations have been incorporated into the following mechanism by Giggins and Pettit[3]. The reaction of CoO and SO_3 forms $CoSO_4$ which forms a low melting point solution with Na_2SO_4. The liquid salt then penetrates the Al_2O_3 scale at cracks. Alternating layers of Al and Cr are formed by selective removal of Al from the alloy presumably by Al-sulfite formation at the liquid/alloy interface where the p_{O_2} is low and then reprecipitation as oxide where the p_{O_2} is higher. The Al-depleted alloy is converted to Cr_2O_3 to form the Cr-rich region and Co which diffuses to the liquid/gas interface forming Co-oxide or sulfate. It is suggested[3] that this mode of attack is not operative at high temperatures because much higher SO_3 pressures are required to form sulfates and sulfites.

Smeggil[30], on the other hand, suggests that the corrosion morphology may be reproduced in the absence of SO_3 in the gas phase if the coatings are exposed to brief thermal excursions and transient reducing conditions and proposes this as an alternate mechanism. Laboratory hot corrosion experiments in which specimens were periodically cycled to 1300°C for 30 seconds in carbonaceous material produced corrosion morphologies similar to those observed in marine turbines and have produced

changes in coating microstructure similar to those observed by Smeggil in marine turbine components. Smeggil does not offer a mechanism for the degradation produced by the high temperature excursions.

The results of the present study have produced microstructures which are qualitatively in agreement with the mechanism proposed by Giggins and Pettit[3] except that, as seen in Figure 68, the Al is concentrated with the sulfur at the reaction front while the bulk of the pit contains only Cr_2O_3. This model must be modified somewhat to explain the corrosion of the Al-free Co-27Cr alloy. In this case it is a Cr_2O_3 scale which is penetrated by the molten salt which may explain the higher SO_3 pressure which is required to produce pitting in Co-27Cr as compared to Co-Cr-Al. However, once the scale has been penetrated the mechanism is the same. Cobalt diffuses outward through the liquid salt to form oxide or sulfate at the salt/gas interface while the chromium is oxidized in-situ.

Cyclic exposures in which the specimens are cycled to room temperature every hour and recoated with Na_2SO_4 every 12 cycles result in pitting of both alloys at lower SO_3 pressures and, as seen from Figure 69, result in severe weight losses from the Co-Cr-Al alloy exposed with $p_{SO_3} = 6 \times 10^{-4}$ atm. Cyclic exposure does not result in significant weight loss for the Co-27Cr alloy exposed under the same conditions, Figure 70. However, cyclic exposure with 10 ppm NaCl in the gas phase results in severe spalling from the Co-Cr alloy, Figure 70, but considerably less spalling from the Co-Cr-Al alloy. The presence of NaCl in the gas also produces a pitting type of attack in Na_2SO_4- coated Co-Cr-Al which is somewhat similar to that produced by SO_3 as seen in Figure 71. However, a major difference is the porous microstructure produced below the pit by the formation of volatile chlorides of Al and

Cr which are transported outward through the pits and converted to oxide in regions of higher p_{O_2}.

Another interesting feature of Figures 69 and 70 is that the combination of SO_3 and NaCl in the gas phase eliminates the severe spalling of the Co-Cr alloy produced by NaCl alone and that for Co-Cr-Al produced by SO_3 alone. This is believed due to the reaction of NaCl and SO_3 to produce Na_2SO_4 and thus reduce the partial pressure of both species in the gas phase.

The mechanisms of low temperature hot corrosion is a subject of containing studies which will also consider the effects of various contaminants in Na_2SO_4 such as K_2SO_4, SiO_2, etc., on the kinetics and morphologies of attack.

4.6.2 Iron Base Coatings

Preliminary experiments on the hot corrosion resistance of Fe-18Cr-6Al alloys and the same alloys modified with Hf and Mo have been started. These alloys have very good resistance to Na_2SO_4 at high temperatures (900-1000°C) producing smaller wieght changes and a little sulfidation. The same alloys are presently being evaluated for their resistance to low temperature hot corrosion influenced by SO_3 and NaCl and to cyclic exposures.

5.0 SUMMARY

The results of this investigation have produced mechanisms for the hot corrosion of a number of pure metals and alloys in the types of atmospheres likely to be obtained in turbines using coal conversion products as fuel. The results of these mechanistic studies suggest the following conclusions regarding application of alloys in these situations.

1. Simple Cr_2O_3-forming alloys of both Co and Ni have good hot corrosion resistance to most of the deposits likely to form in turbines

burning coal conversion products with the exception of deposits containing considerable amounts of chlorides.

2. The presence of carbide phases is detrimental to the hot corrosion resistance of both Ni and Co alloys.
3. The complex alloy compositions characteristic of superalloys result in susceptibility to serve hot corrosion, the extent of which is sensitive to salt composition, particularly for Ni-base alloys.
4. Conclusion 3 suggests that uncoated alloys will not be able to provide the required combination of corrosion resistance and high-temperature strength for any of the components in turbines running on coal gas.
5. Several alloys including Co-18Cr-6Al-1Hf, Co-27Cr, Co-20Ni-27Cr, Ni-50Cr, and Fe-18Cr-6Al-Hf have corrosion resistance for use as coatings and claddings at high temperatures (900-1000°C).
6. The problem of low temperature hot corrosion (700-800°C) must still be investigated for the types of deposits likely to form in coal fired systems before selection of reliable coatings can be made.

References

1. J. Stringer, "Hot Corrosion of High Temperature Alloys, Alloys", in Properties of High Temperature Alloys, Z. A. Foroulis and F. S. Pettit, eds., The Electrochemical Society, p. 513, 1976.

2. J. A. Goebel and F. S. Pettit, "Alloy-Molten Slag Reactions Associated with Hot Corrosion of Alloys," in Metal-Slag-Gas Reactions and Processes, Z. A. Foroulis and W. W. Smeltzer, eds., The Electrochemical Society, p. 693, 1975.

3. C. S. Giggins and F. S. Pettit, "Hot Corrosion Degradation of Metals and Alloys - A Unified Theory", Pratt and Whitney Aircraft, Final Report to Air Force Office of Scientific Research on Contract No. F44620-76-C-0123, June, 1979.

4. G. C. Fryburg, R. A. Miller, C. A. Stearns, and F. J. Kohl, "Formation of Na_2SO_4 and K_2SO_4 in Flames Doped with Sulfur and Alkali Chlorides and Carbonates", NASA Technical Memorandum Tm-73794, 1977.

5. J. F. G. Condé, N. Birks, and M. G. Hocking, paper presented at 4th Conference on Gas Turbines in Marine Environments, Annapolis, MD, June 1979.

6. M. B. Cutrone, Progress Rept. on ERDA, Contract No. EX-76-C-1765, July 15, 1977.

7. E. A. Gulbransen, G. H. Meier, W. Linhart, and T. Huang, "Thermodynamic Stability Diagrams for Condensed Phases in Selected Metal-Surface-Oxygen Systems between 1150°K, and 1450°K", DOE Rept. FE-2484-3, November, 1977.

8. H. Lux, Z. fur Elektrochem., 45, 303, 1939.

9. A. W. Coats, D. J. A. Dear, and D. Penfold, J. Inst. Fuel, 41, 129 (1968).

10. G. K. Moiseev and G. K. Stepanov, Electrochemistry of Molten and Solid Electrolytes, 3, 39 (1966) translated from Russian by Consultants Bureau, New York.

11. G. K. Moiseev and G. K. Stepanov, Electrochemistry of Molten and Solid Electrolytes, 5, 101 (1967).

12. G. K. Moiseev and G. K. Stepanov, Electrochemistry of Molten and Solid Electrolytes, 4, 91 and 99 (1967).

13. J. A. Goebel and F. S. Pettit, Met. Trans., 1, 1943 (1970).

14. R. F. Reising and D. P. Krause, Corrosion, 30, 131 (1974).

15. D. R. Chang, R. Nemoto, and J. B. Wagner, Jr., Met. Trans., 7A, 803 (1976).

16. M. R. Wootton and N. Birks, Corr. Sci., 12, 829 (1972).

17. W. C. Fang and D. A. Shires, "SO_3 Transport in Liquid Sodium Sulfate", unpublished research.

18. R. Reising, Corrosion, 31, 159 (1975).

19. K. P. Peters, D. P. Whittle, and J. Stringer, Corr. Sci., 16 791 (1976).

20. J. A. Goebel and F. S. Pettit, "Hot Corrosion of Cobalt-Base Alloys", Final Report on Air Force Contract F 33615-72C-1757, 1975.

21. D. M. Johnson, D. P. Whittle, and J. Stringer, Con. Sci., 15, 645 (1975).

22. J. A. Goebel, F. S. Pettit and G. W. Gouard, Met. Trans., 4, 261 (1973).

23. N. S. Bornstein, M. A. DeCrescente, and H. A. Roth, Met. Trans., 4, 1799 (1973).

24. N. S. Bornstein and M. A. DeCrescente, Trans. TMS-AIME, 245, 1947 (1969).

25. J. B. Johnson, J. R. Nicholls, R. E. Hurst, and P. Hancock, Corr. Sci., 18, 527 and 543 (1978).

26. F. Fryburg, F. Kohl, and C. Stearns, "Hot Corrosion Studies of Four Nickel-Base Superalloys, NASA TRW VIA, B-1900, Alloy 713C, and IN-738", in Properties of High Temperature Alloys, Z. A. Foroulis and F. S. Pettit, eds., Electrochem. Soc., Princeton, NJ, 1977, pp.

27. T. T. Huang and G. H. Meier, "The Initiation of Hot Corrosion in Nickel Base Alloys", progress report on NASA Grant No. NSG-3214, November 1979.

28. M. E. El-Dahshan, J. Stringer, and D. P. Whittle, Cobalt, 57, 182 (1972).

29. R. A. Barkalow and F. S. Pettit, "Marine Gas Turbine Hot Corrosion Dependence on Ingested Salt Levels", Pratt and Whitney Aircraft, Final Report to Naval Research Laboratory on Contract N00173-77-C-0206, April 1979.

30. J. G. Smeggil "Study of the Effects of Gaseous Environment on the Hot Corrosion of Superalloy Materials", Quarterly Report to NASA Lewis Research Center on Contract NAS3-21376, December 1978.

"Table I "Weight Changes (mg/cm^2) for Ni-base Alloys after 48 hr at 977°C in 1 atm O_2, Coated with 1 mg/cm^2 Salt"

Alloy	Na_2SO_4	Na_2SO_4 + K_2SO_4	Na_2SO_4 + C	Na_2SO_4 + SiO_2	Na_2SO_4 + TiO_2	K_2SO_4	$CaSO_4$
Ni-20Cr	+1.8	-1.0	-1.3	-2.1	-0.1	-0.25	-0.1
Ni-6Al	+17.6	+16.0	+18.1	+23.4	+7.4	+6.7	+2.7
Ni-10Cr-4Al	+15.2	+23.9	+4.7	+8.7	+3.4	+1.5	+0.9
Ni-50Cr	-1.0	-1.0	-2.1	-4.5	-0.25	-1.0	+0.3
IN-738	+28	+14	+13	+34	+68	+1.4	+2.3
Ni						+19.9	+4.0

Table II "Weight changes (mg/cm^2) after 48 hours in O_2 Coated with 1 mg/cm^2 Salt"

Alloy	(900°C) No Salt	(900°C) Na_2SO_4	(900°C) Na_2SO_4 (20% NaCl)	(900°C) NaCl	(750°C) NaCl
Co-20Cr	11.3		11.7 (s)	45	13.2
Co-20Ni -20Cr	3.22		2.8 (s)	12	2.95
Co-27Cr	0.92	4.69	2.6 (s)	30	1.04 (s)
Co-20Ni -27Cr	1.95	0.42	-7.9 (s)	28	7.1
Co-20Ni -20Cr -5Ti	1.38	1.11	1.8 (s)	14.5	3.9
Co-18Cr 6Al-1HF	0.30	-0.28	-0.3 (s)	2.5	0.8
FSX-414 FSX-418	0.28 0.20	-0.18 -0.73	-5 (s) -0.13	11.9 9.6	1.36 5.24

(s) indicates extensive scale spalling.

Table III "Weight changes (mg/cm^2) after 48 hrs. at 750°C"

Gas Composition	O_2		O_2 + 1000 ppm SO_2 $p_{SO_3} = 6x10^{-4}$ atm		O_2 + 1% SO_2 $p_{SO_3} = 6x10^{-3}$ atm	
Alloy	No Salt	1 mg/cm^2 Na_2SO_4	No Salt	1 $\frac{mg}{cm^2}$ Na_2SO_4	No Salt	1 mg/cm^2 Na_2SO_4
Co-20Cr	1.5	0.4	0.43	0.04	0.95	5.2
Co-27Cr	0.09	0.05	0	-0.13	0.09	1.9
Co-18Cr-6Al	0.05	-0.05	0.05	-0.14	0.04	$-17.6_{(S)}$
Co-18Cr-6Al-1Hf	0.1	0	0.13	0.44	0.06	$-20.9_{(S)}$
Co	10	6.2	8.3	9.3	8.3	$-8.6_{(S)}$
Ni-20Cr	0.14	0.14	0.24	0.04	0.09	2.3
Ni-23Cr	0.09	-0.08	0.17	0.12		
Ni-18Cr-6Al	0.03	-0.03	0.11	-0.08	0	0.2
Ni	0.6	2.9	0.8	1.8	1.5	9.4

(S): Scale spalled off during cooling to room temperature

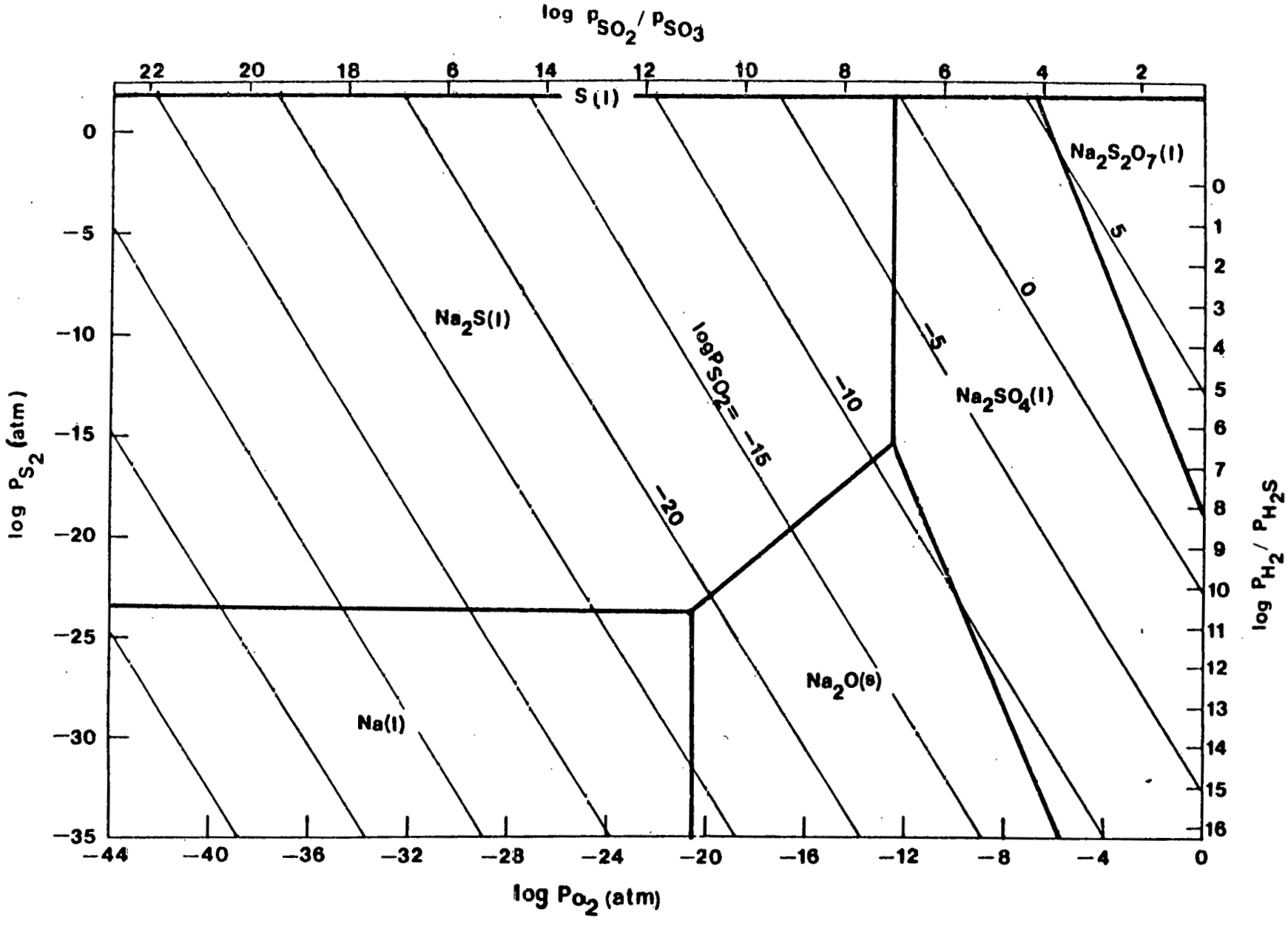

Figure 1 Condensed Phase Stability Diagram for the Na-S-O System at 1250°K.

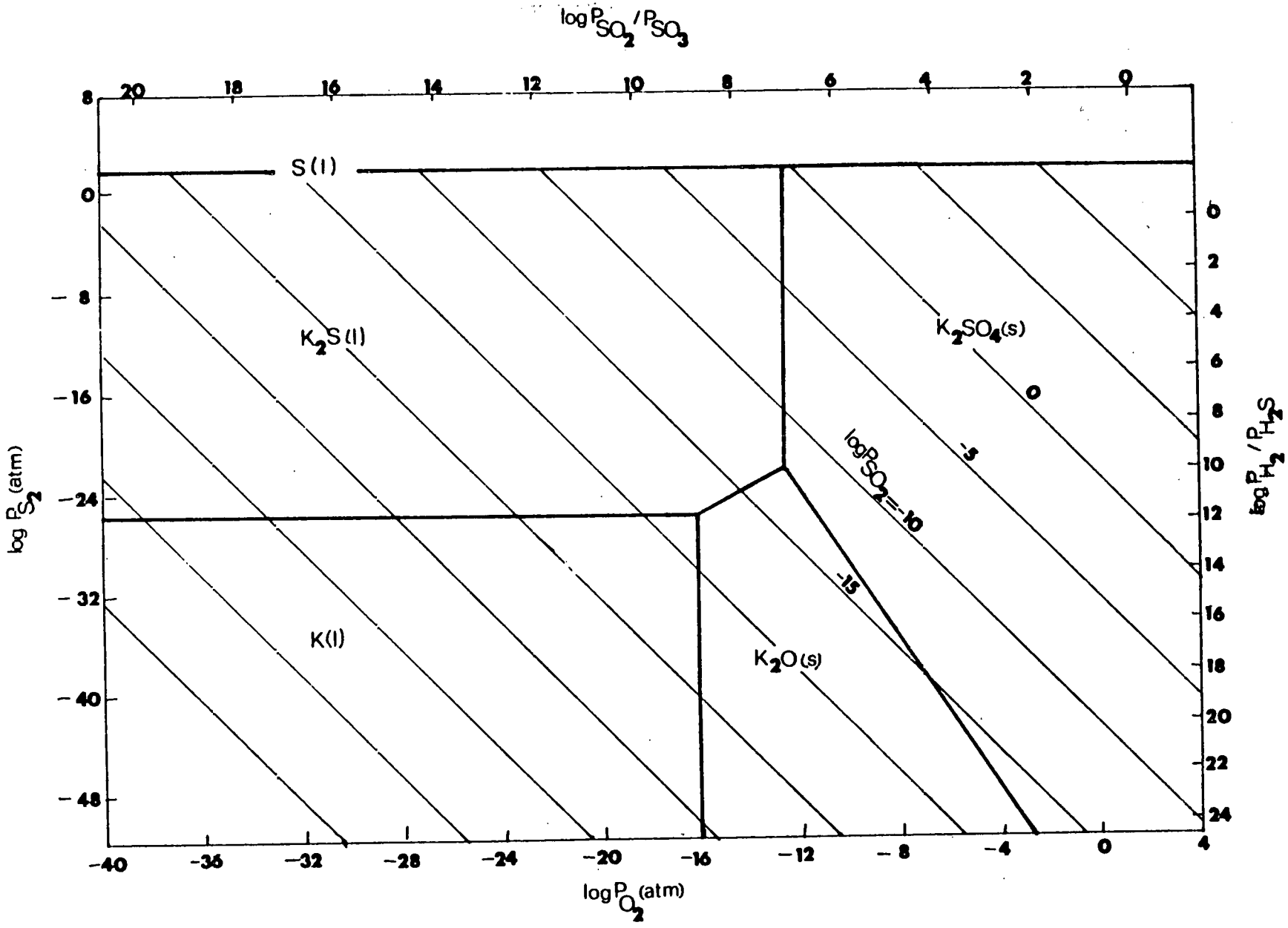

Figure 2 Condensed Phase Stability Diagram for the K-S-O System at 1250°K.

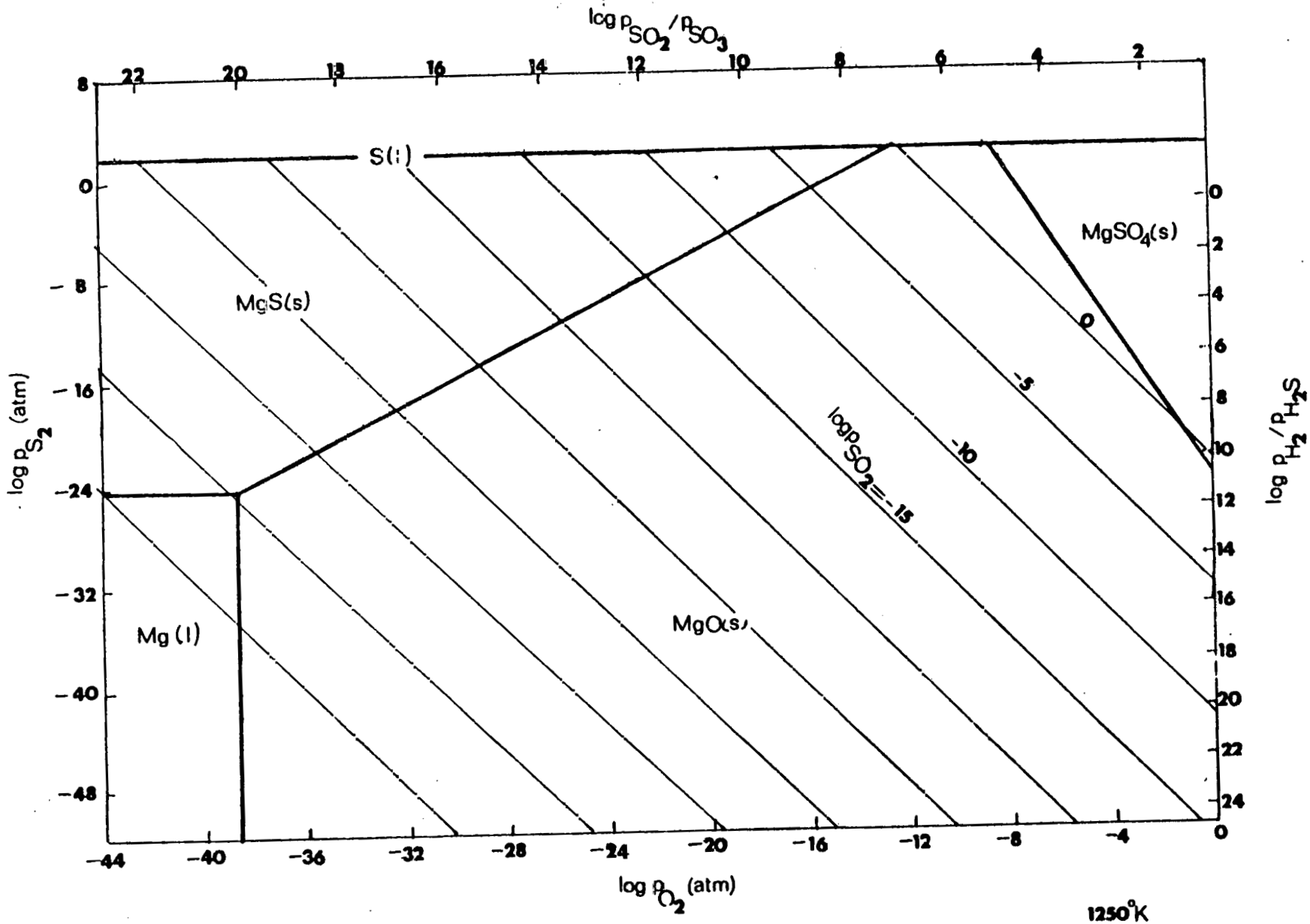

Figure 3 Condensed Phase Stability Diagram for the Mg-S-O System at 1250K.

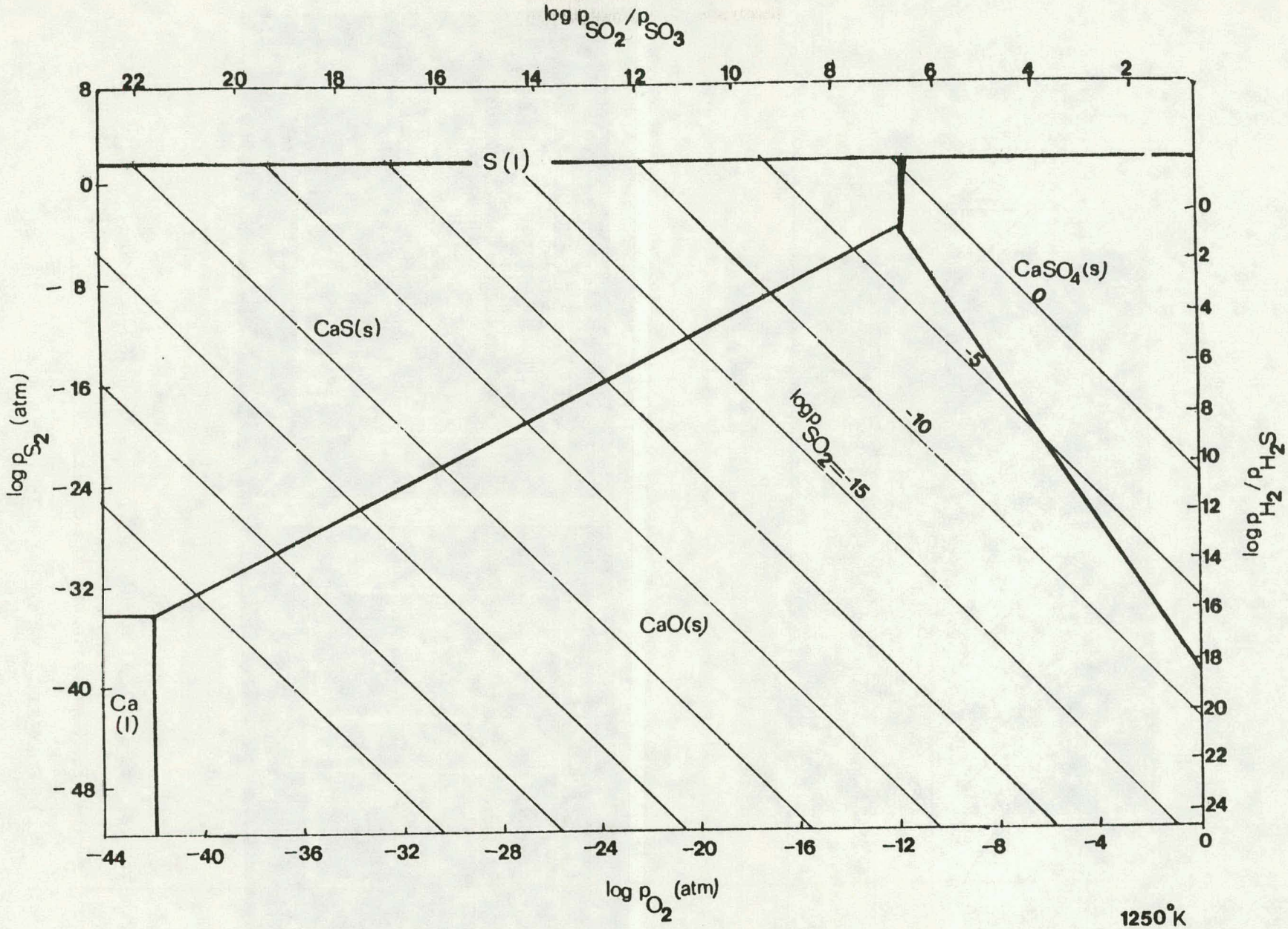

Figure 4 Condensed Phase Stability Diagram for the Ca-S-O System at 1250K.

a.

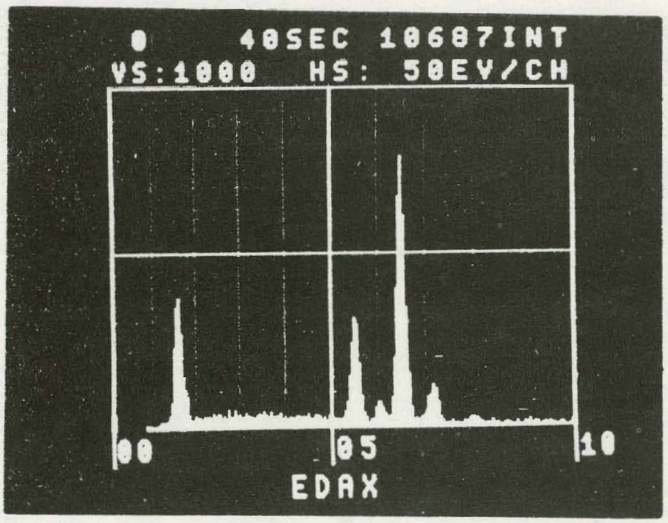

b.

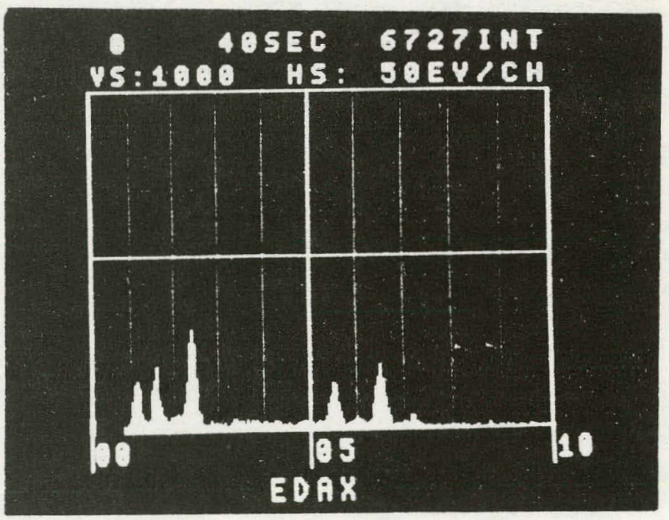

c.

Figure 5. (a) Fe-18Cr-6Al oxidized 2 hrs. with Na_2SO_4 coating.

(b) EDAX analysis of bare oxide.

(c) EDAX analysis of the salt.

a.

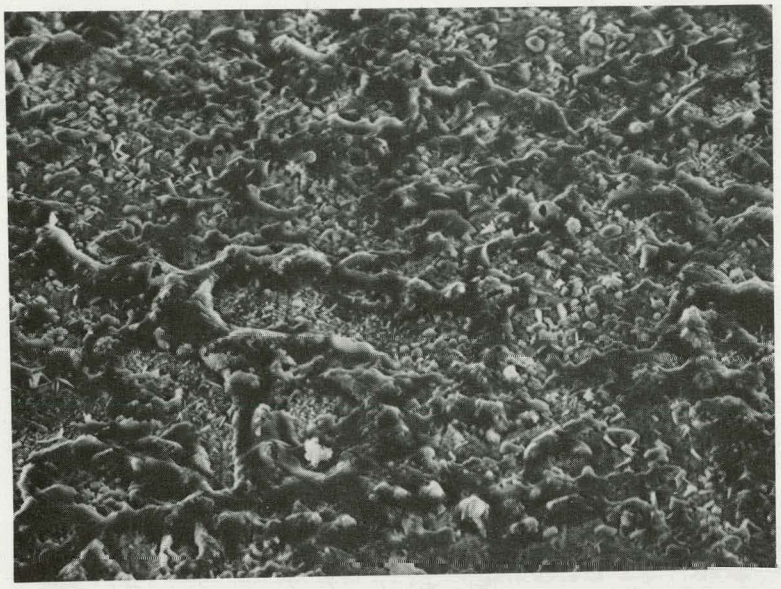

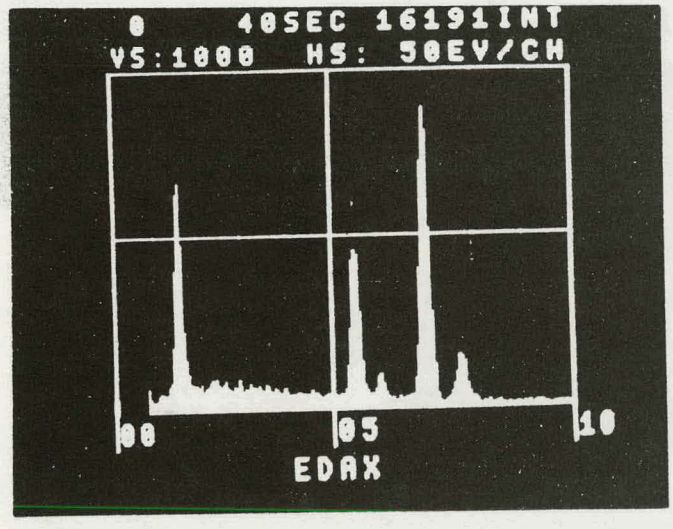

b.

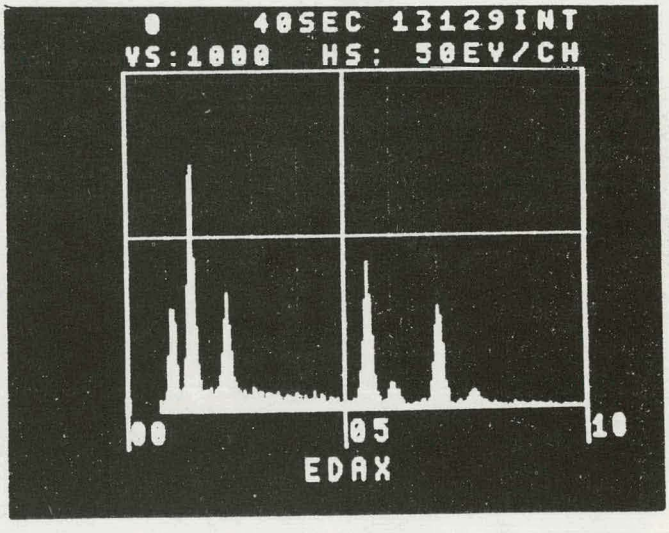

c.

Figure 6 (a) Co-18Cr-6Al oxidized 2 hrs. with Na_2SO_4 coating.

(b) EDAX analysis of bare oxide.

(c) EDAX analysis of salt.

a.

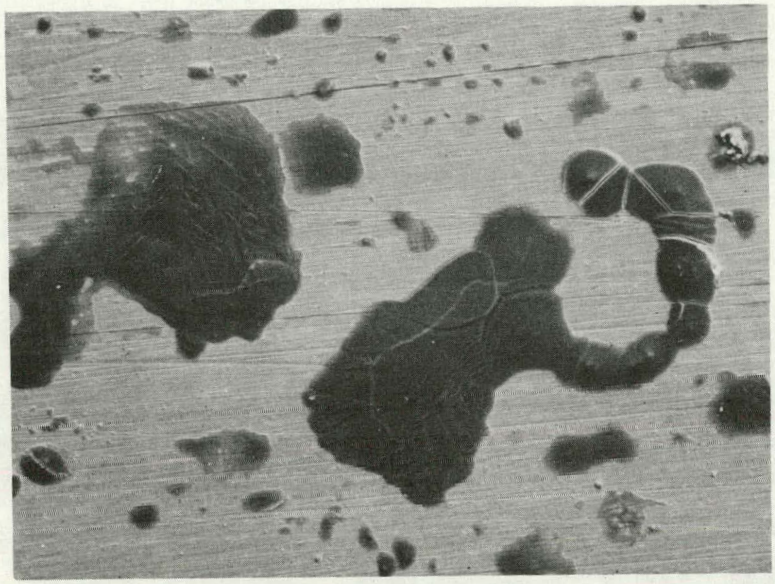

b.

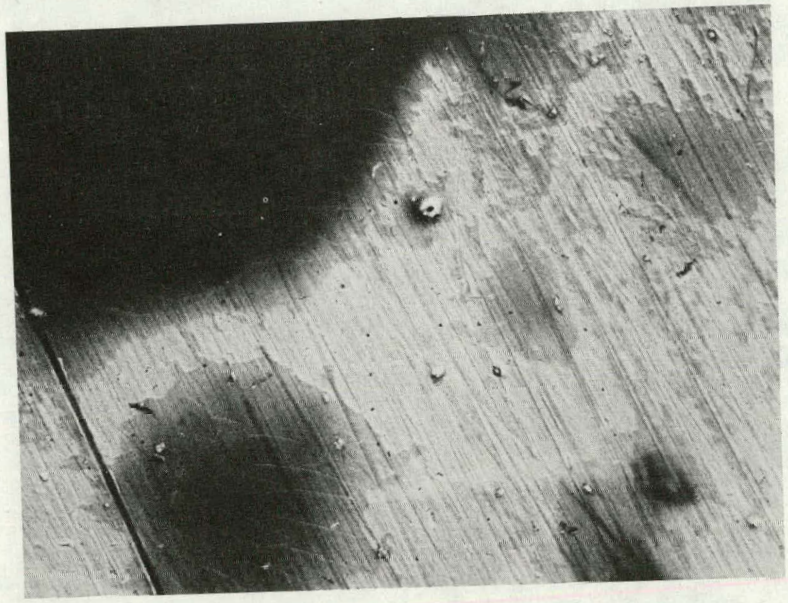

Figure 7 (a) Co-18Cr-6Al preoxidized for 30 min., sprayed with Na_2SO_4, and oxidized for 30 min. at 900°C x 200.

(b) Fe-18Cr-6Al preoxidized for 30 min., sprayed with Na_2SO_4, and oxidized for 30 min. at 900°C x 200.

a.

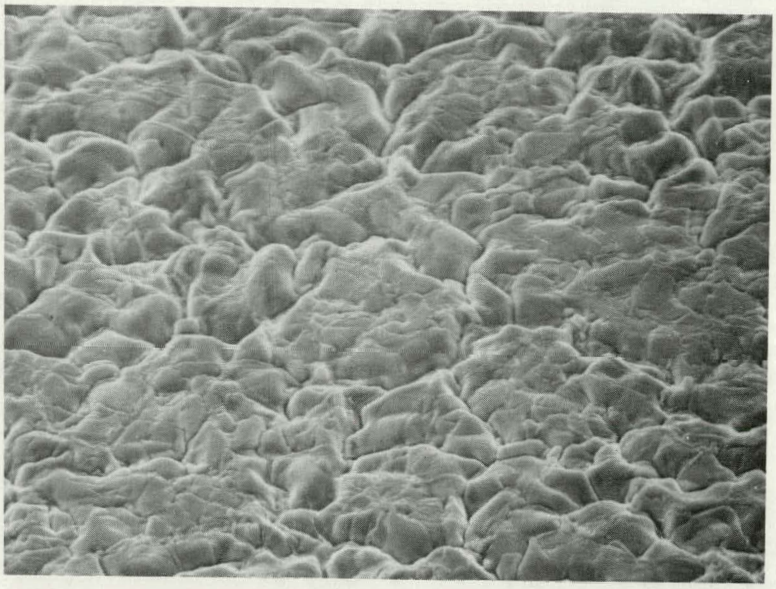

b.

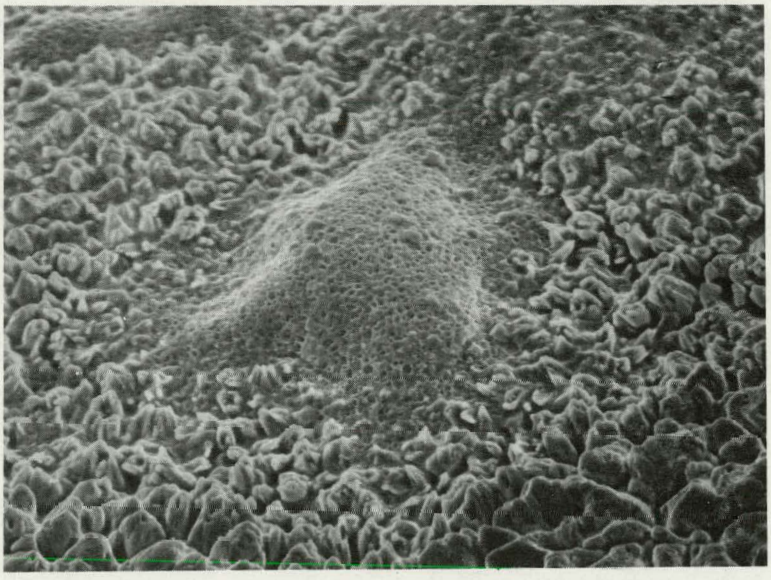

Figure 8 (a) Pure Fe preoxidized for 30 min. at 900°C x 1000.

(b) Preoxidized Fe sprayed with Na_2SO_4 and oxidized for 30 min. at 900°C x 1000.

a.

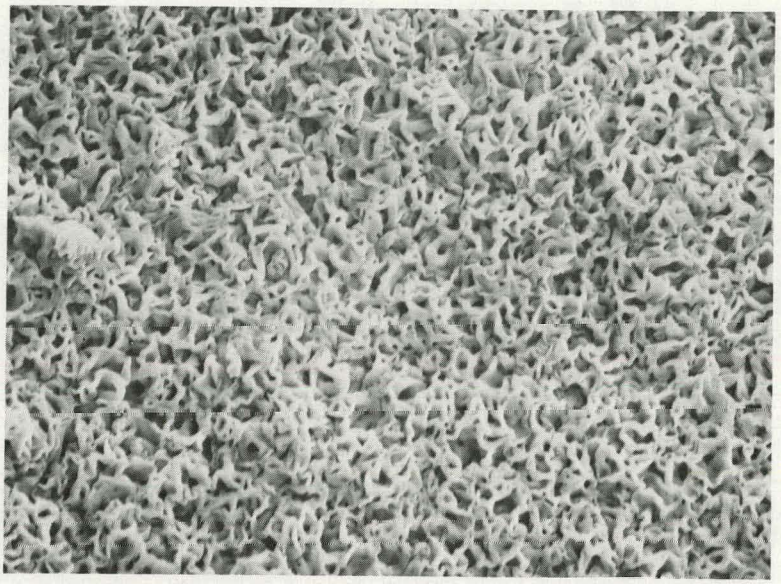

b.

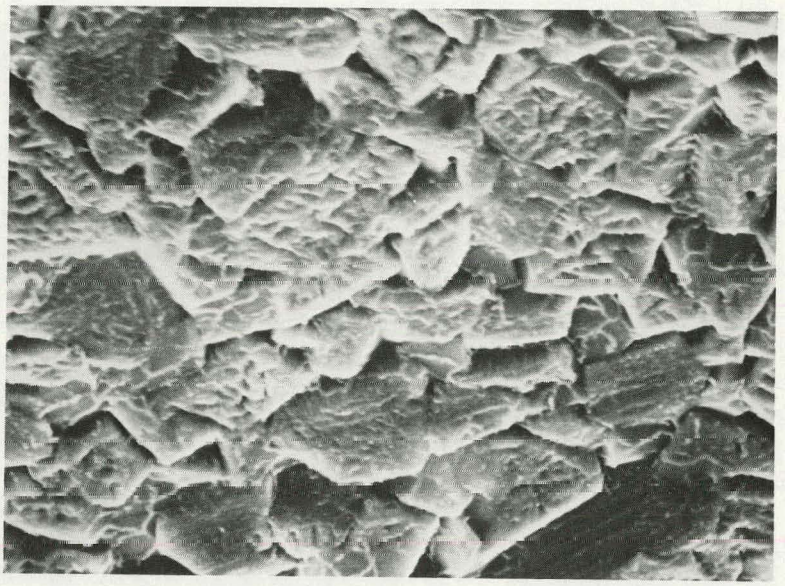

Figure 9 (a) Pure Co preoxidized for 30 min. at 900°C x 2000.

(b) Preoxidized Co sprayed with Na_2SO_4 and oxidized for 30 min. at 900°C x 2000.

a.

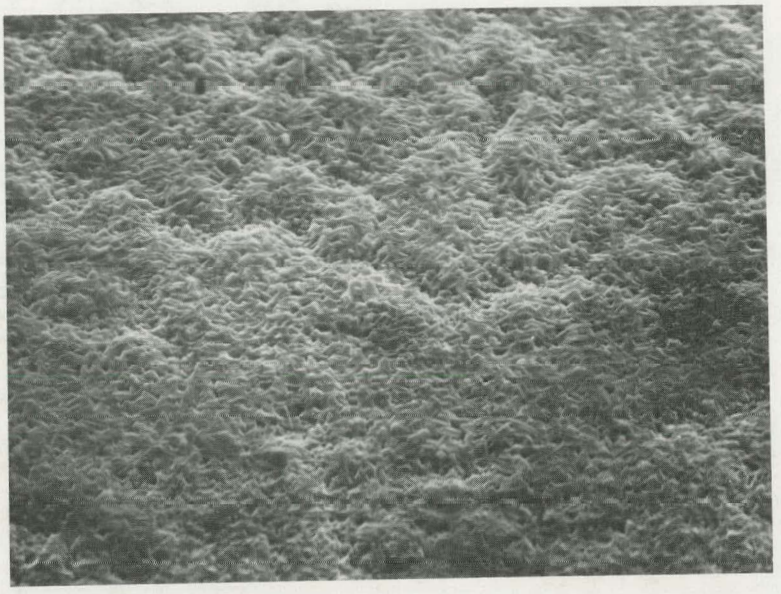

b.

Figure 10 (a) Pure Ni preoxidized for 30 min. at 900°C x 2000.

(b) Preoxidized Ni sprayed with Na_2SO_4 and oxidized for 30 min. at 900°C x 2000.

a.

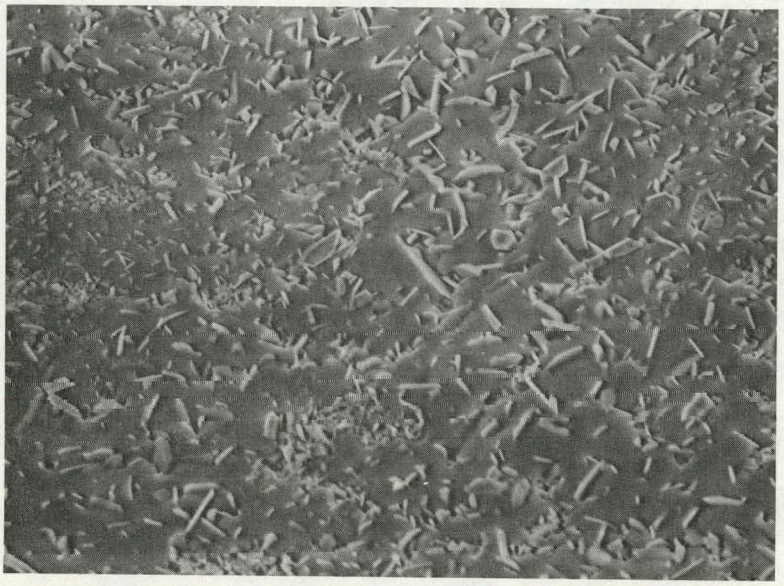

b.

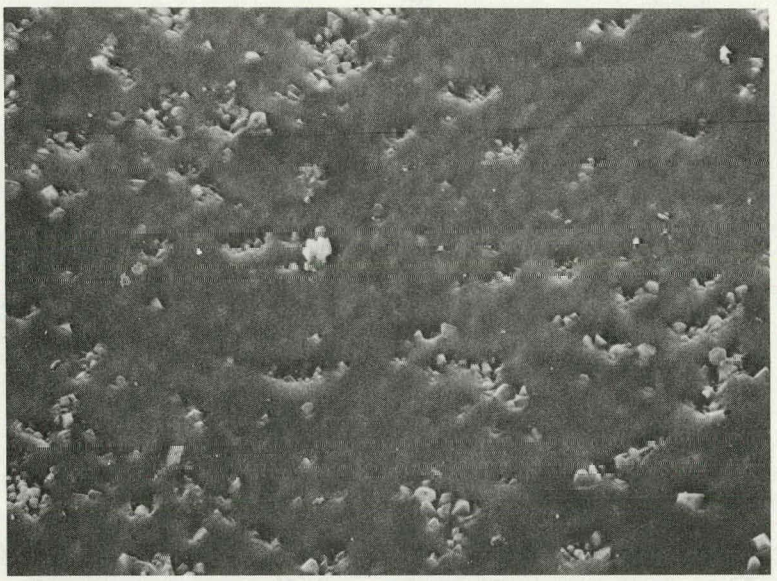

Figure 11 (a) Pure Cr oxidized 30 min. at 900°C with Na_2SO_4 coating.

(b) Co-27Cr-20Ni oxidized 30 min. at 900°C with Na_2SO_4 coating.

a.

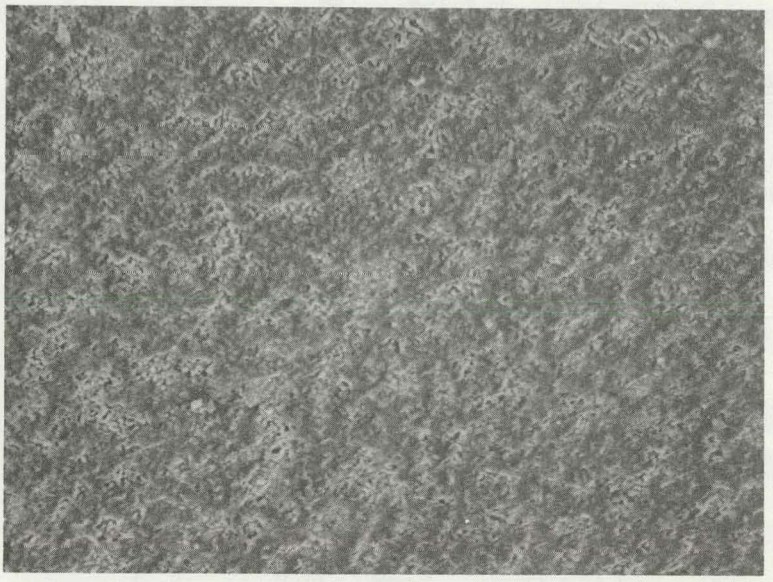

b.

Figure 12 (a) Ni-20Cr oxidized for 30 min. at 900°C with Na_2SO_4 coating.

(b) Ni-50Cr oxidized for 30 min. at 900°C with Na_2SO_4 coating.

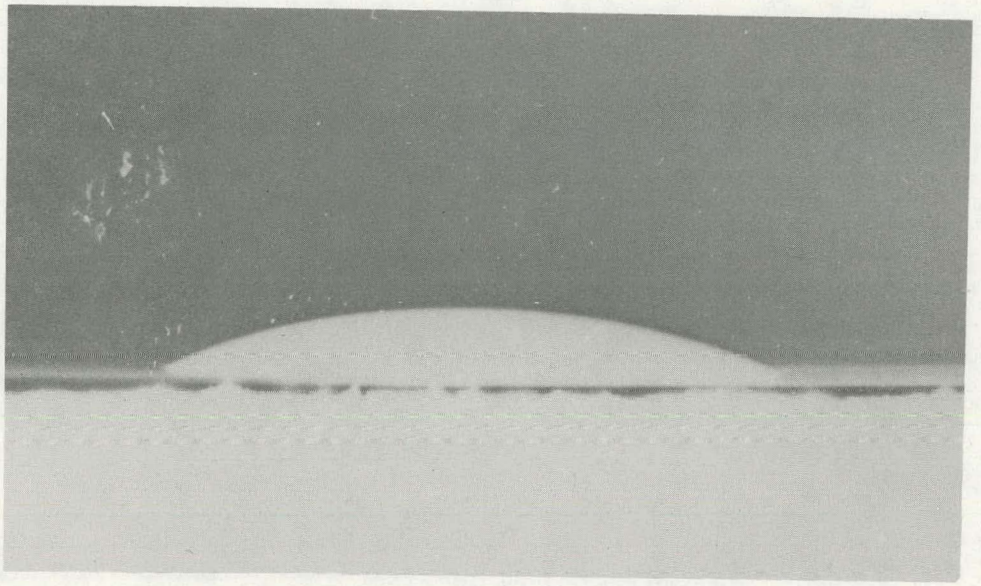

Figure 13 Spreading of Na_2SO_4 on Pt at 900°C

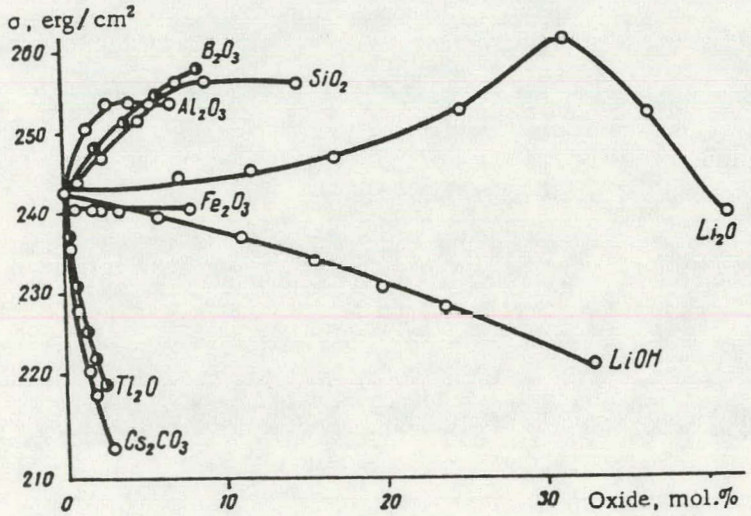

Figure 14 The effect of various additives on the surface tension of molten Li_2CO_3 at 765°C. (Ref. 12)

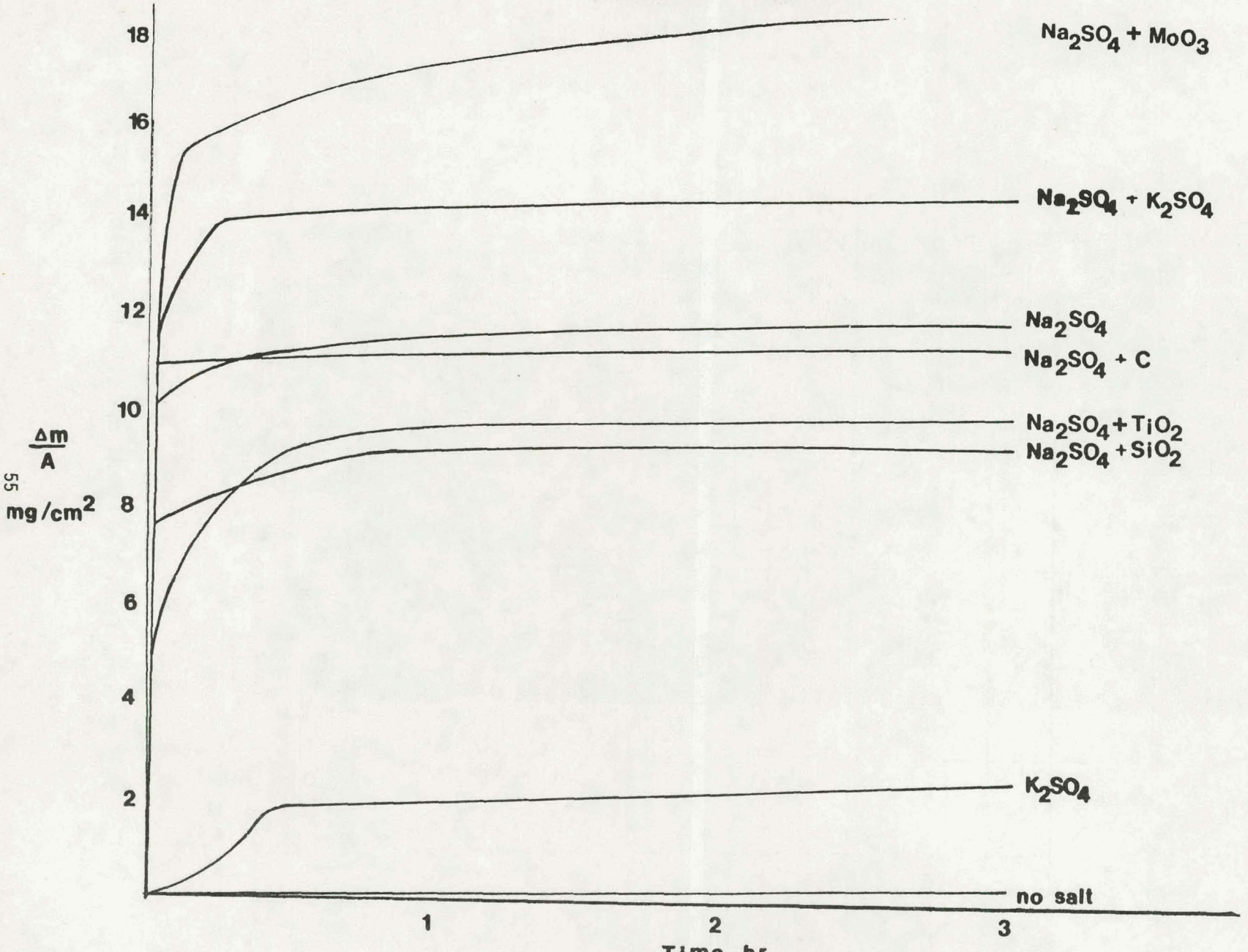

Figure 15 Rate of oxidation of Ni at 900°C in oxygen with 1 mg/cm^2 coatings of various salts

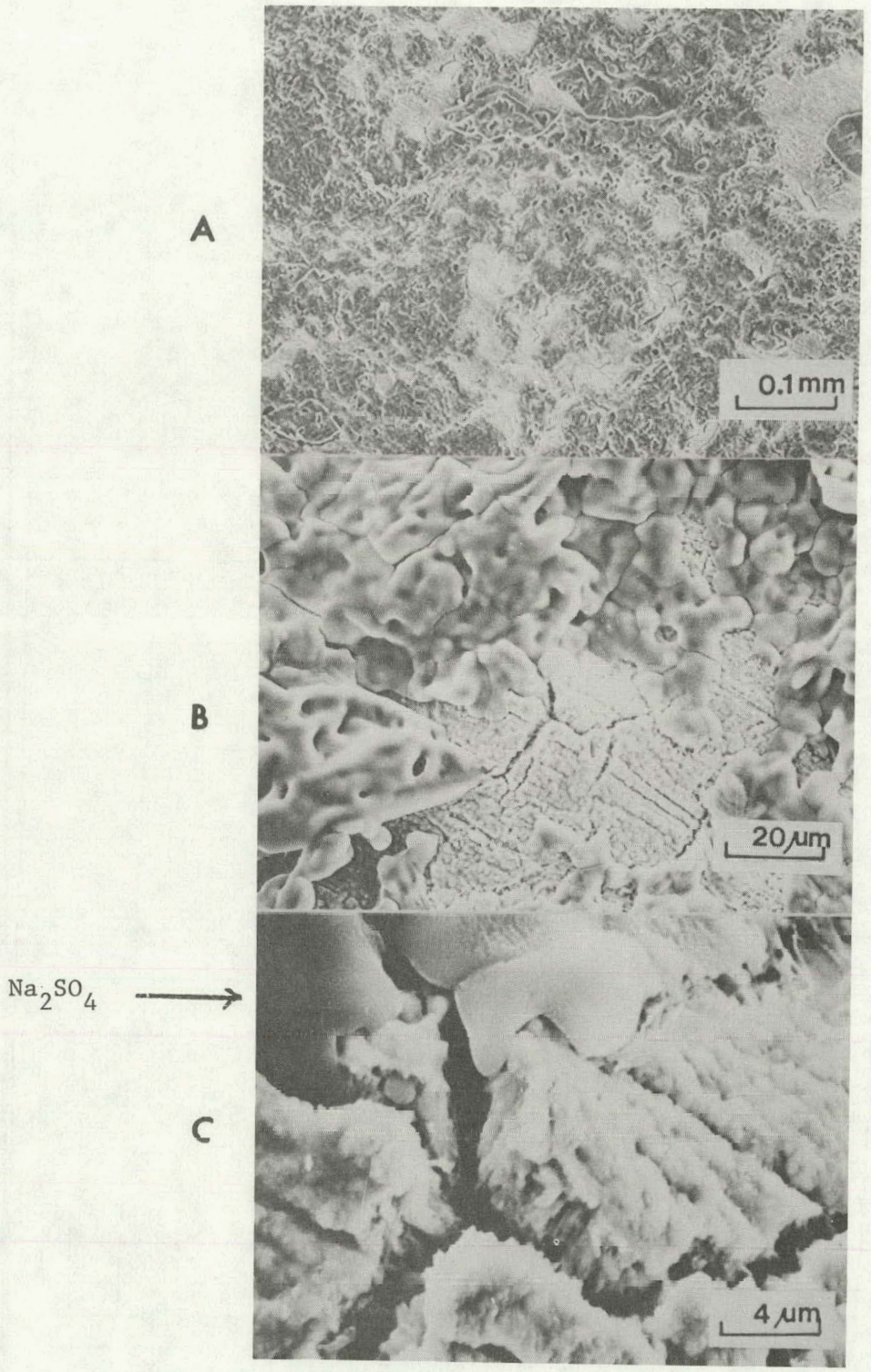

Figure 16 (a) Surface of nickel specimen coated with 1 mg/cm^2 Na_2SO_4 and oxidized at 890^{o}C for 10 sec.

(b) (c) Details of (a).

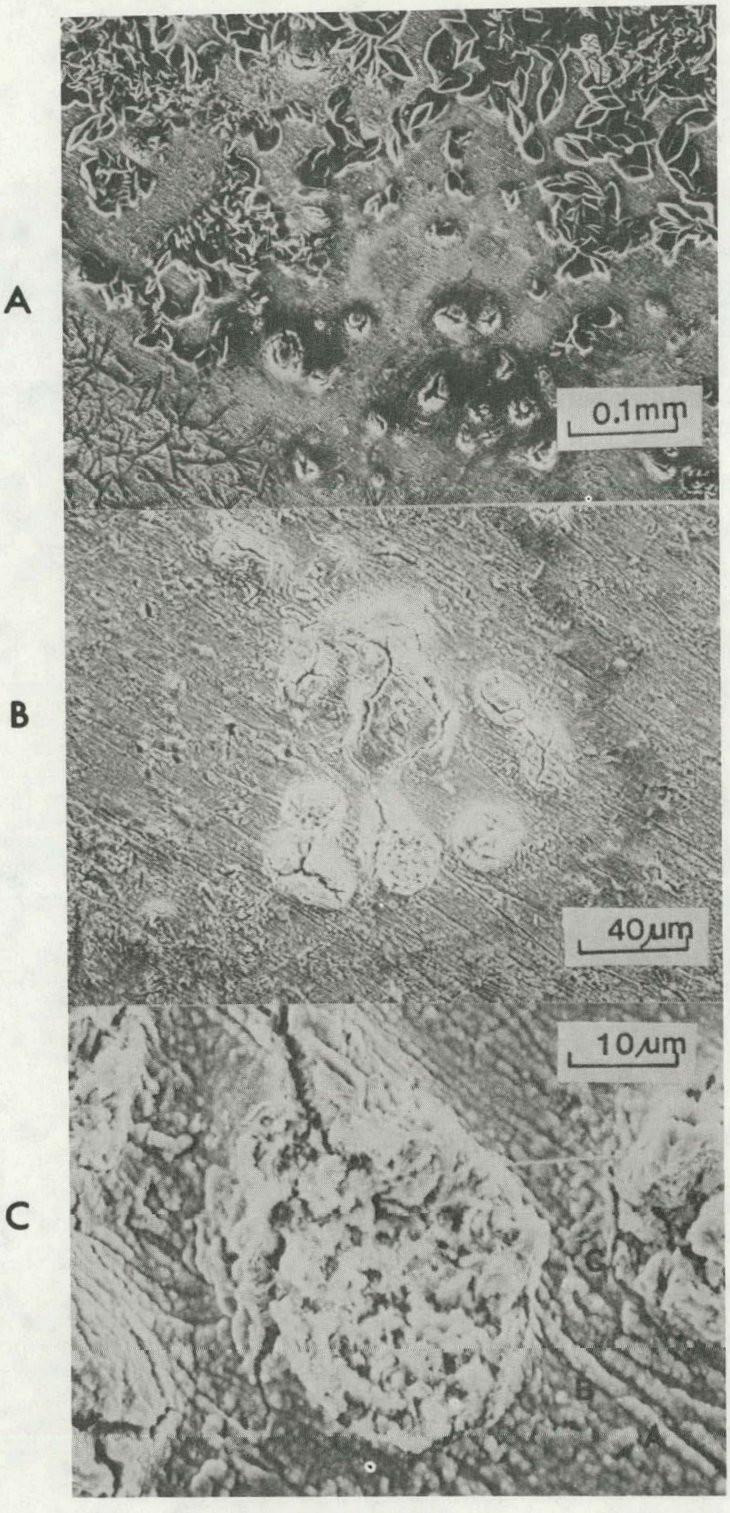

Figure 17 (a) (b) (c) Surface of nickel specimen coated with 1 mg/cm^2 Na_2SO_4 and oxidized at 890^{o}C for 10 seconds.

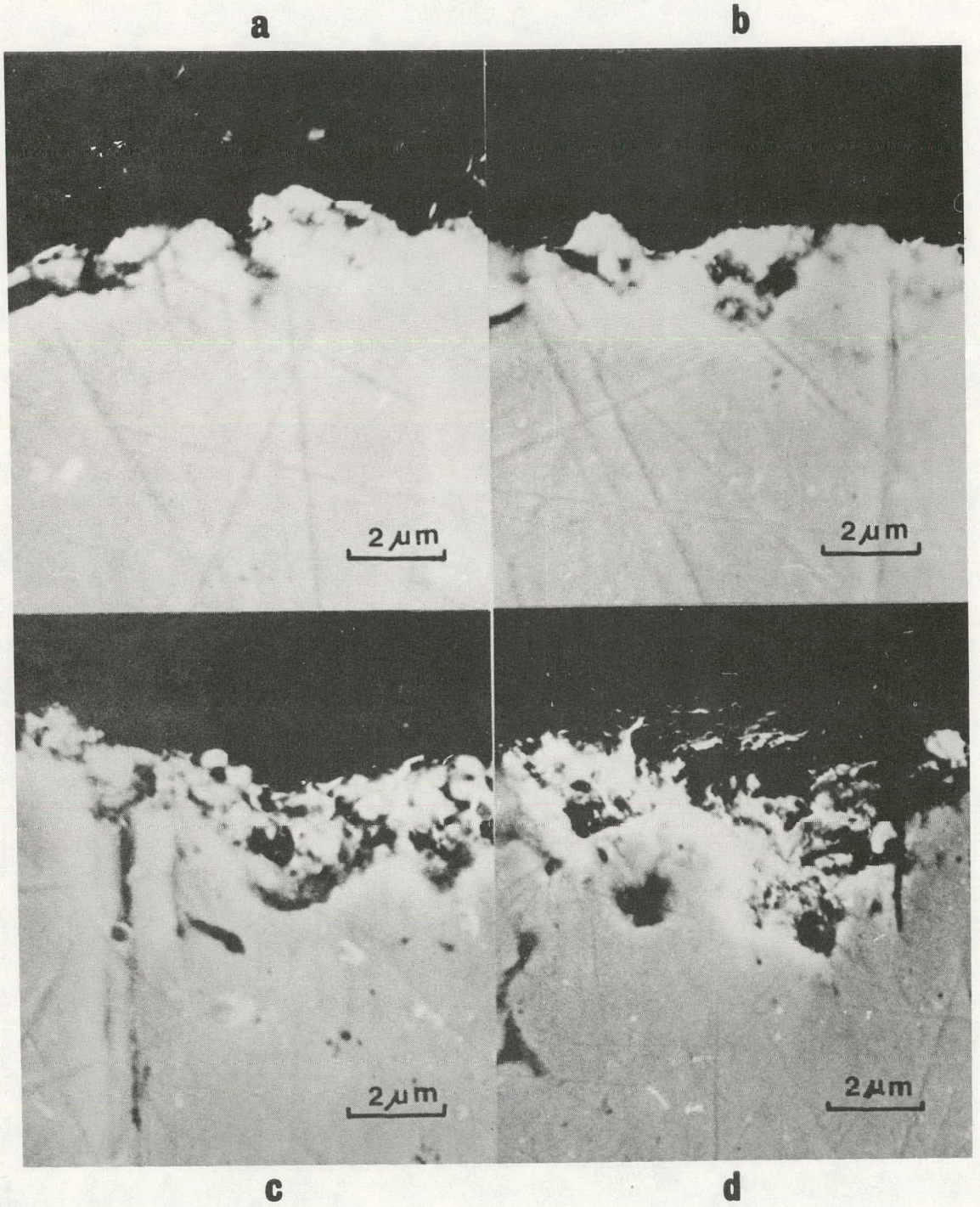

Figure 18 (a) (b) (c) (c) Cross sections of nickel oxidized at 890°C for 10 sec.

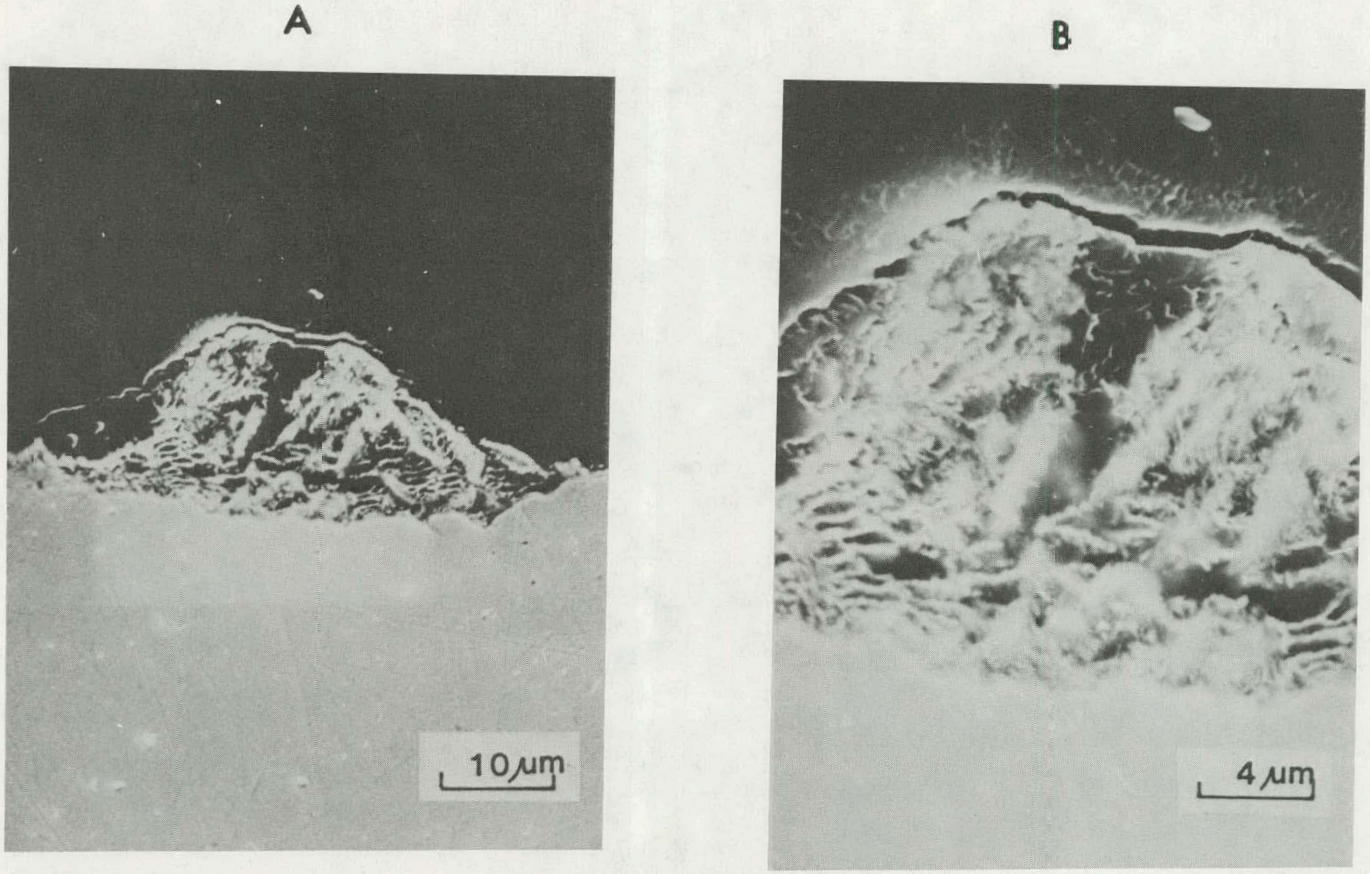

Figure 19 (a) Another area of the same specimen in Figure 18.

(b) Detail of (a).

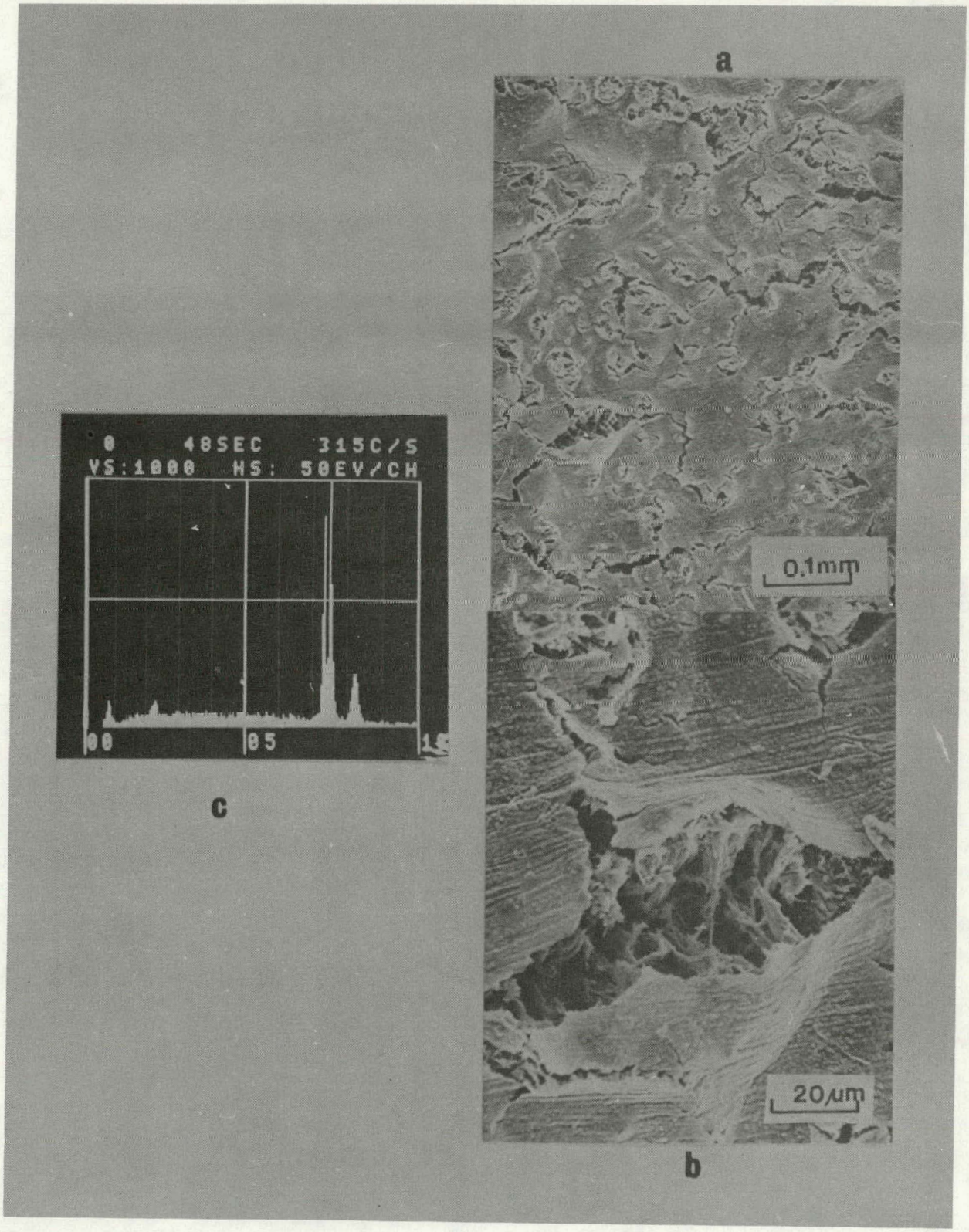

Figure 20 (a) Surface of nickel specimen coated with 1 mg/cm^2 Na_2SO_4 and oxidized at 890^{o}C for 30 sec.

(b) Detail of (a).

(c) EDAX of the surface.

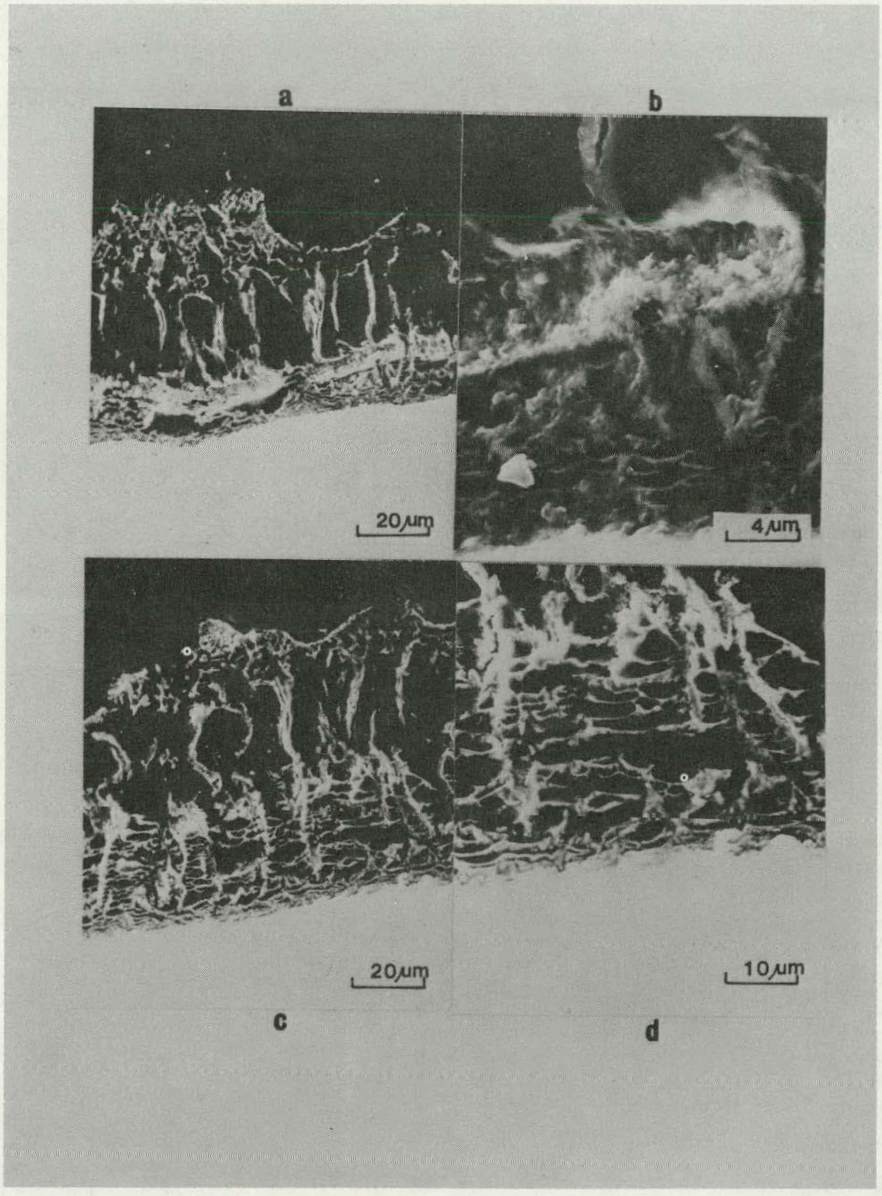

Figure 21 (a) (c) Cross sections of the same specimen as in Figure 20.

(b) (d) Detail (a) (c).

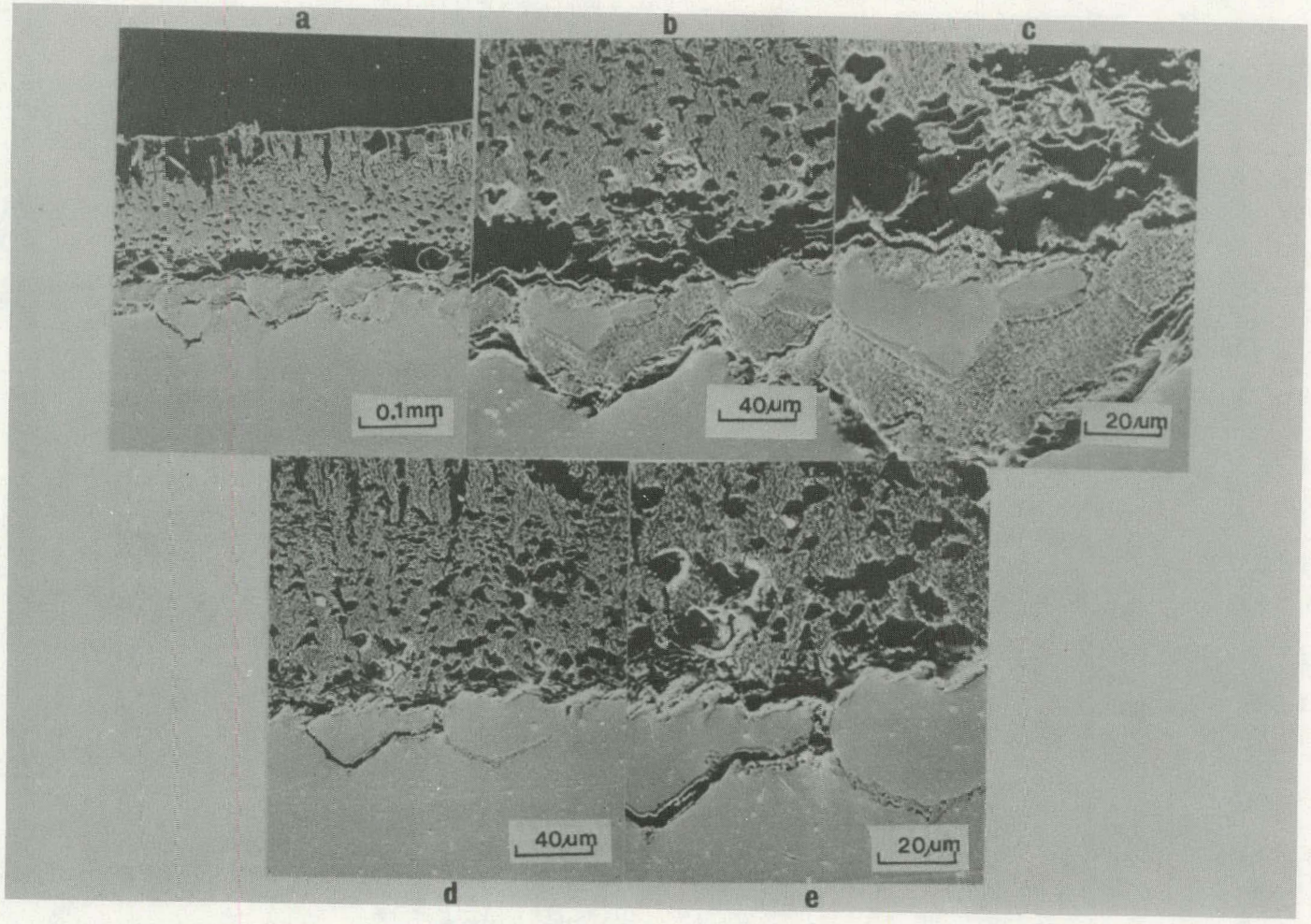

Figure 22 (a) (b) (c) (d) (e) Nickel coated with Na_2SO_4 (1 mg/cm^2) oxidized at 900^oC for 180 minutes.

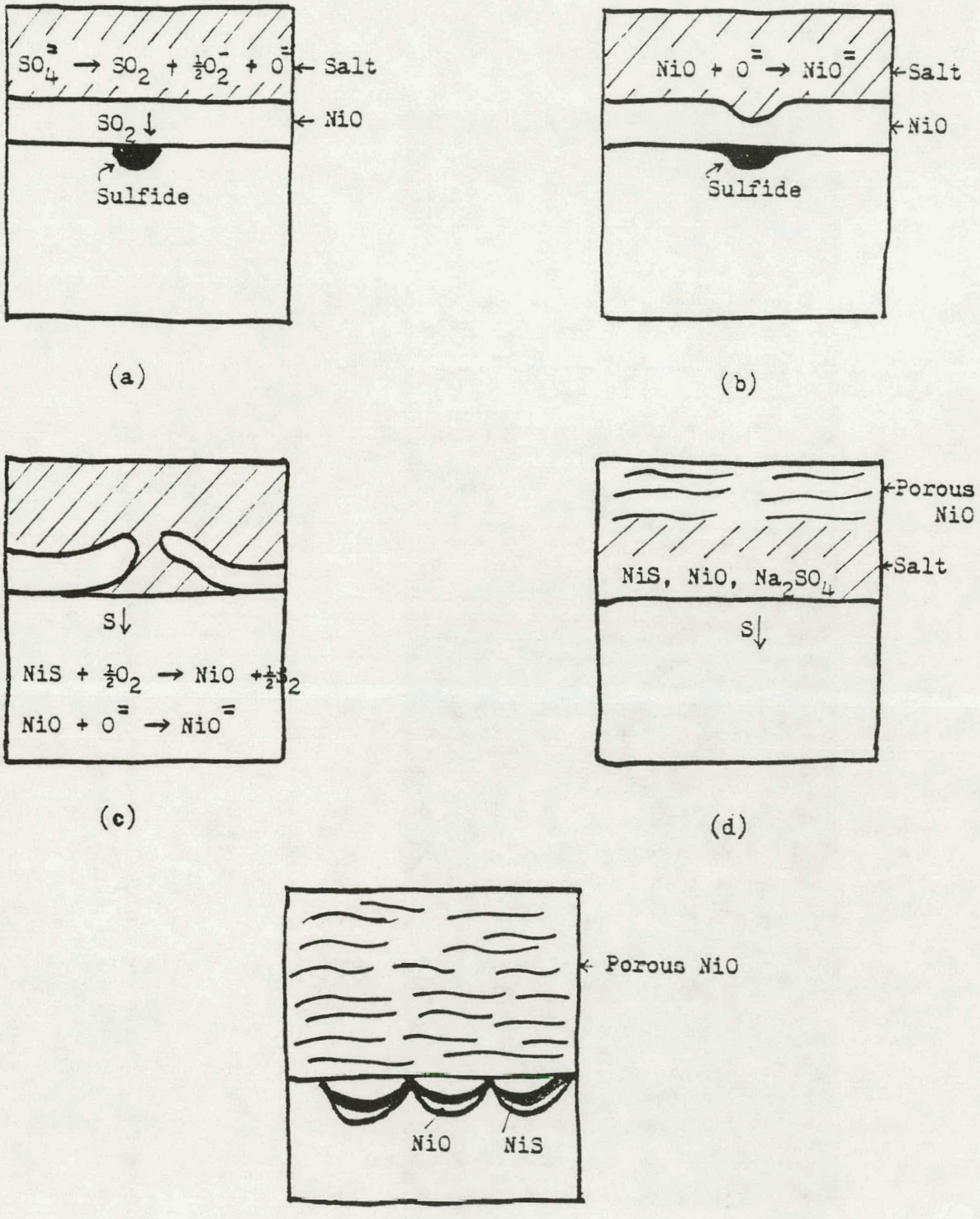

Figure 23 A schematic diagram to illustrate the Na_2SO_4-induced hot corrosion of pure nickel in one atm O_2.

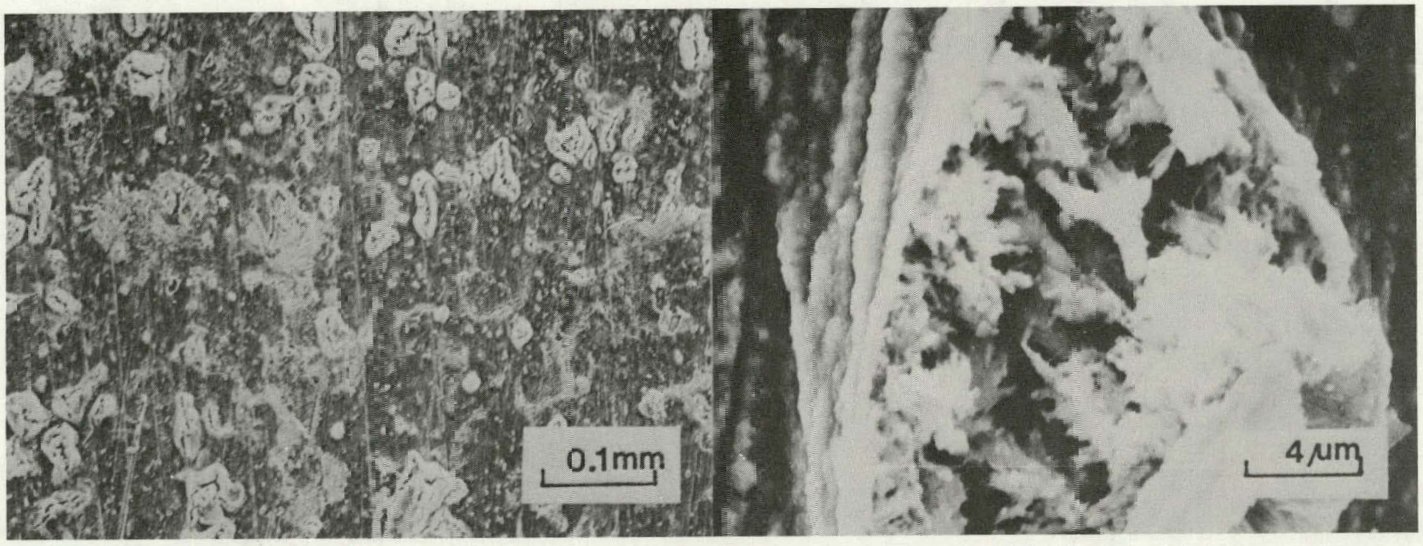

Figure 24 Surface of nickel specimen coated with $Na_2SO_4 + K_2SO_4$ oxidized at 890°C for 10 seconds.

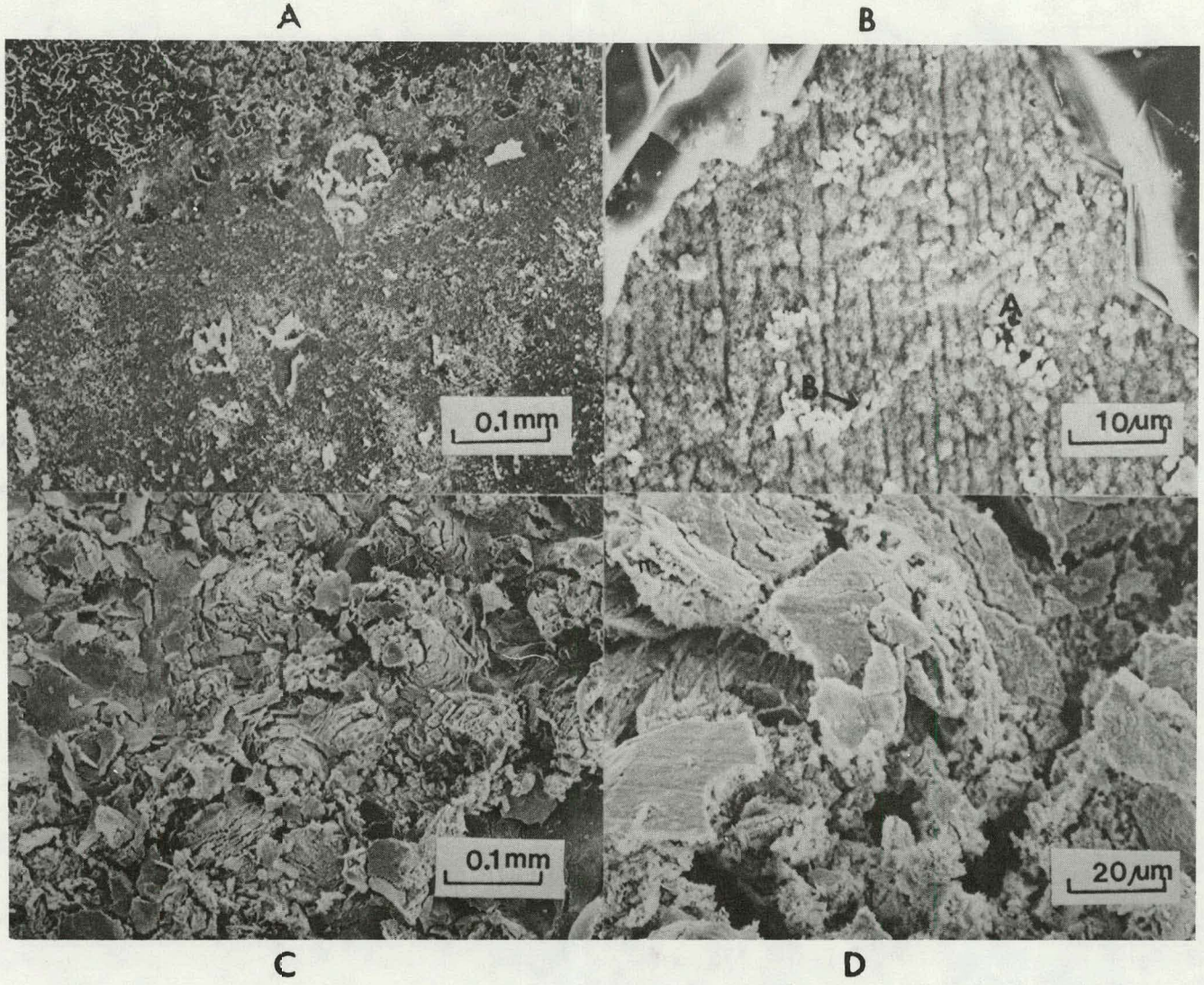

Figure 25 (a) (b) Surface of nickel specimen coated with Na_2SO_4 + TiO_2 (1 mg/cm^2) oxidized at 890°C for 30 sec.

(c) (d) Surface of nickel specimen coated with Na_2SO_4 + TiO_2 oxidized at 900°C for 15 min.

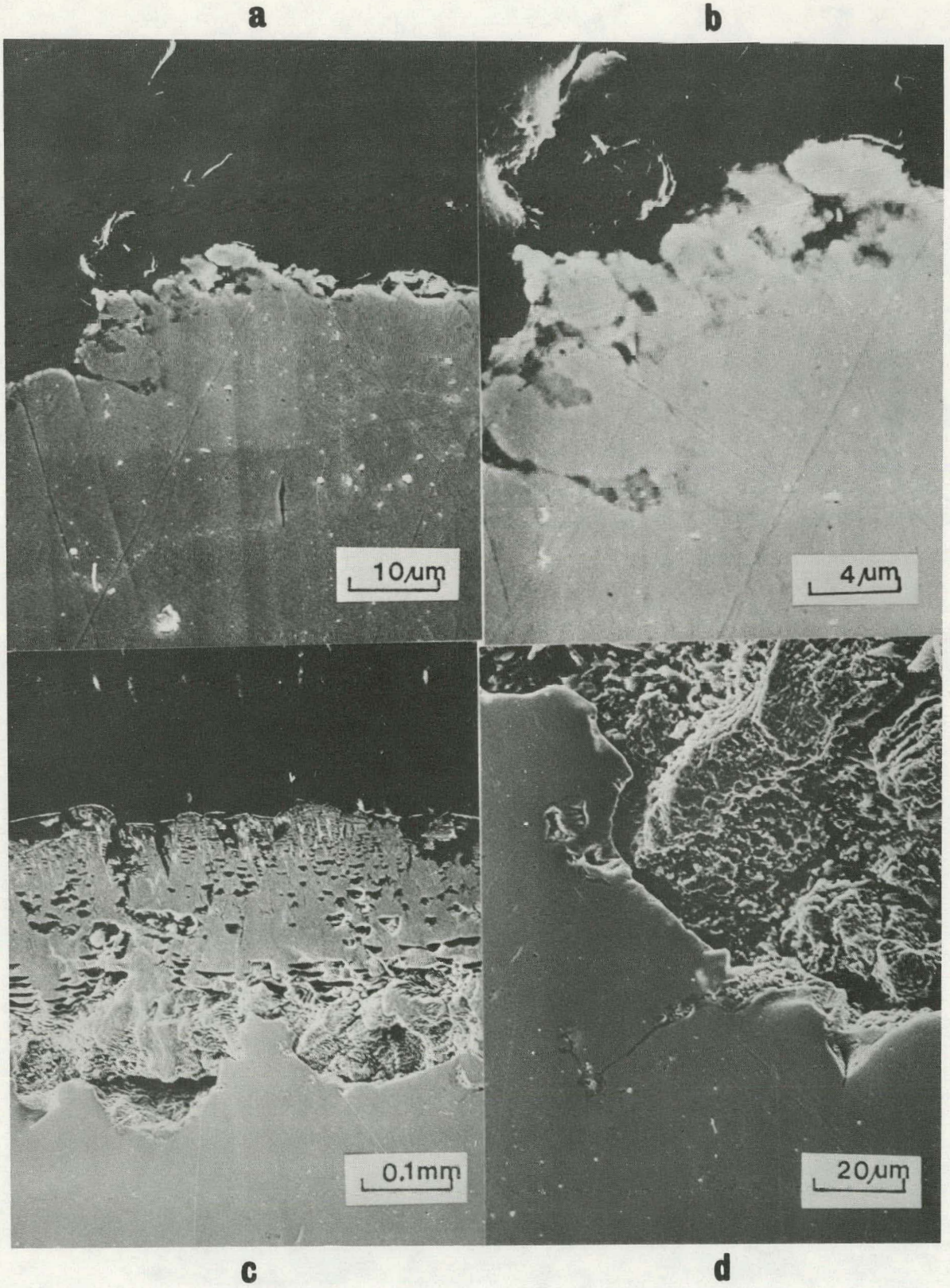

Figure 26 (a) (b) Cross section of nickel coated with Na_2SO_4 + TiO_2 (1 mg/cm^2) oxidized at 890°C for 30 sec.

(c) (d) Cross sections of nickel coated with Na_2SO_4+ TiO_2 oxidized at 900°C for 15 min.

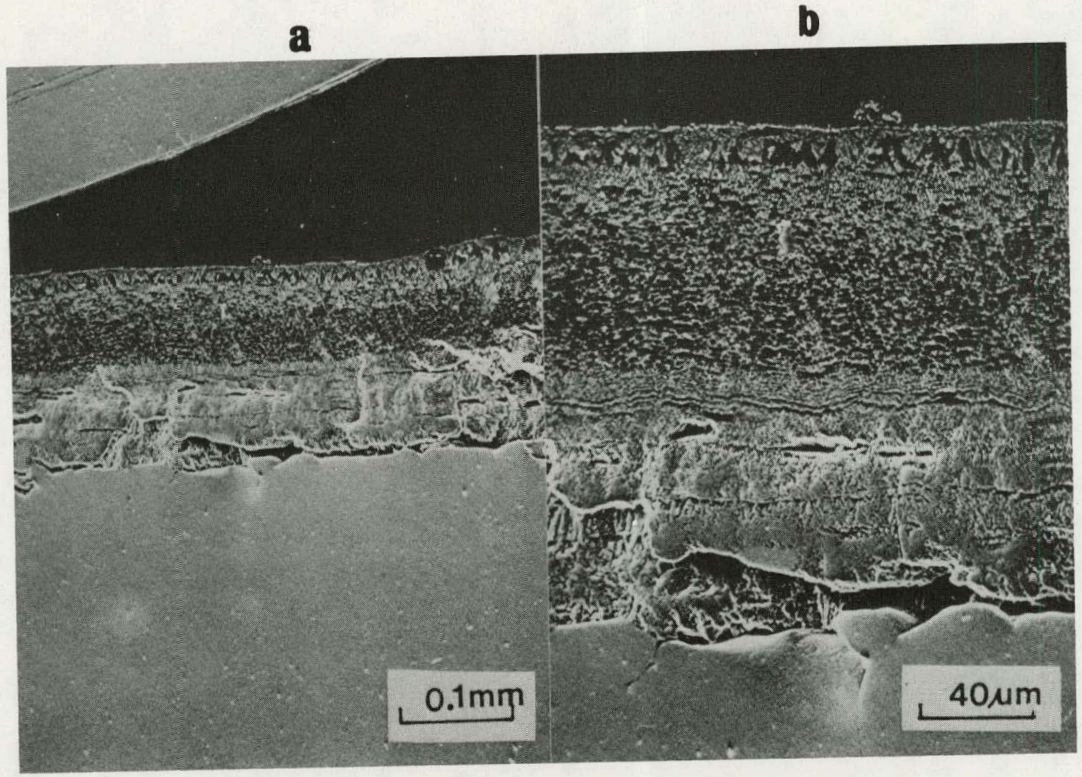

Figure 27 (a) Ni coated with Na_2SO_4 + MoO_3 (1 mg/cm^2) oxidized at 900°C for 3 hrs.

(b) same as (a).

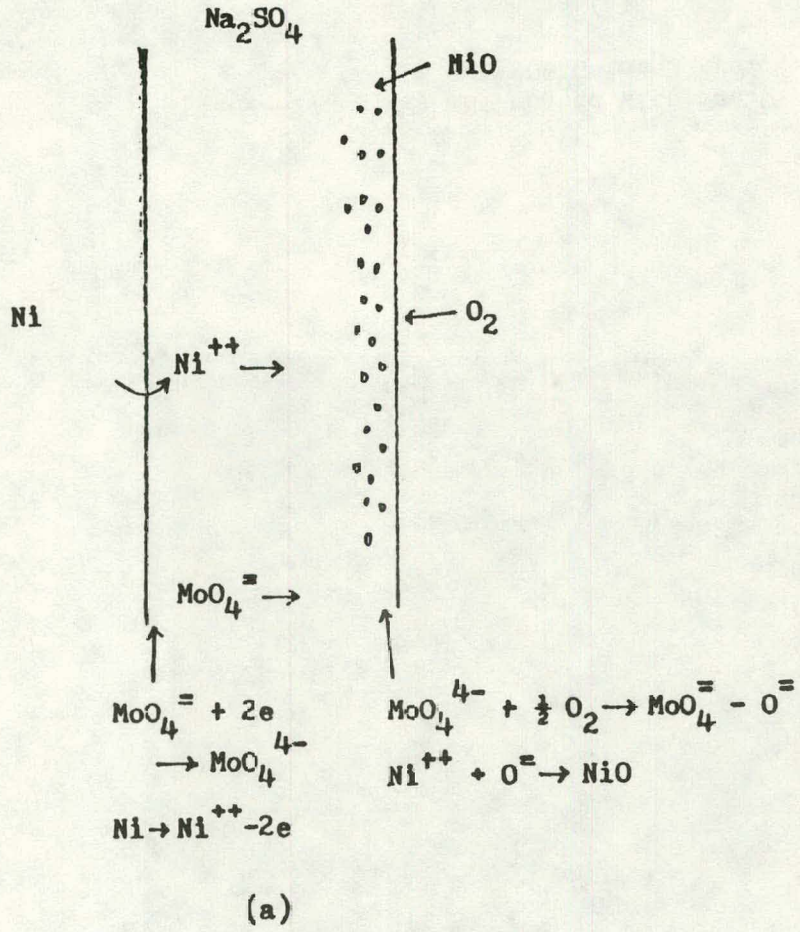

Figure 28 A schematic diagram to illustrate the MoO_3-modified Na_2SO_4 induced hot corrosion of pure nickel in one atm O_2.

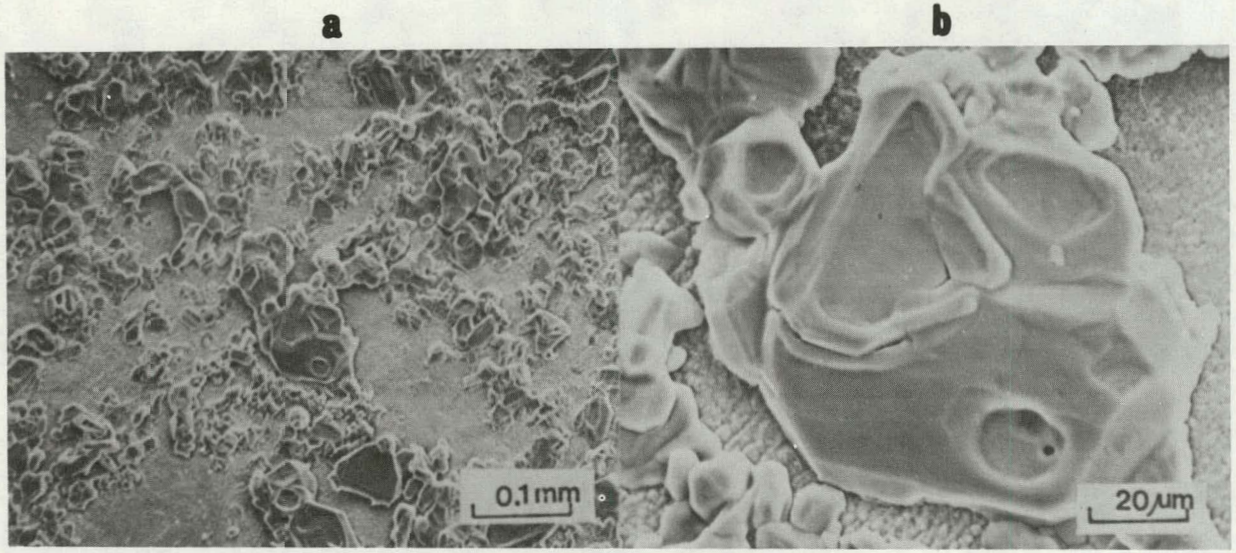

Figure 29 (a) Surface of Ni specimen coated with K_2SO_4 (1 mg/cm^2) oxidized at 900°C for 40 min.

(b) detail of (a).

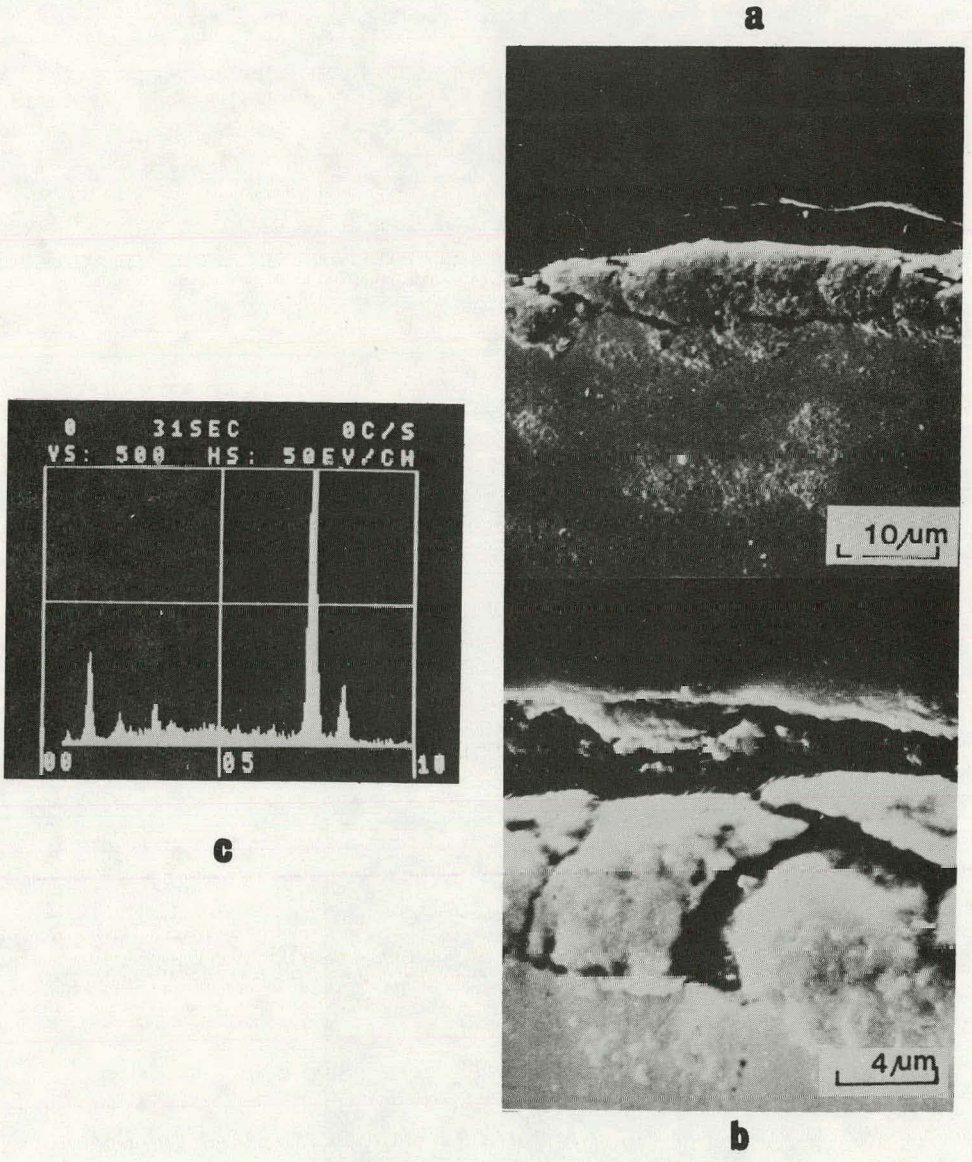

Figure 30 (a) Cross-section of nickel specimen coated with K_2SO_4 (1mg/cm^2) oxidized at 900°C for 40 min.

(b) detail of (a).

(c) EDAX of dark region in the scale.

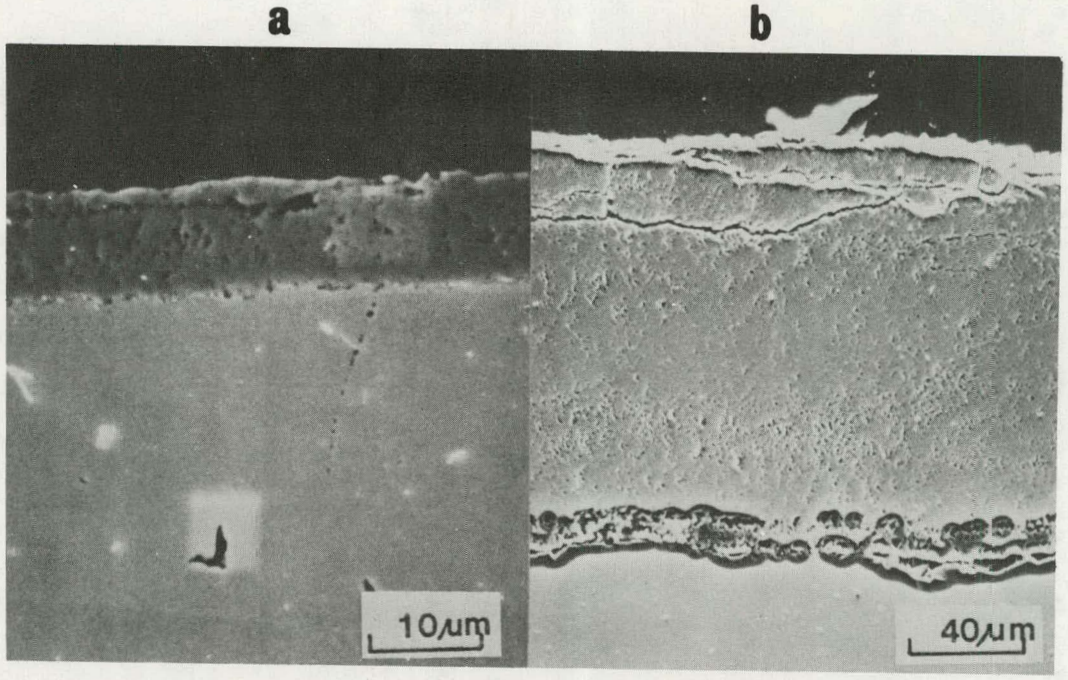

Figure 31 (a) Ni coated with K_2SO_4 ($1mg/cm^2$) oxidized at 900^oC for 3 hrs.

(b) Ni coated with K_2SO_4 ($1mg/cm^2$) oxidized at 977^oC for 48 hrs.

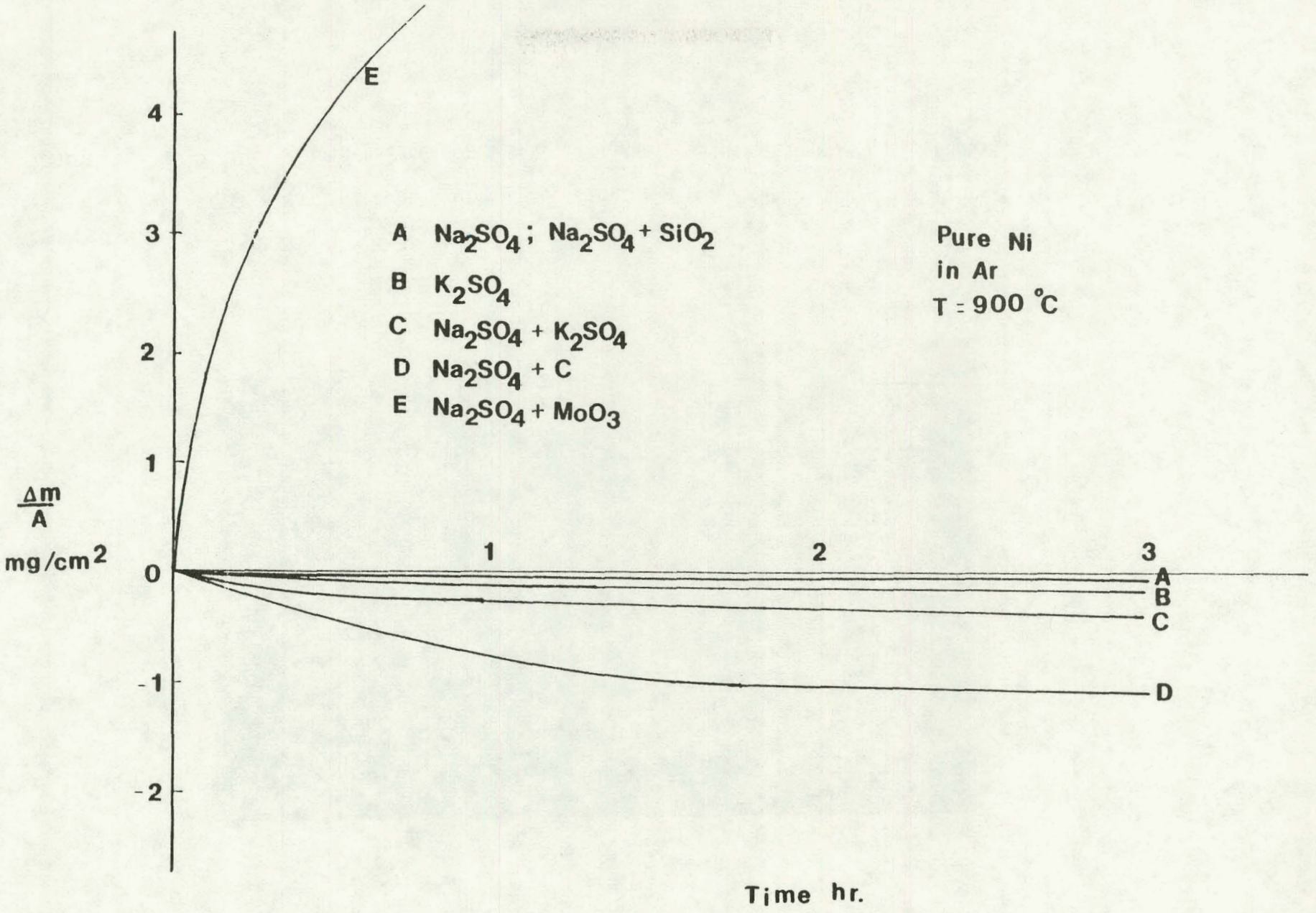

Figure 32 Weight change vs Time for Pure Nickel coated with 1 mg/cm^2 salt reacted in Ar at 900^o C.

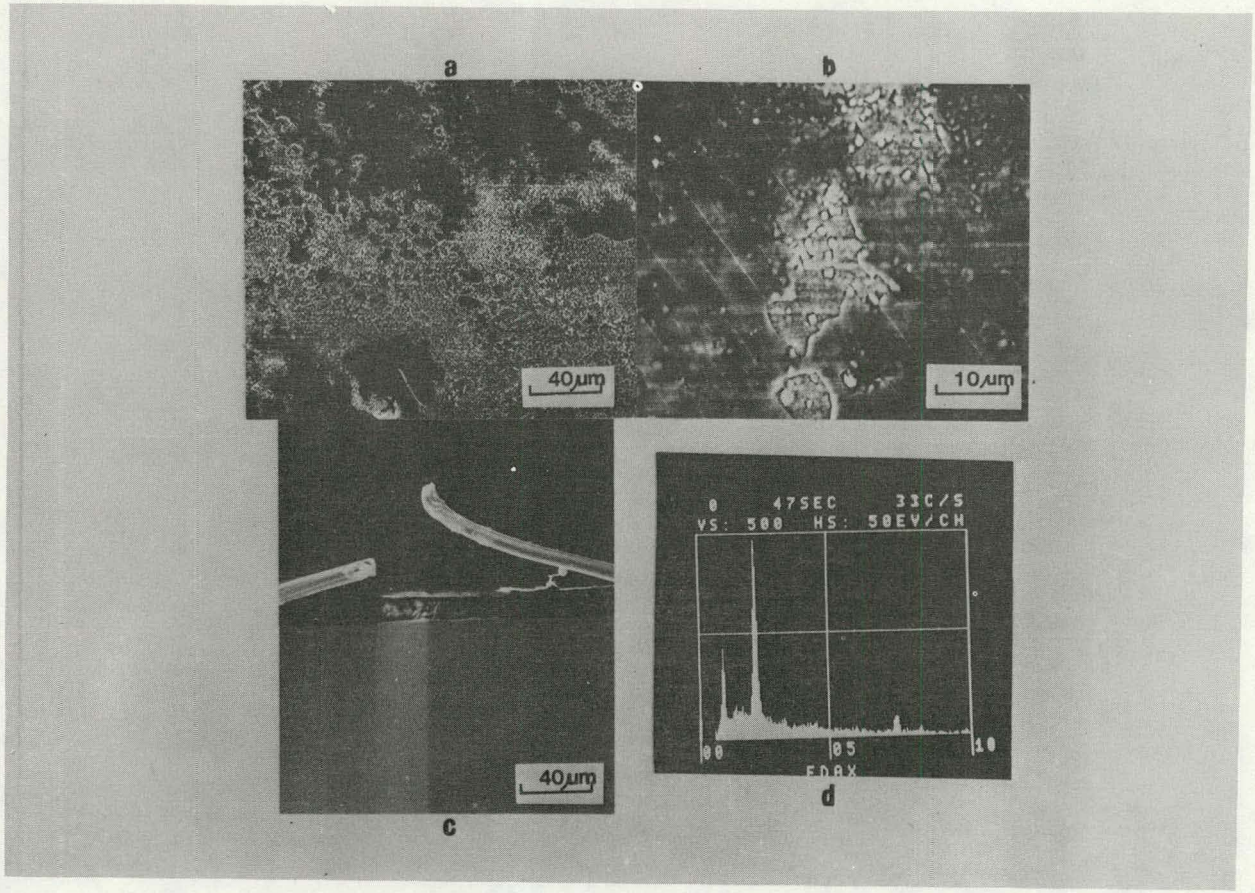

Figure 33 (a) Ni coated with Na_2SO_4 ($1mg/cm^2$) reacted in Ar at 900^oC for 40 min.

(b) same as (a).

(c) Cross-section of the specimen.

(d) EDAX of outer region in (c).

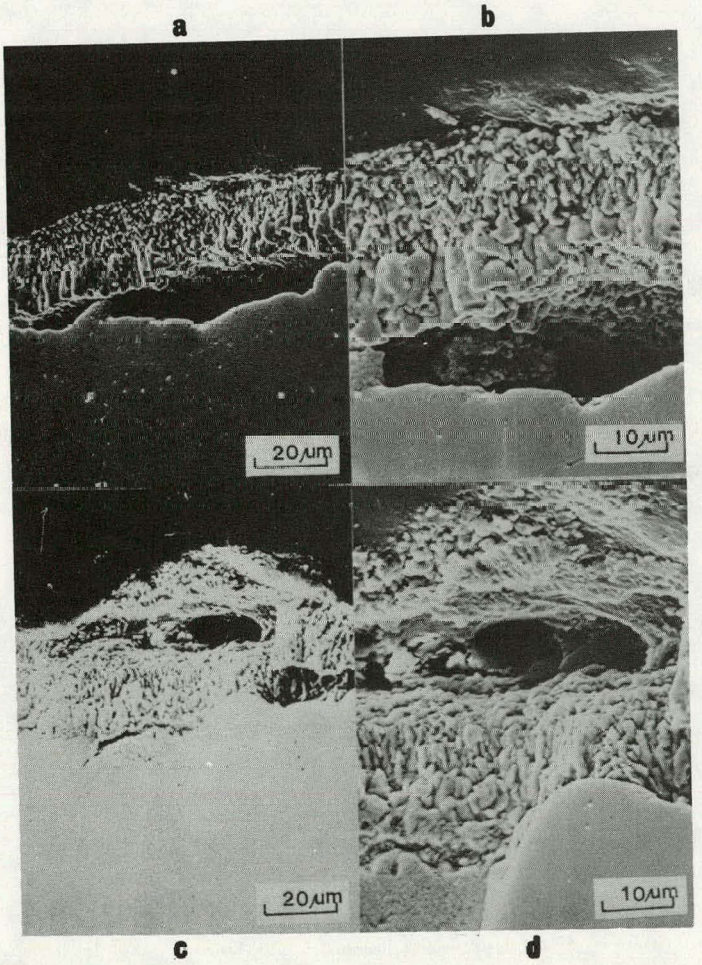

Figure 34 (a) (b) (c)$_2$(d) The scale of Nickel coated with Na_2SO_4 + MoO_3 (1mg/cm^2) reacted in Ar at 900^{o}C for 3 hours.

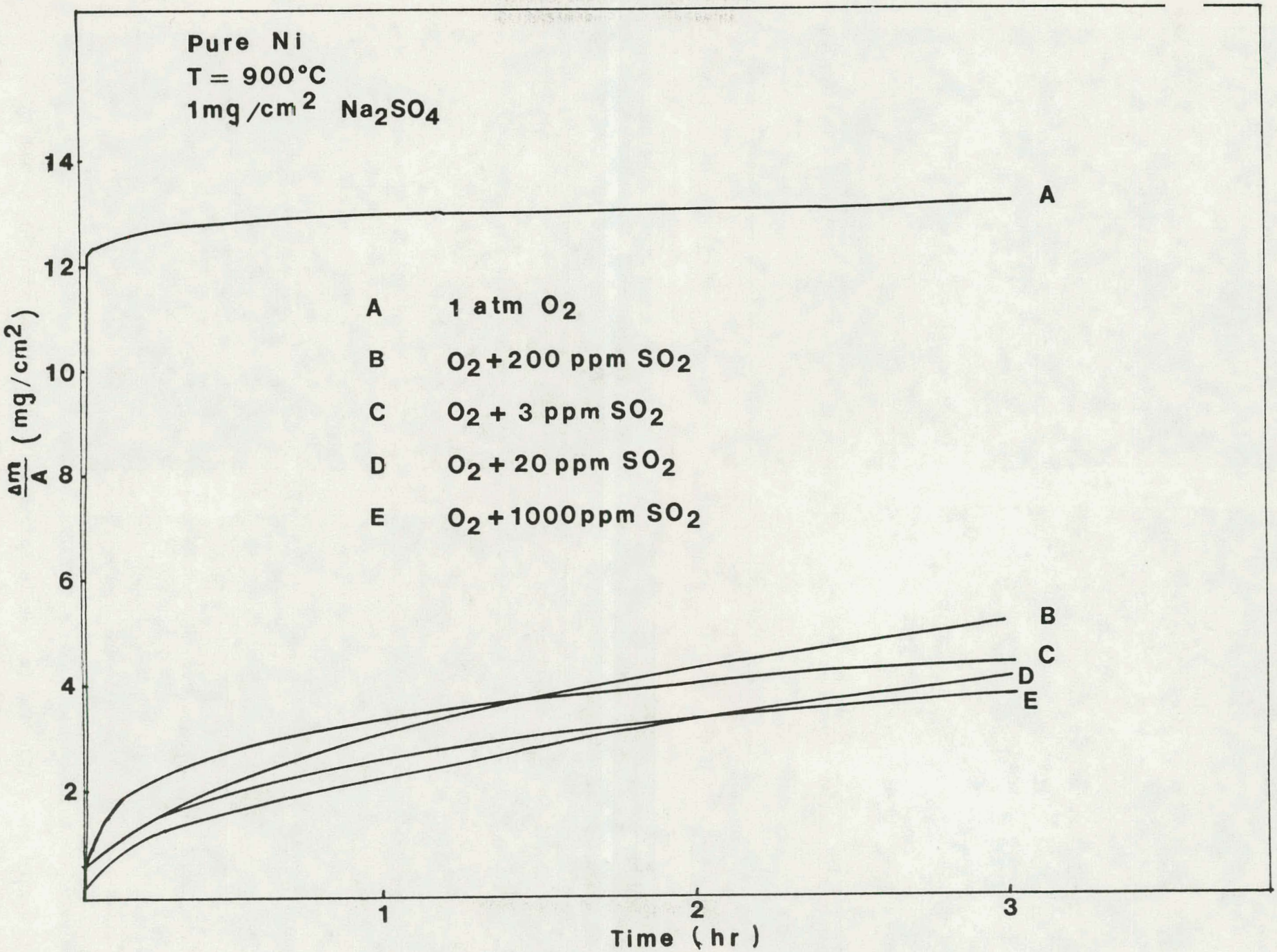

Figure 35 The rate of oxidation of Na_2SO_4-coated Ni at 900° C in various atmospheres

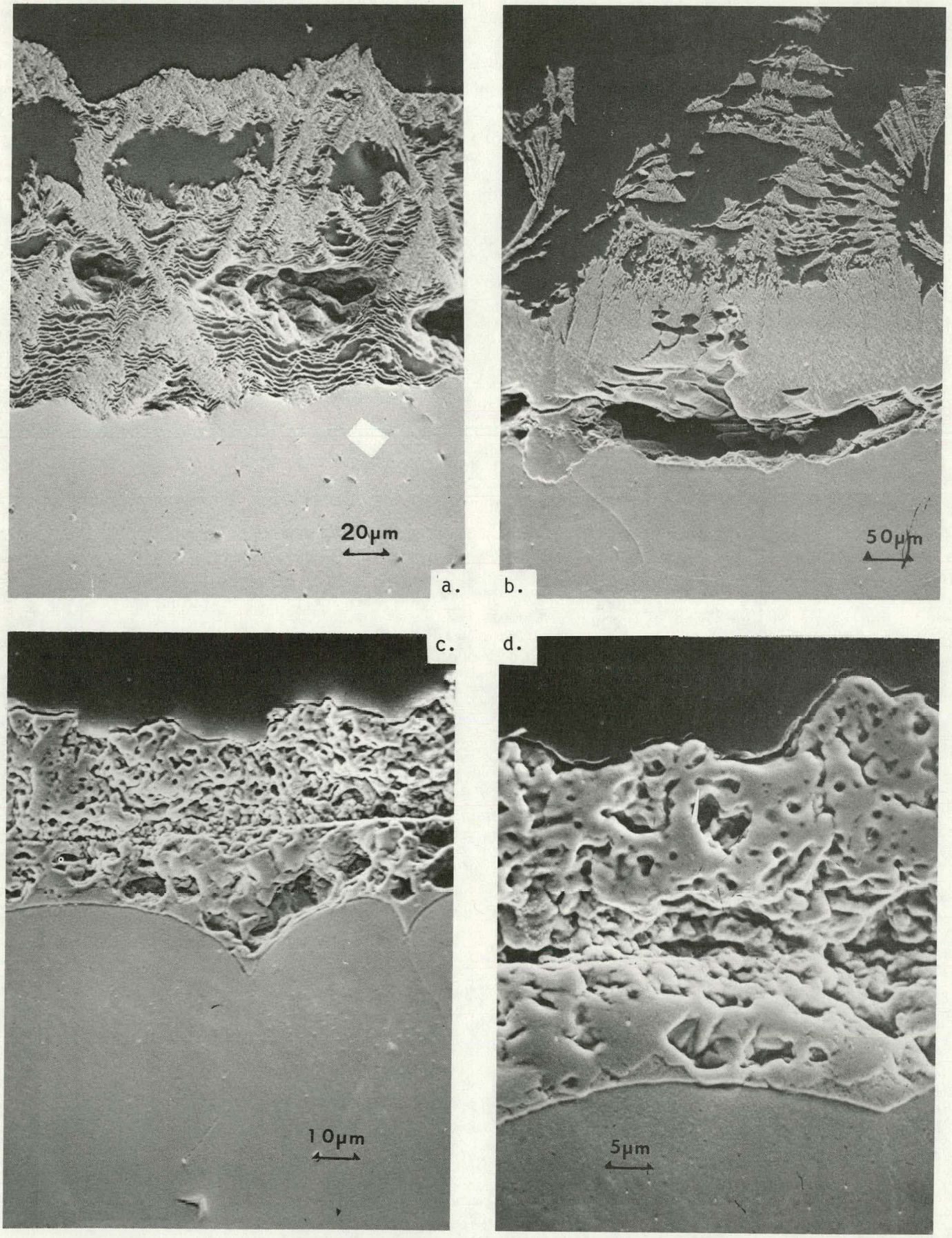

Figure 36 (a) and (b) Scale formed on Na_2SO_4-coated Ni in O_2 at 900°C.
(c) and (d) Scale formed on Na_2SO_4-coated Ni in O_2+20ppm (SO_2+SO_3).

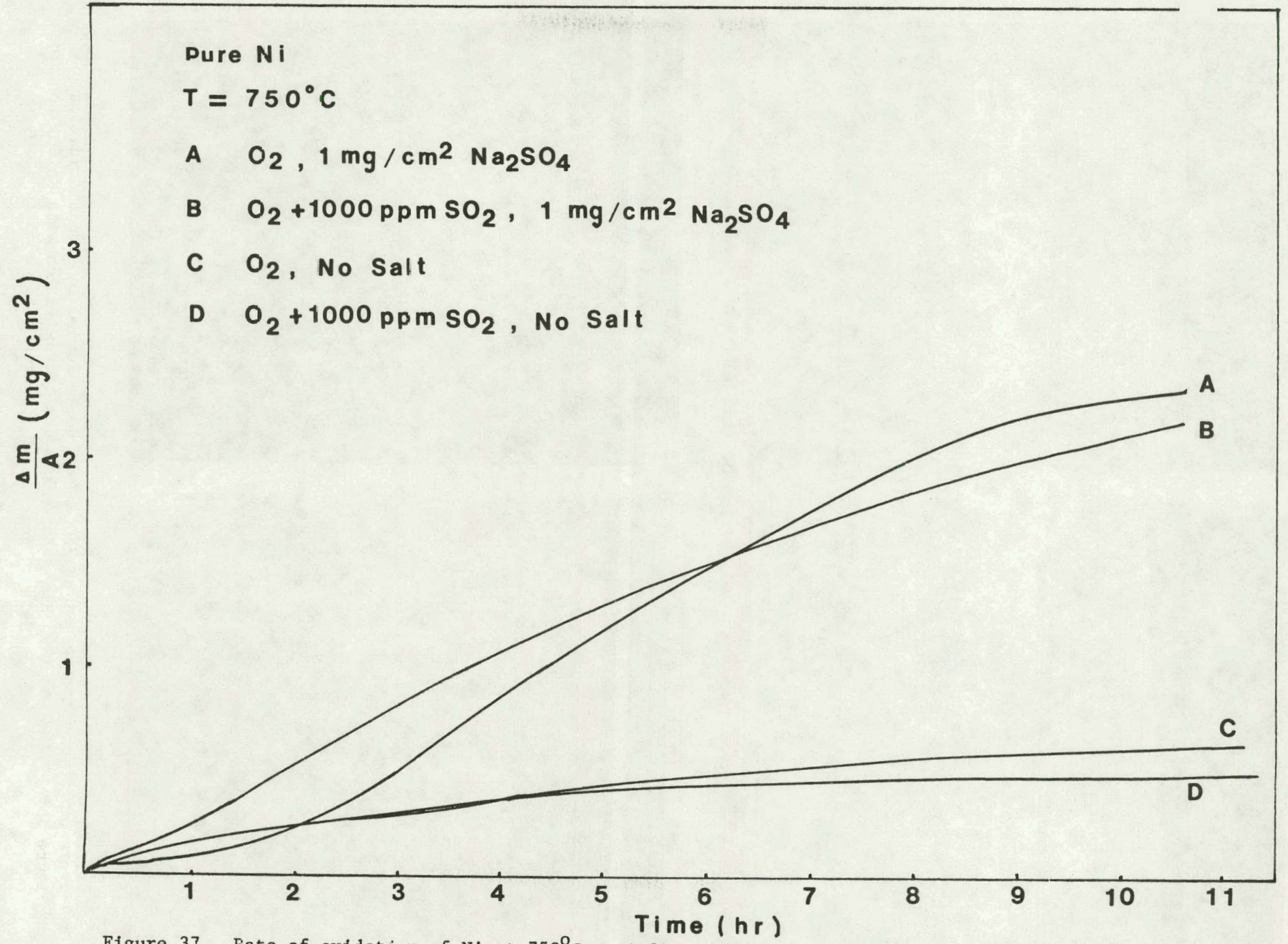

Figure 37 Rate of oxidation of Ni at 750°C as influenced by Na_2SO_4 deposits and (SO_2+SO_3) in the gas phase.

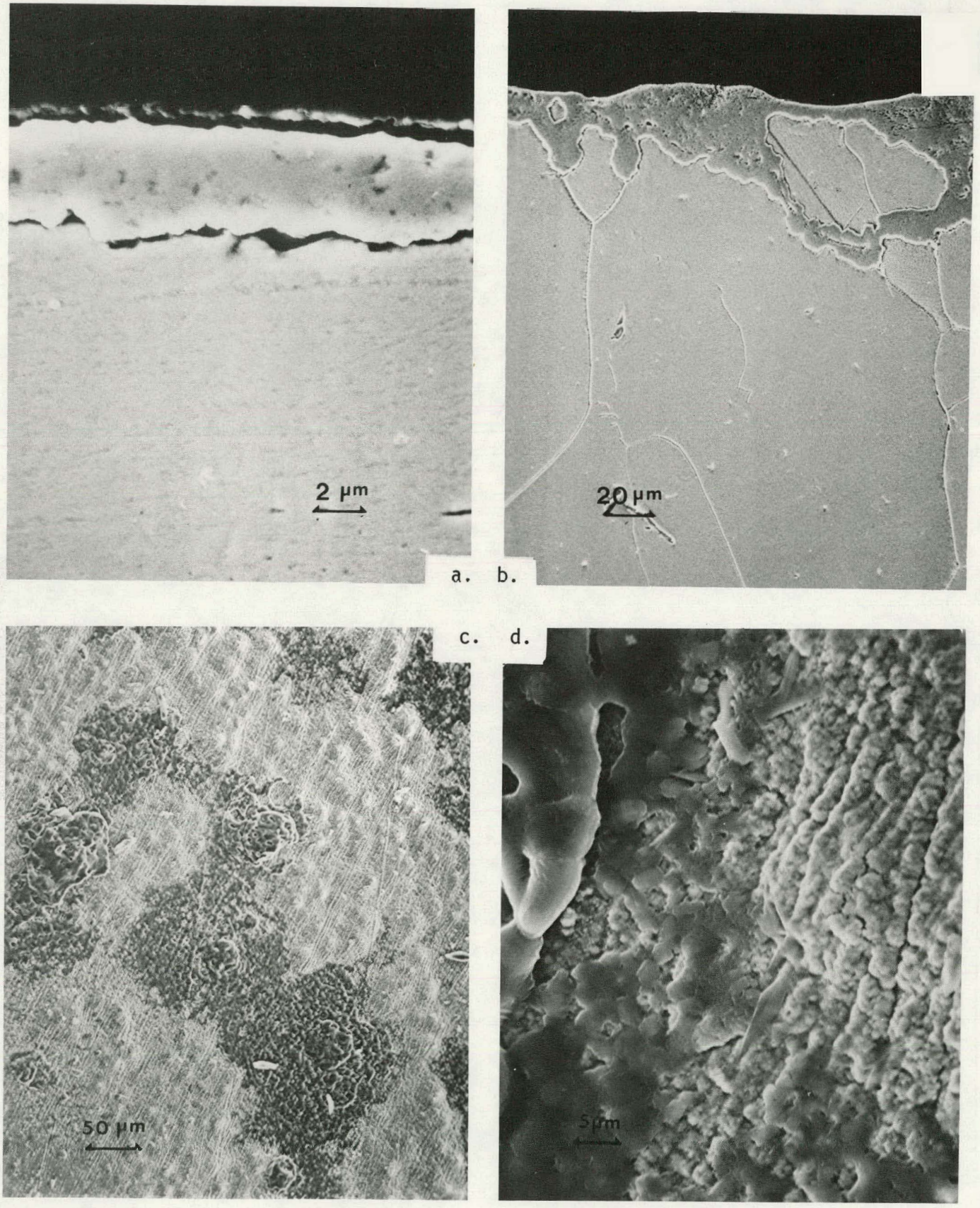

Figure 38 Oxidation of Ni at 750°C (a) Scale formed in simple oxidation after 48 hrs. (b) Scale formed after oxidation with Na_2SO_4 coating. (c) and (d) Salt on surface of specimen after 30 min. in O_2.

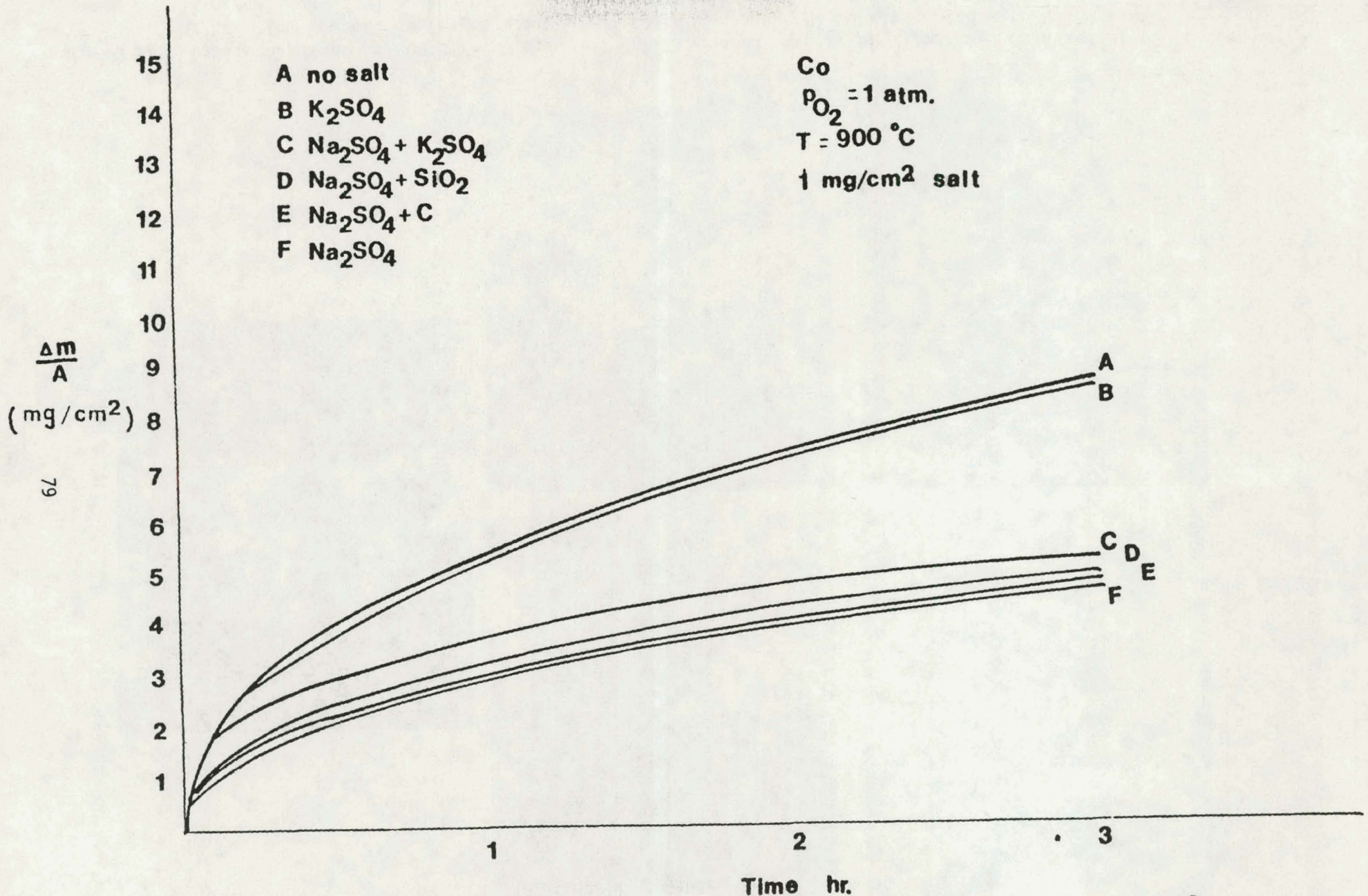

Figure 39 Weight change vs Time for pure Cobalt coated with 1 mg/cm^2 salt in 1 atm O_2 at 900°C.

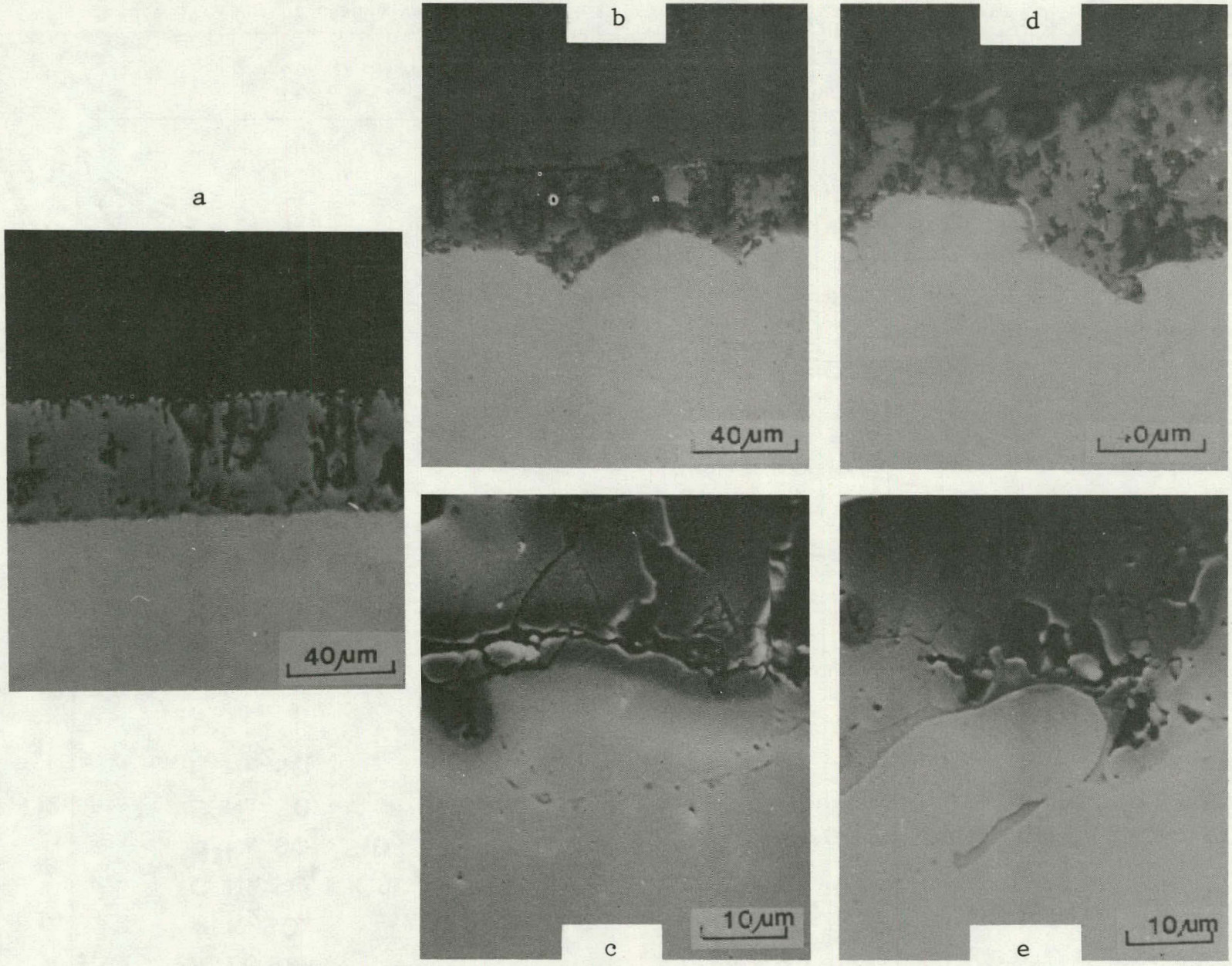

Figure 40 (a) Cobalt oxidized at 900°C for 3 hrs. (b) Cobalt coated with Na_2SO_4 (1mg/cm^2) oxidized at 900°C for 3 hrs. (c) Detail of (b) at the scale/metal interface. (d) Cobalt coated with Na_2SO_4+K_2SO_4 (1mg/cm^2) oxidized at 900°C for 3 hrs. (e) Detail of (d) at the scale/metal interface.

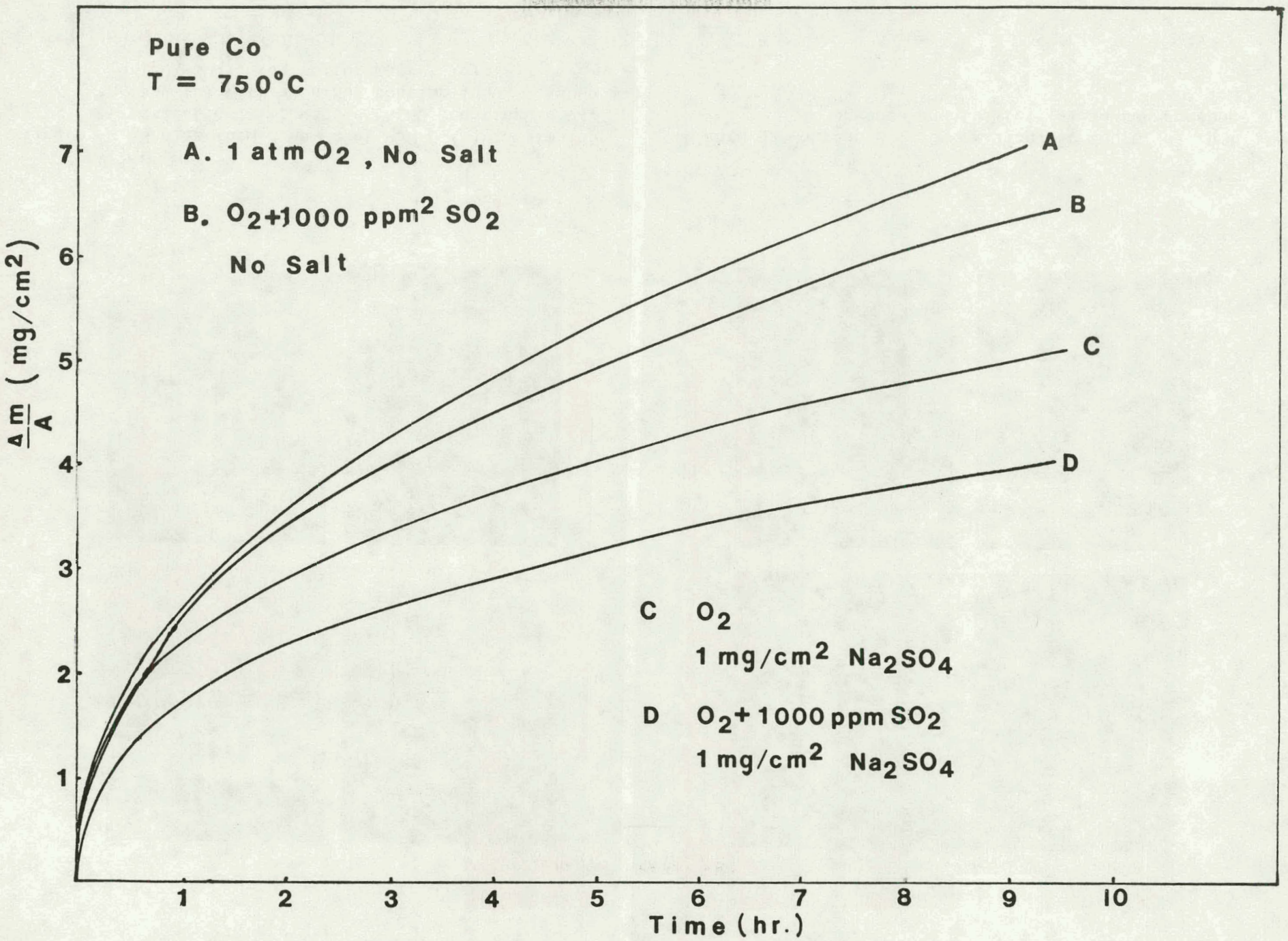

Figure 41 Rate of oxidation and hot corrosion of Co at 750°C.

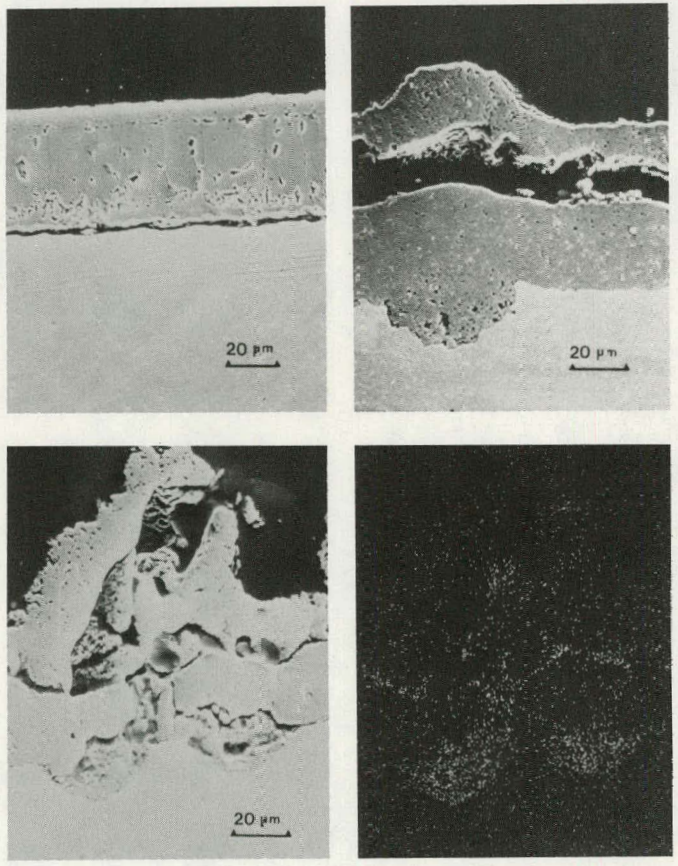

Figure 42 Scales formed on Co at 750°C (a) in simple oxidation, (b) with a Na_2SC_4 coating in O_2, and (c) with a Na_2SO_4 coating in O_2 + 1000ppm (SO_2+SO_3), (d) sulfur map of (c).

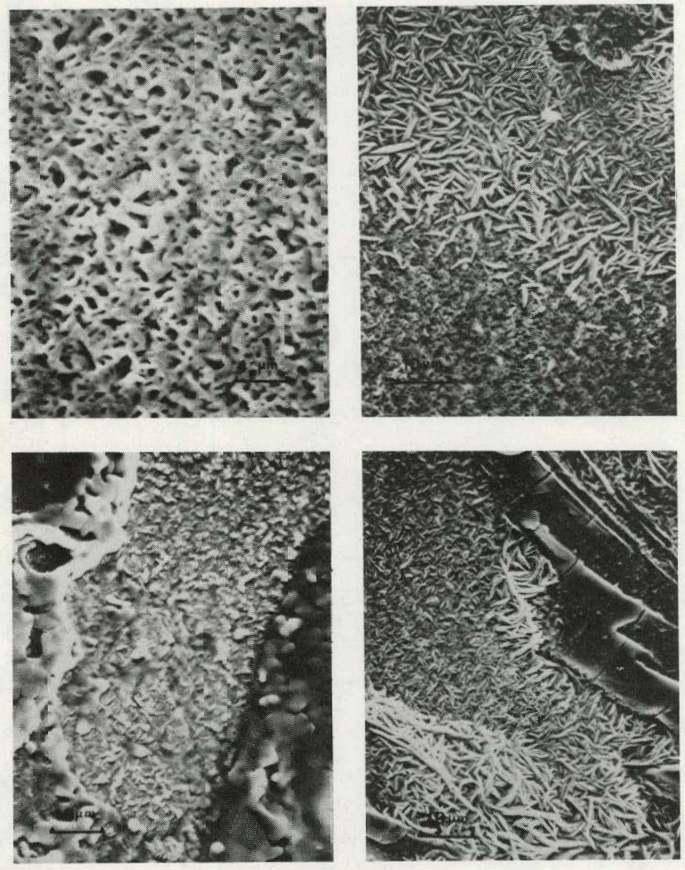

Figure 43 Surfaces of Co oxidized at 750°C (a) in in absence and (b) (c) (d) in the presence of Na_2SO_4.

a.

b.

c.

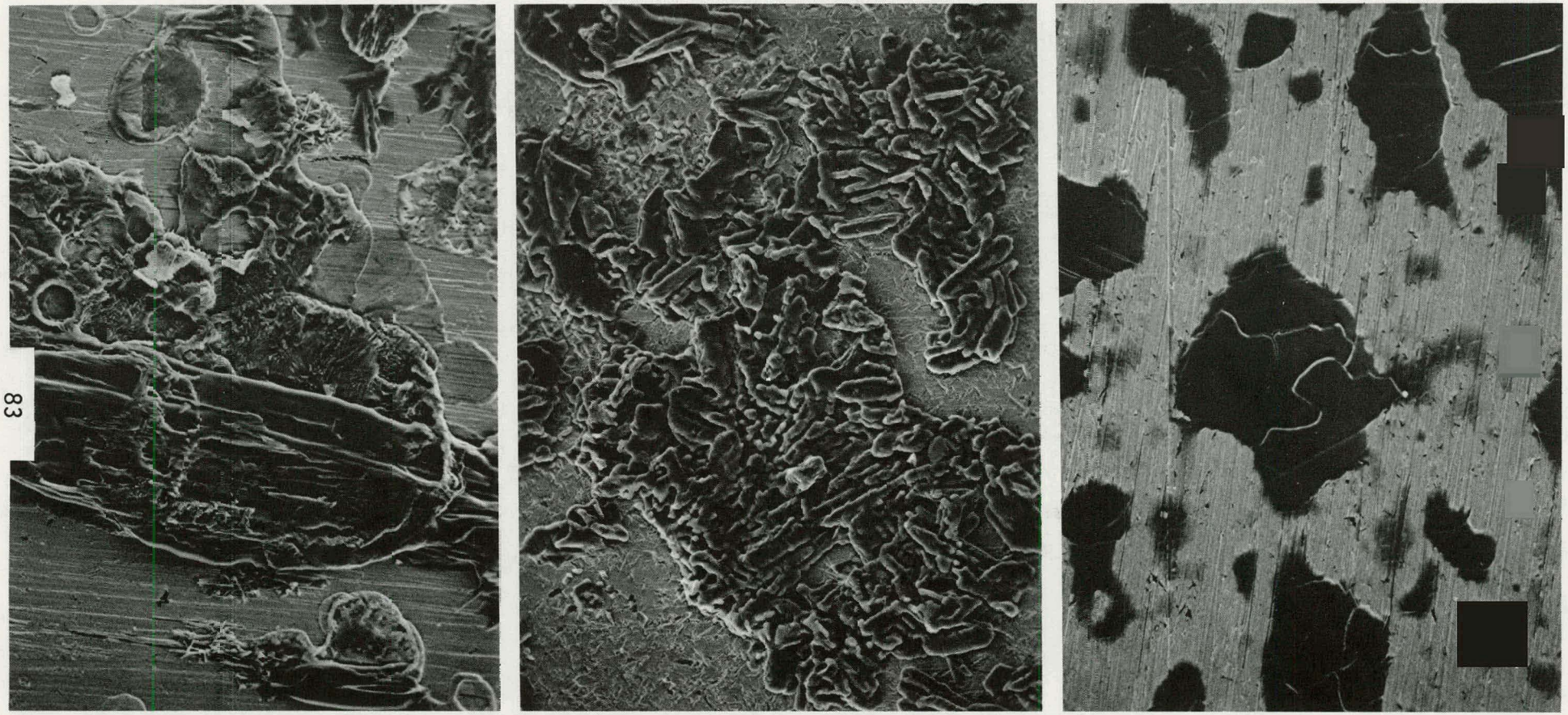

400 x

400 x

100 x

Figure 44 Na_2SO_4 coatings ($1mg/cm^2$) on Pt. (a) as sprayed, (b) after heating to 750^oC, and (c) after heating to 900^oC.

a. b. c.

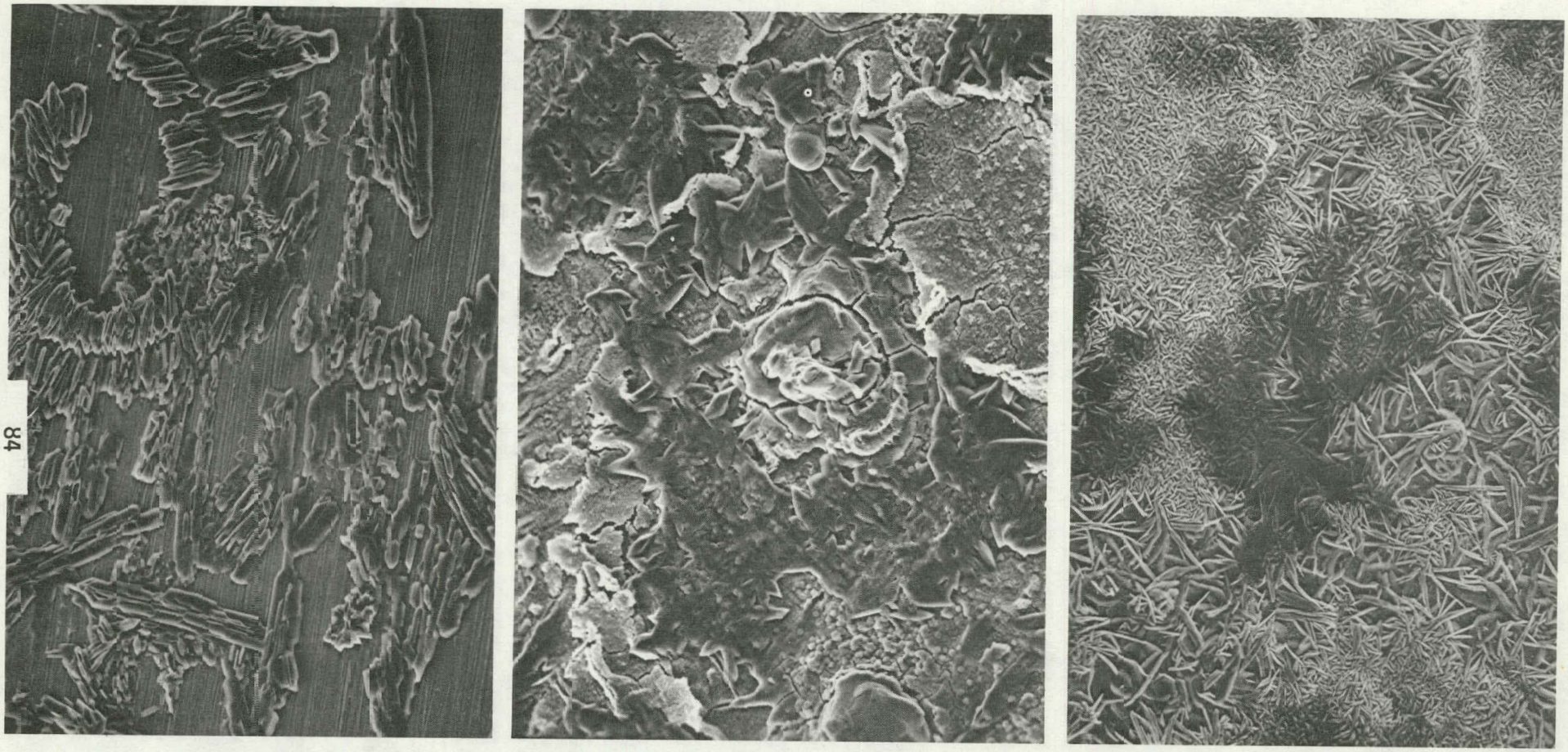

Figure 45 Na_2SO_4 coatings ($1mg/cm^2$) in Co (a) as sprayed, (b) after heating to 750^oC, and (c) after heating to 900^oC (all magn. 400 x).

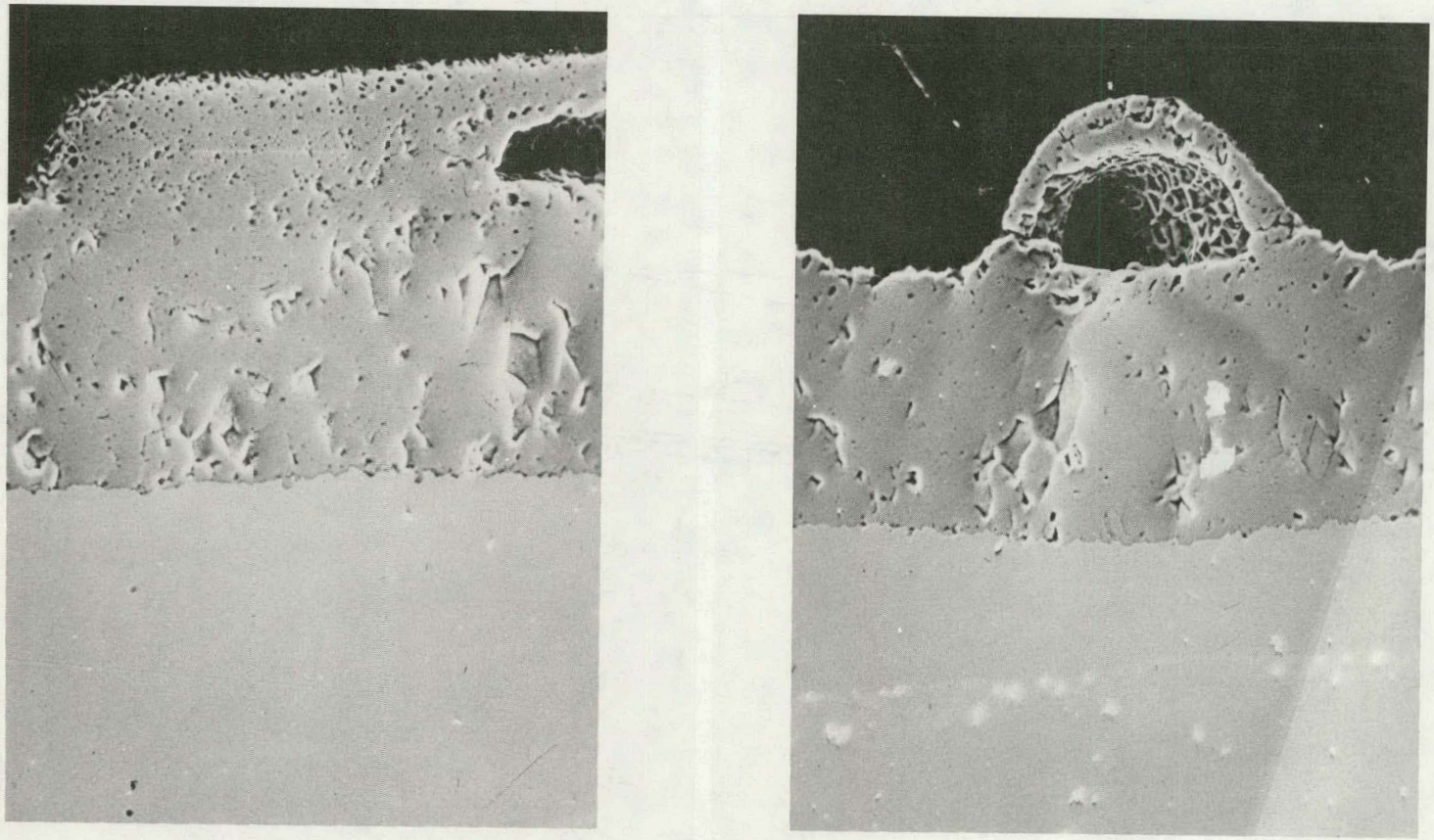

Figure 46 Scales formed on pure Co at 750°C in O_2 + 1000 ppm (SO_2 + SO_3) in the absence of Na_2SO_4 x 800.

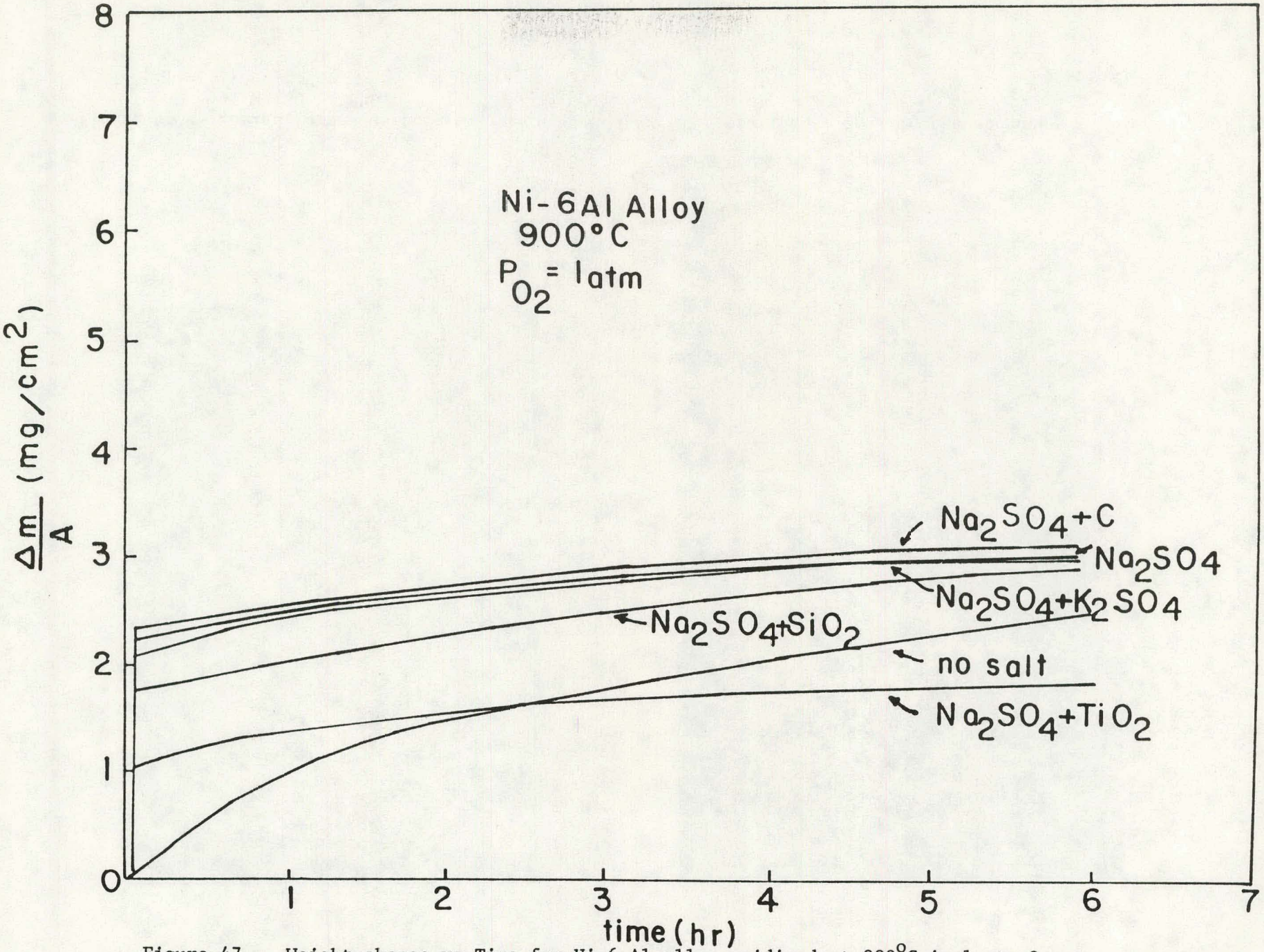

Figure 47 Weight change vs Time for Ni-6 Al alloy oxidized at 900°C in 1 atm O_2.

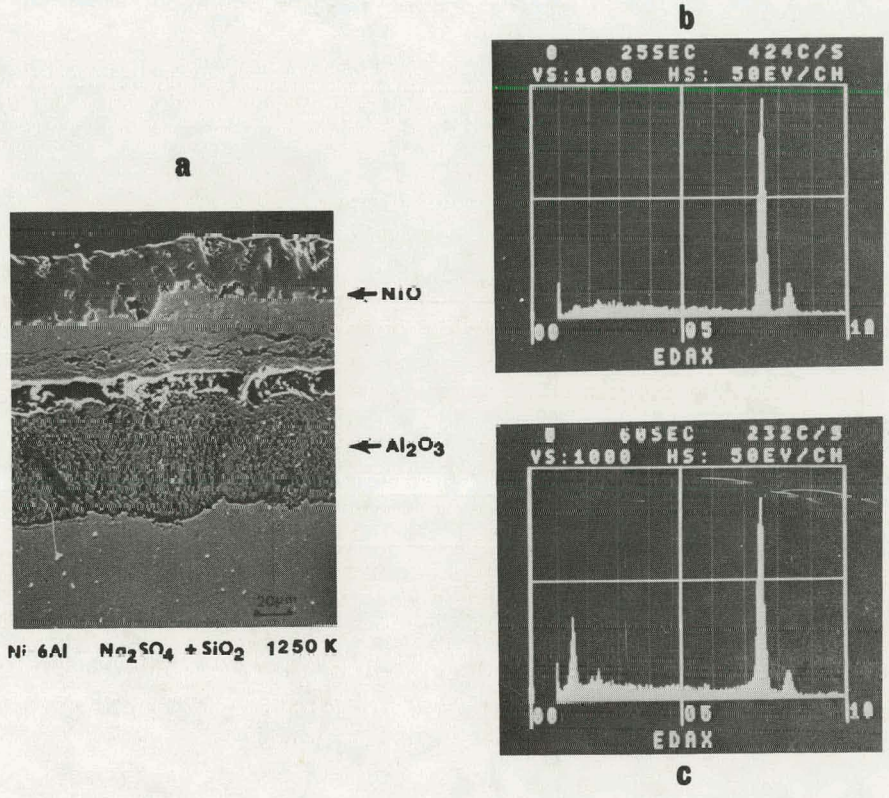

Figure 48 Ni-6Al alloy oxidized at 977°C for 48 hrs. with Na_2SO_4 ($1mg/cm^2$) coating.

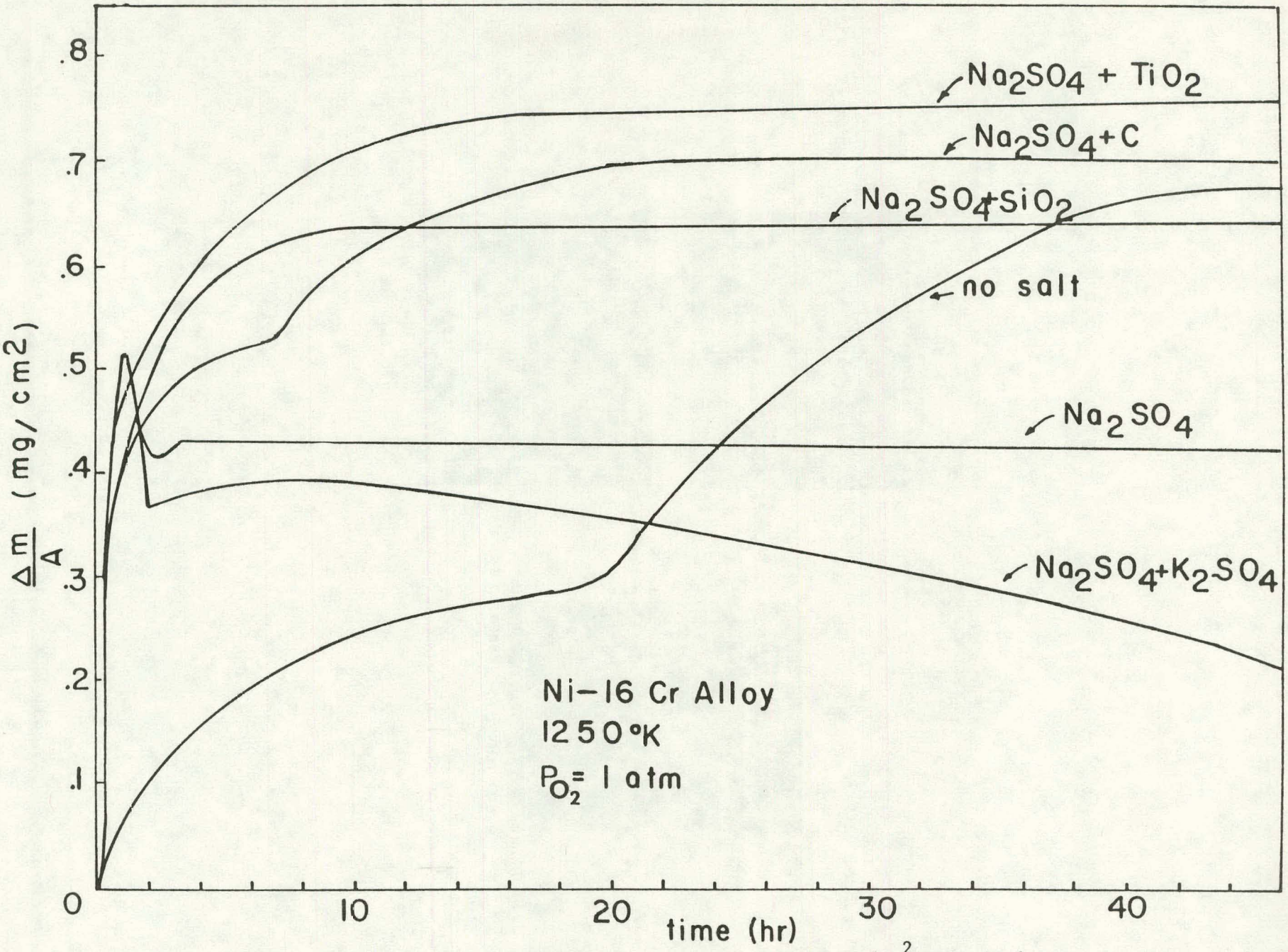

Figure 49 Weight change vs Time for Ni-16 wt% Cr coated with 1 mg/cm^2 salt in 1 atm O_2 at 977°C.

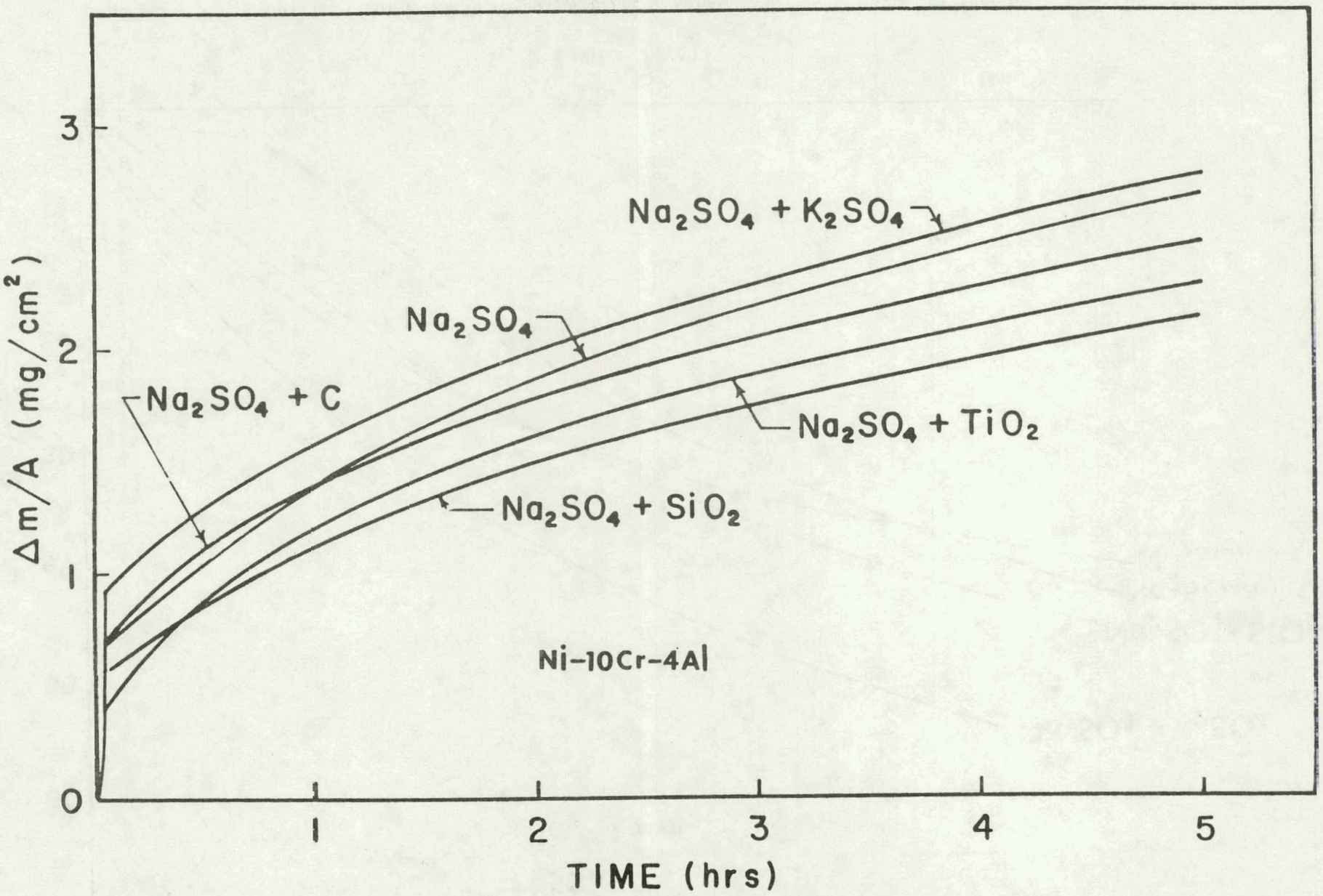

Figure 50 Weight change vs Time for Ni-10 Cr-4 Al alloy coated with 1 mg/cm^2 salt in 1 atm O_2 at 900°C.

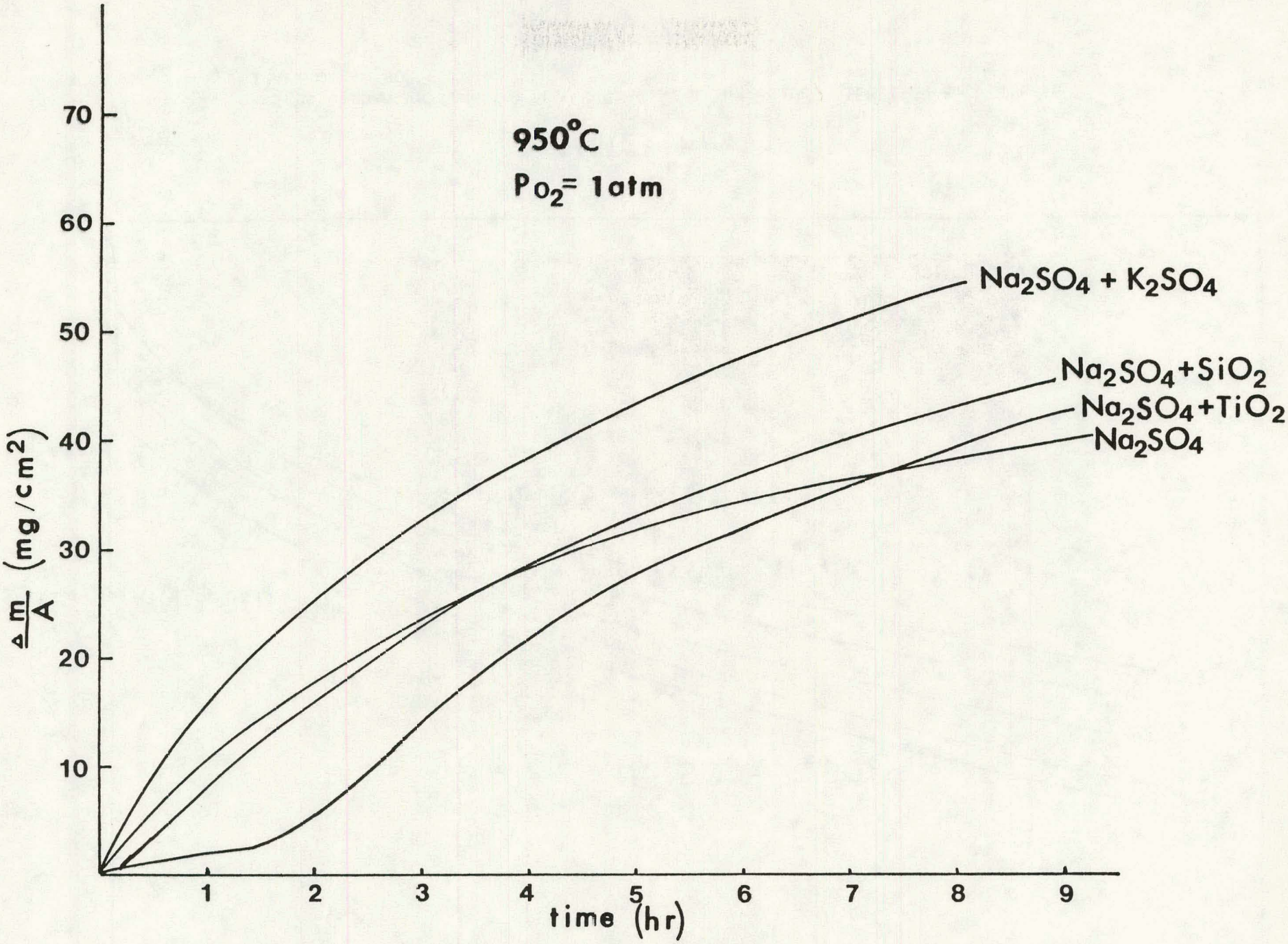

Figure 51 Weight change vs Time for B-1900 oxidized at 950°C with various salt coatings.

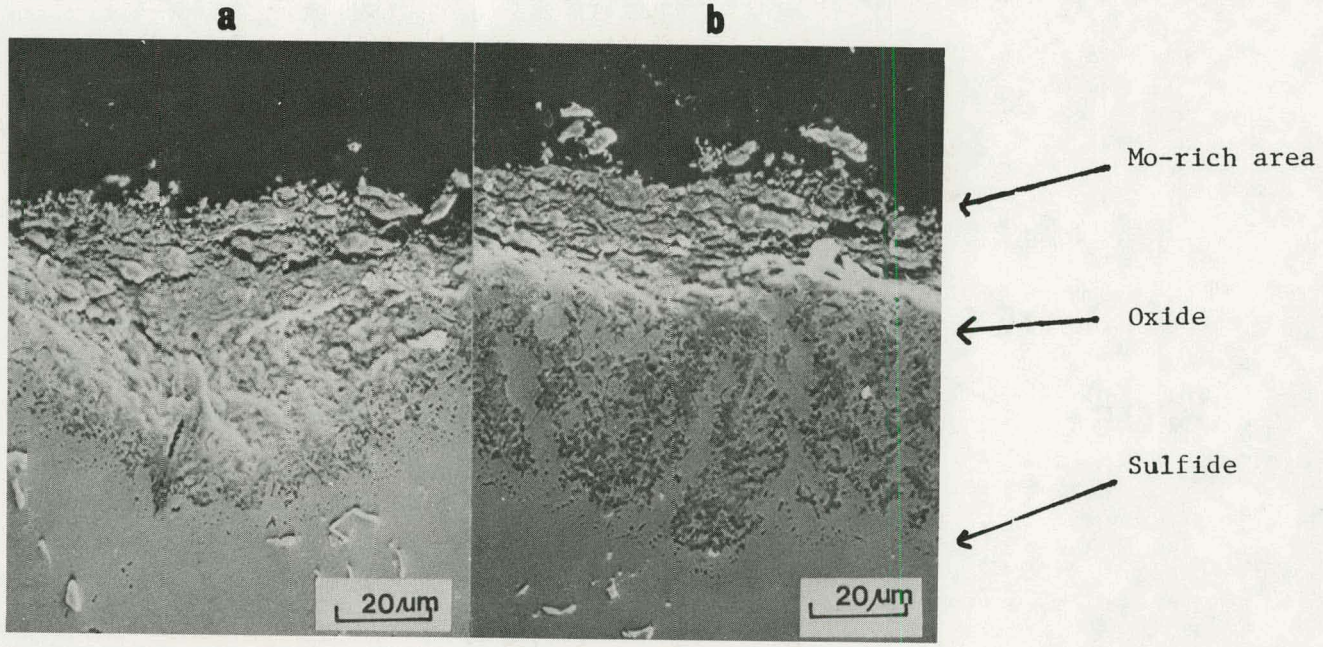

Figure 52 (a) (b) The scale of B-1900 coated with Na_2SO_4 ($1mg/cm^2$) oxidized at 950^oC for 10 hrs.

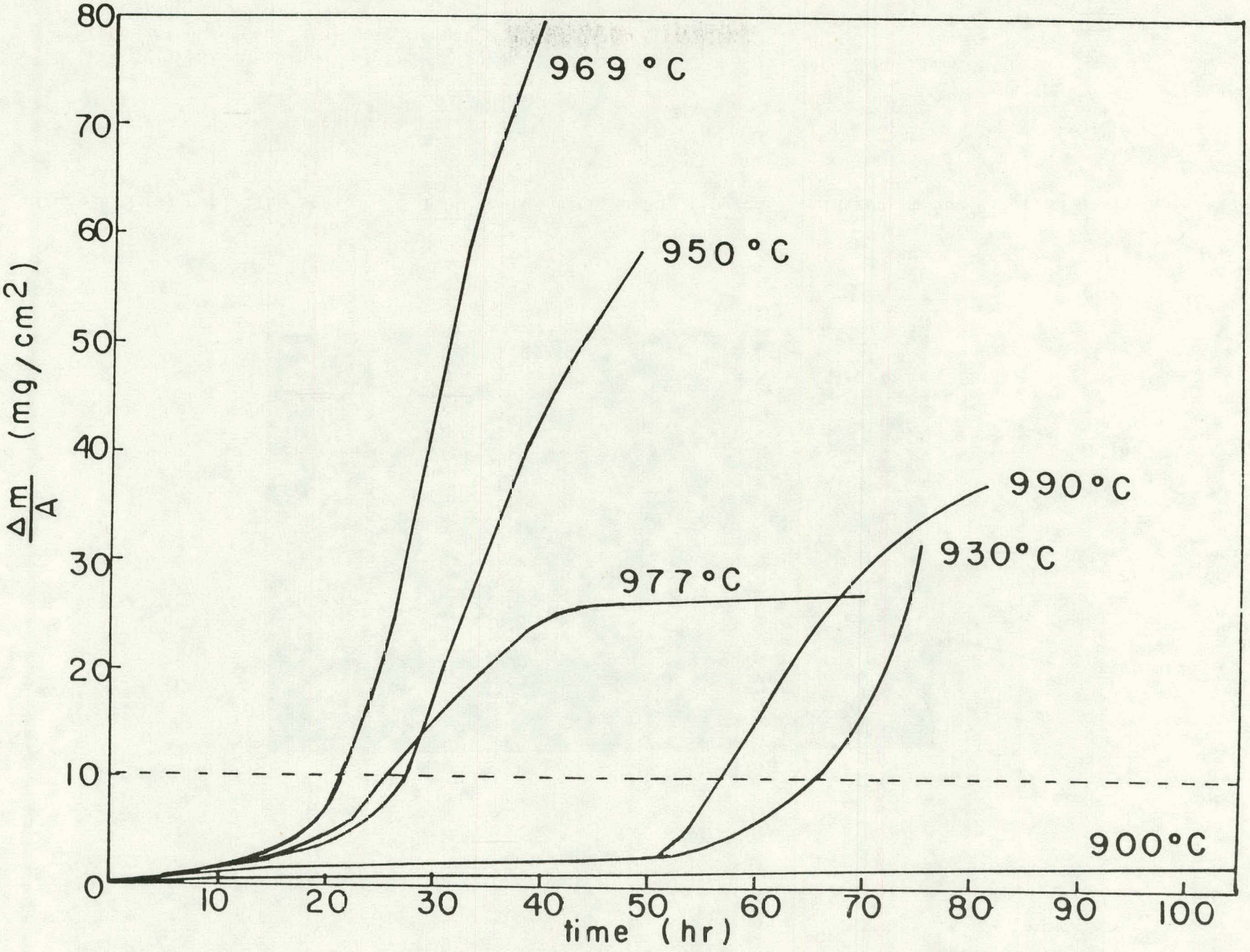

Figure 53 Weight Change vs Time for IN-738 coated with 1 mg/cm^2 Na_2SO_4 in 1 atm O_2.

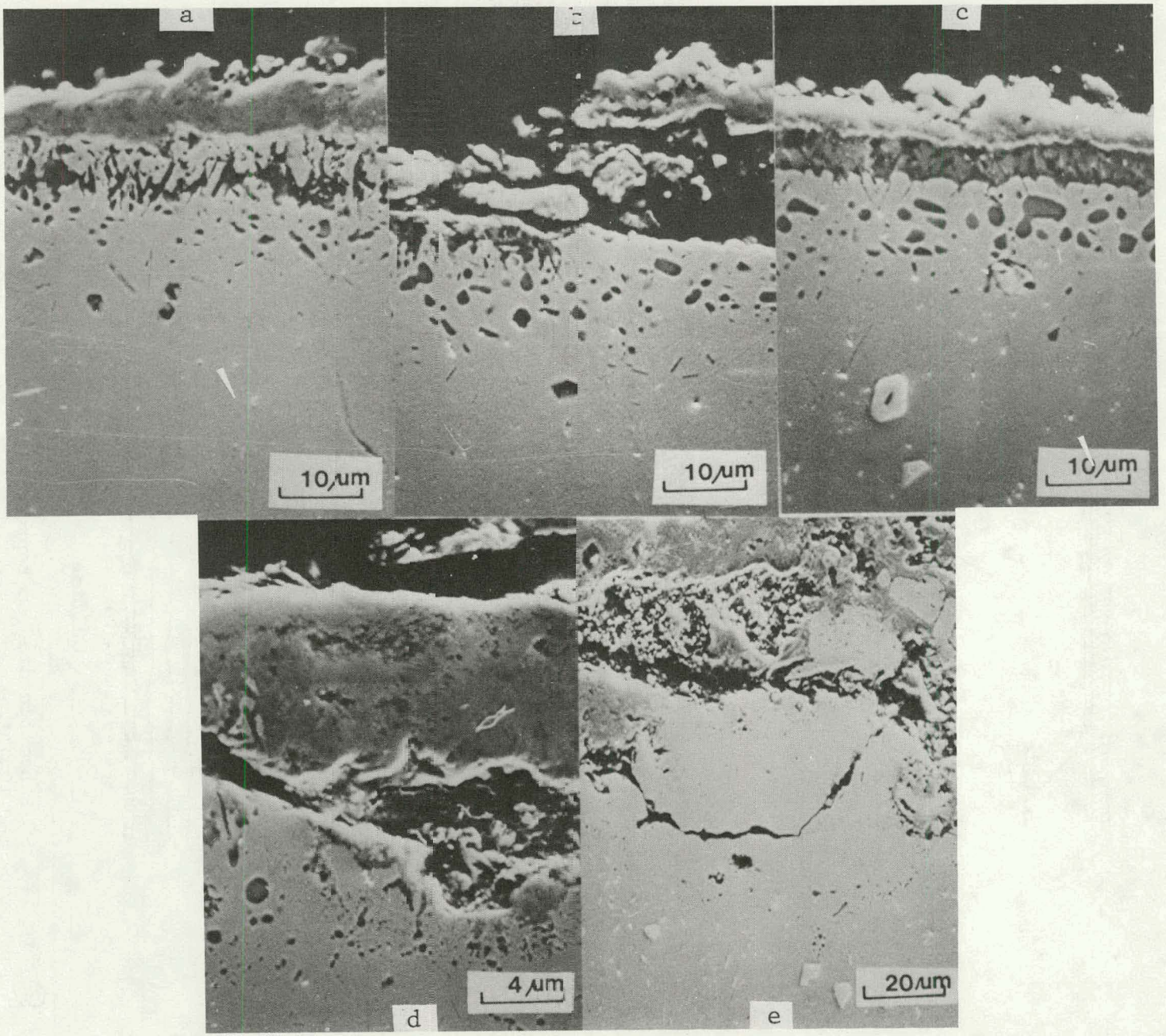

Figure 54 1N-738 oxidized 10 hrs. at 970°C with 1mg/cm^2 coating of Na_2SO_4. (a) Specimen center. (b) (c) (d) Transition region. (e) Scale near corner.

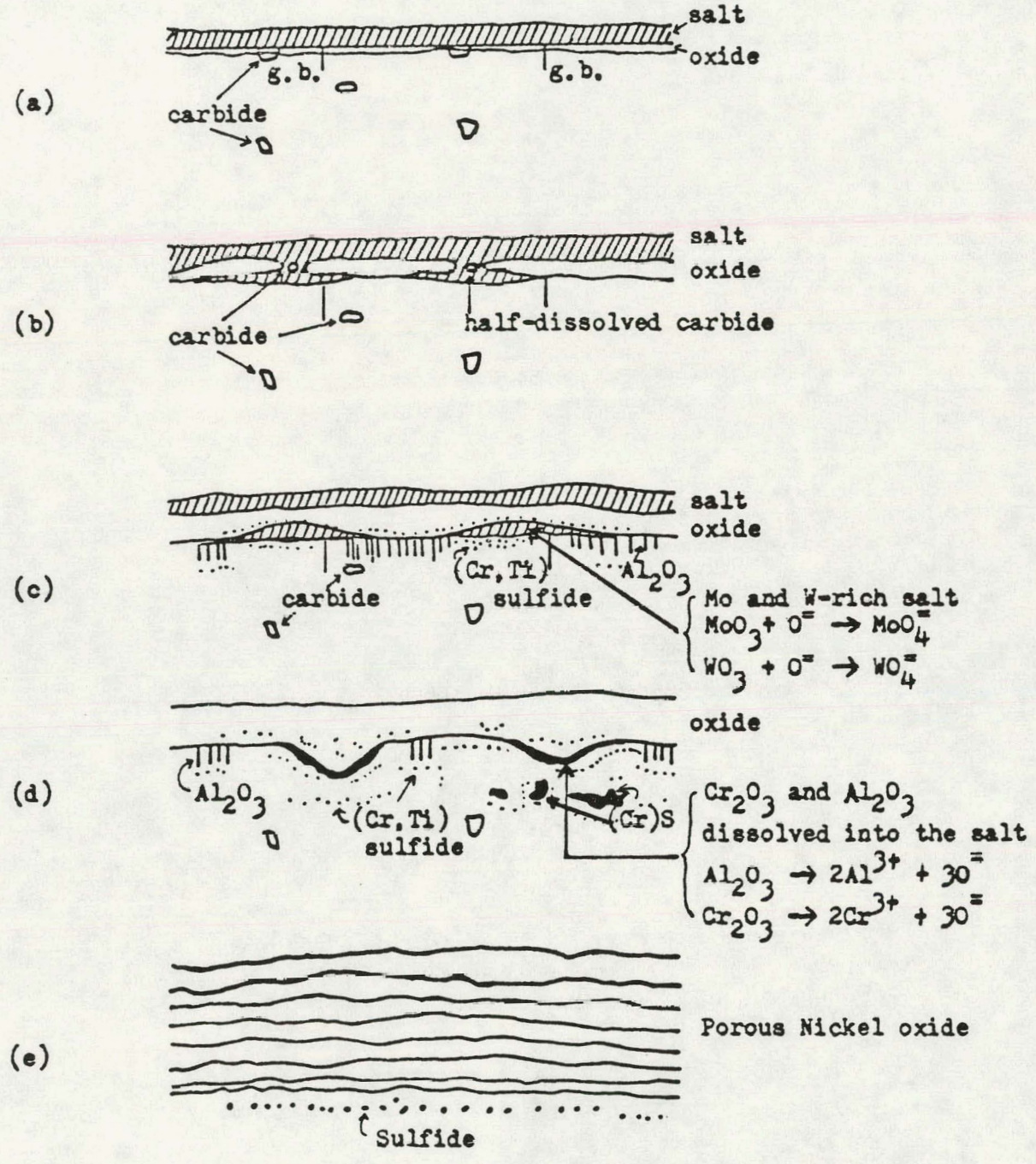

Figure 55 A schematic diagram representing the hot corrosion attack of IN-738-like alloys.

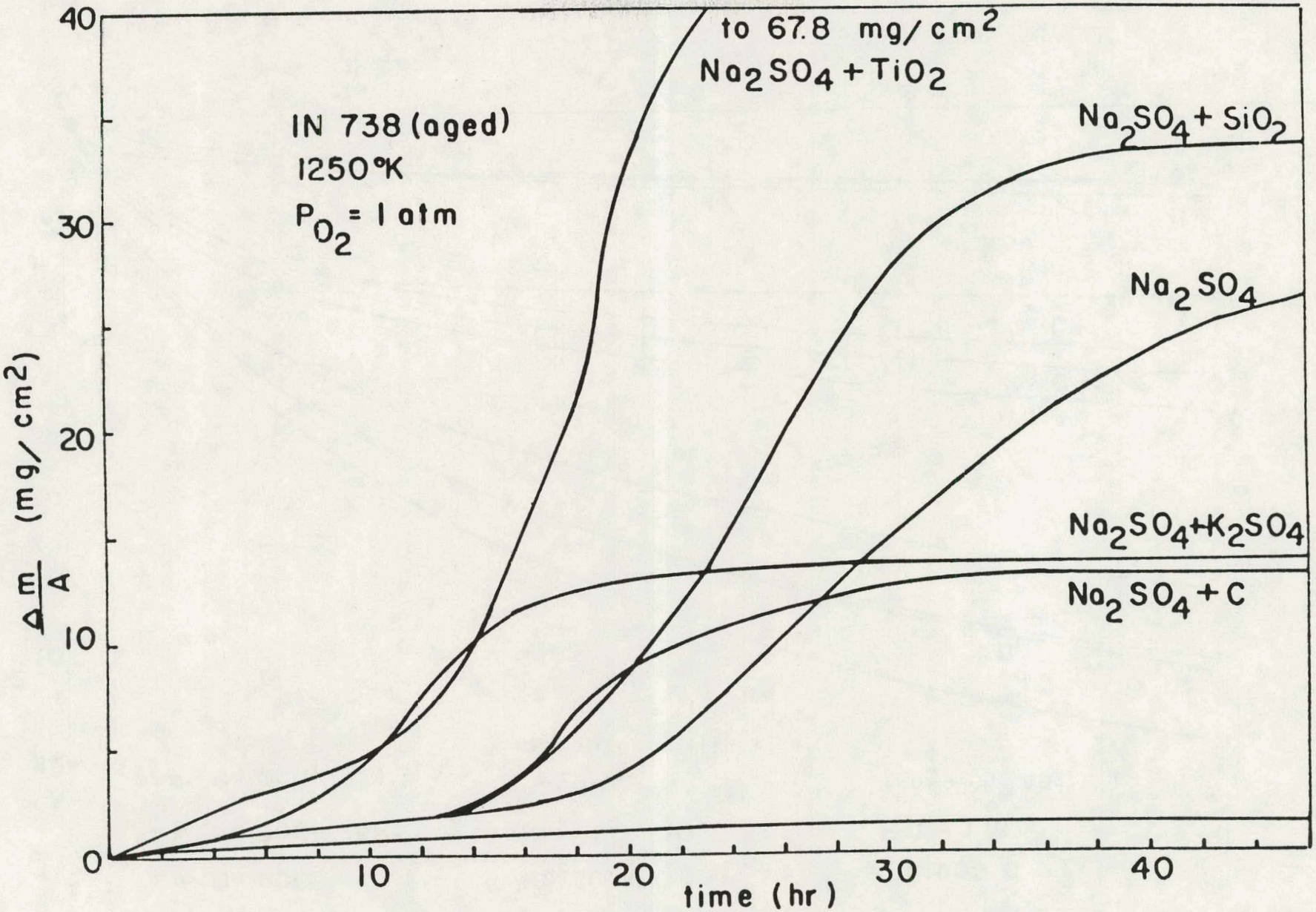

Figure 55 Weight Change vs Time for IN-738 coated with 1 mg/cm^2 salt in 1 atm O_2 at 977°C.

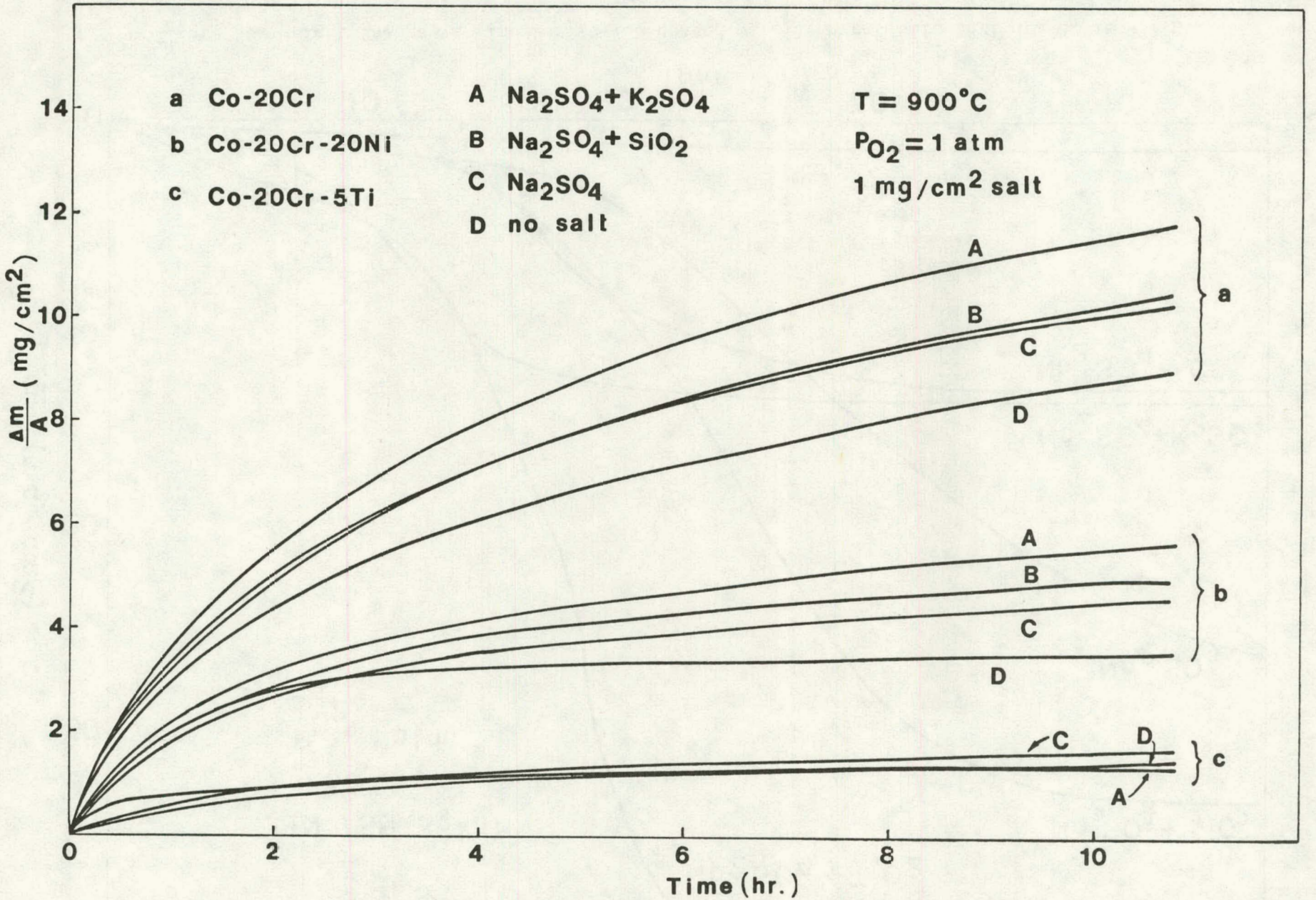

Figure 57 The effect of Ni and Ti on the hot corrosion of Co20wt%Cr

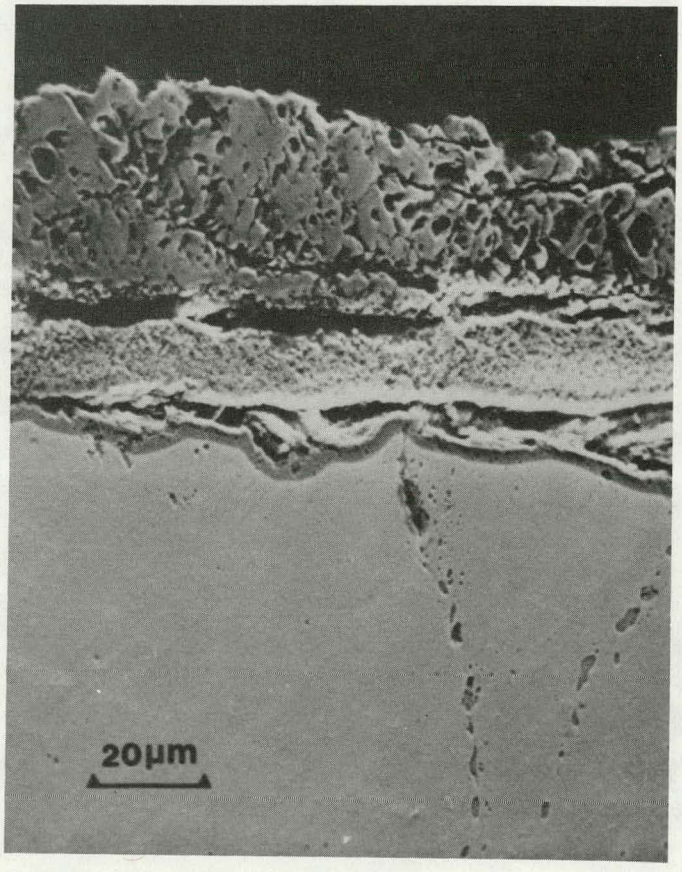

Figure 58 Scale formed on Co-20wt%Cr coated with 1 mg/cm^2 Na_2SO_4 + K_2SO_4 and oxidized 48 hours in atm at 900°C.

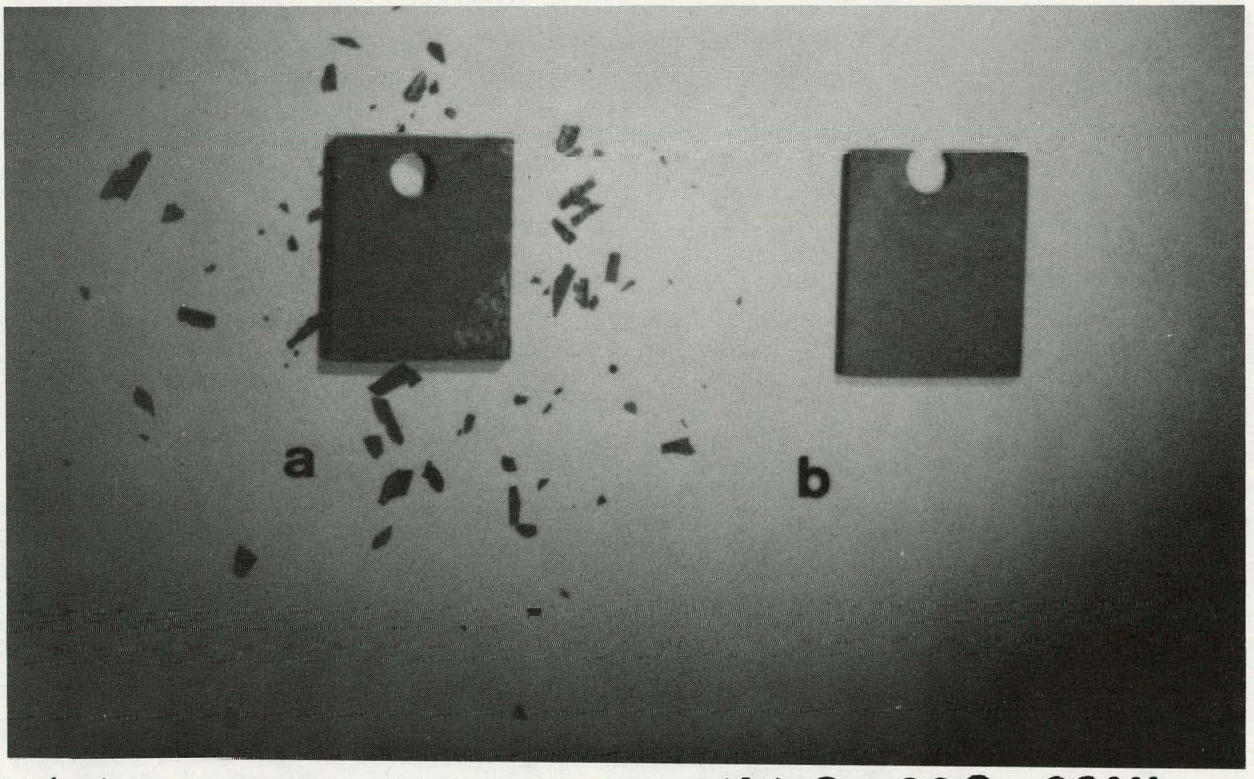

Figure 59 Effect of Ni on the Spalling of Scales from Co-20Cr.

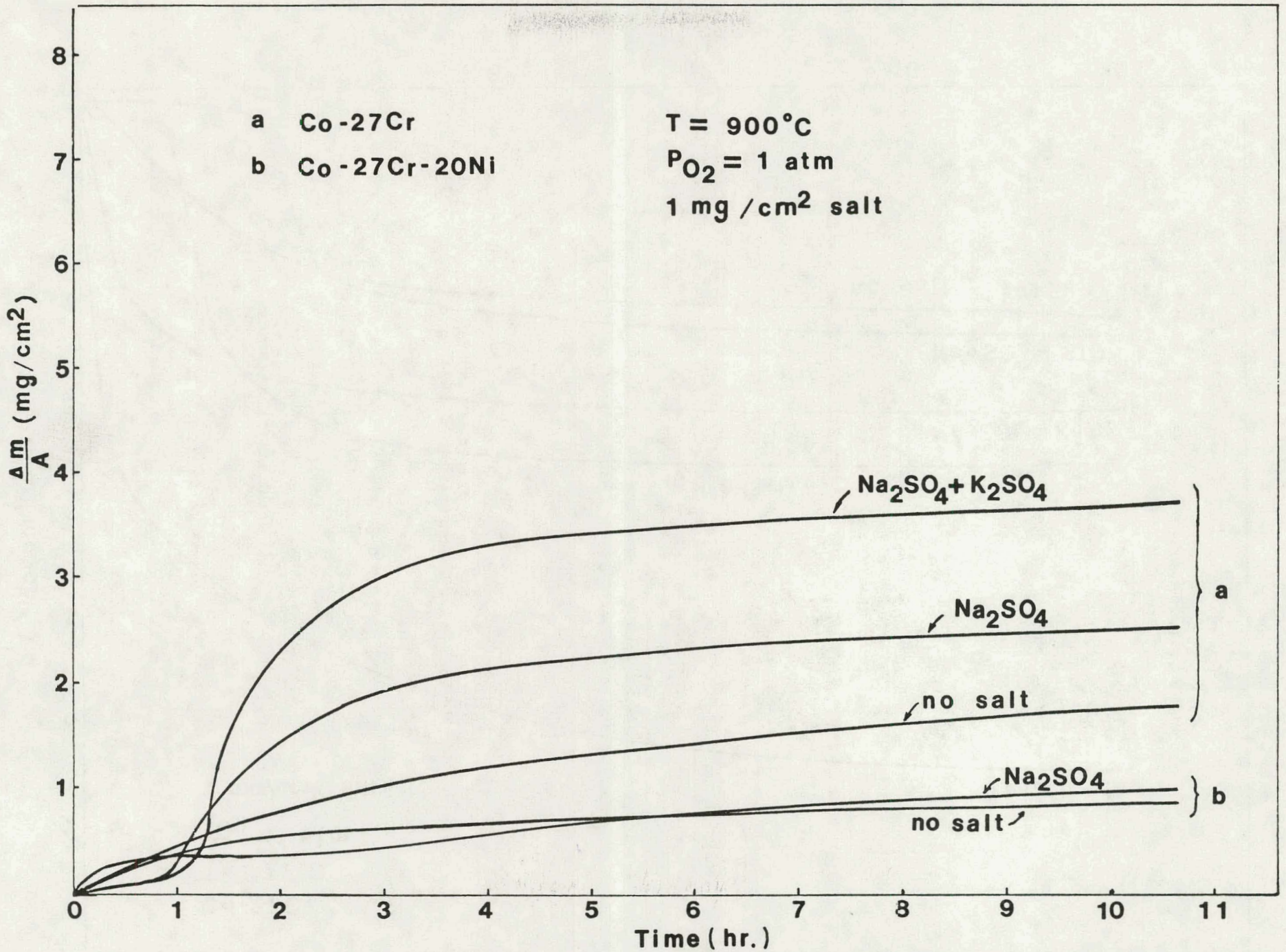

Figure 60 Oxidation rates of Co-27wt%Cr and Co-27wt%Cr-20wt%Ni with and without salt coatings at 900°C.

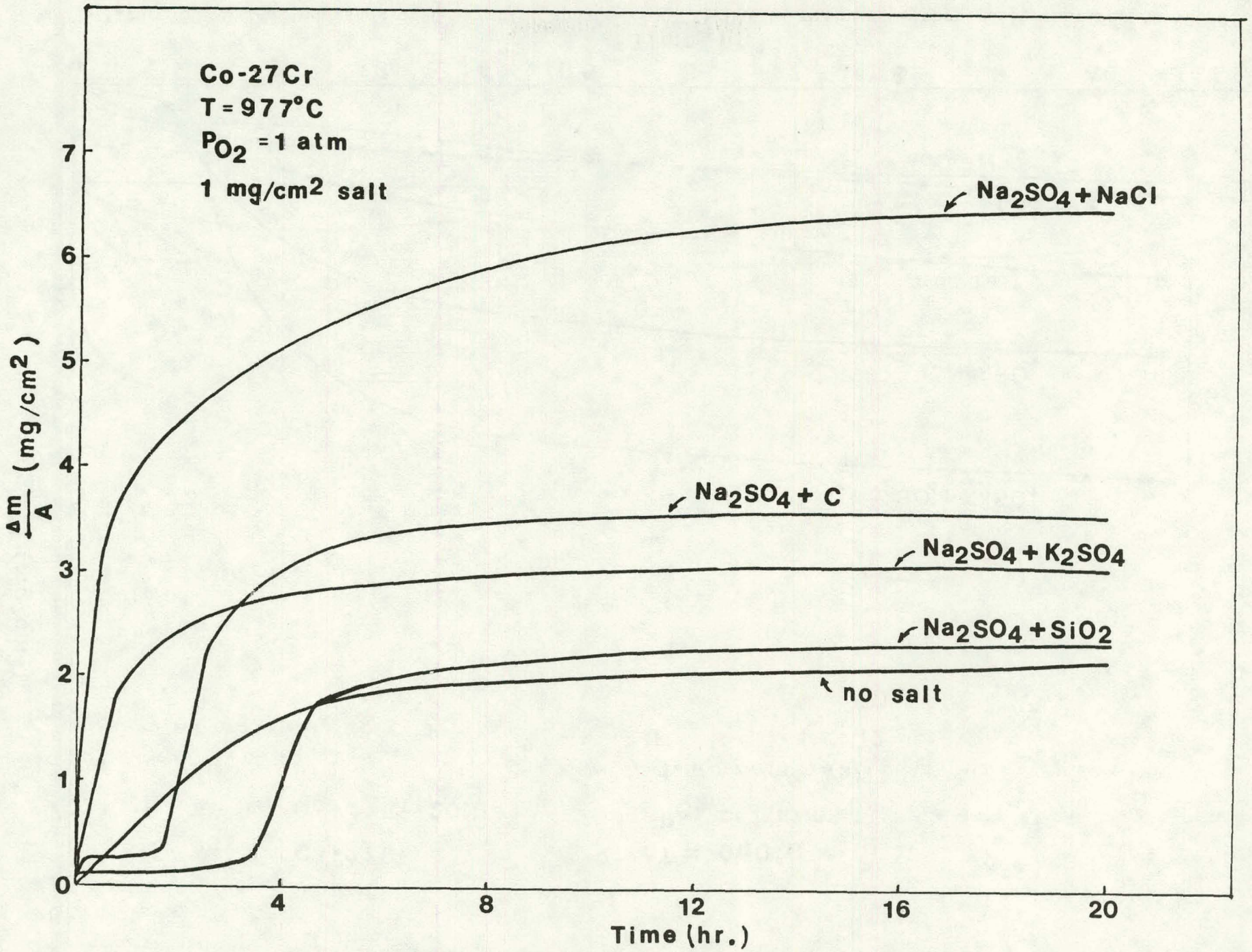

Figure 61 The effect of deposit composition on the oxidation rate of Cr-27wt%Cr at 977°C.

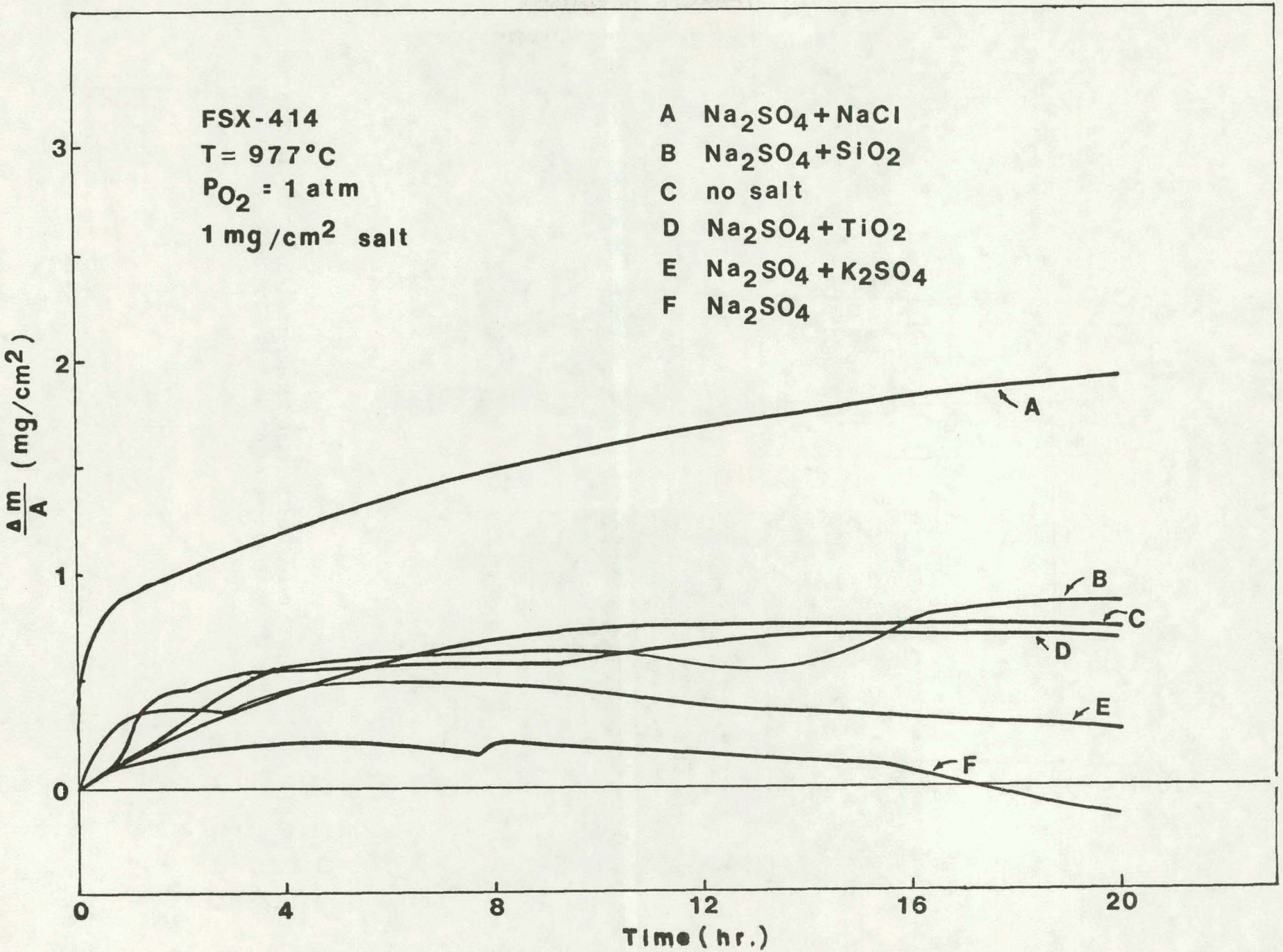

Figure 62 The effect of deposit composition on the oxidation rate of FSX-414 at 977°C.

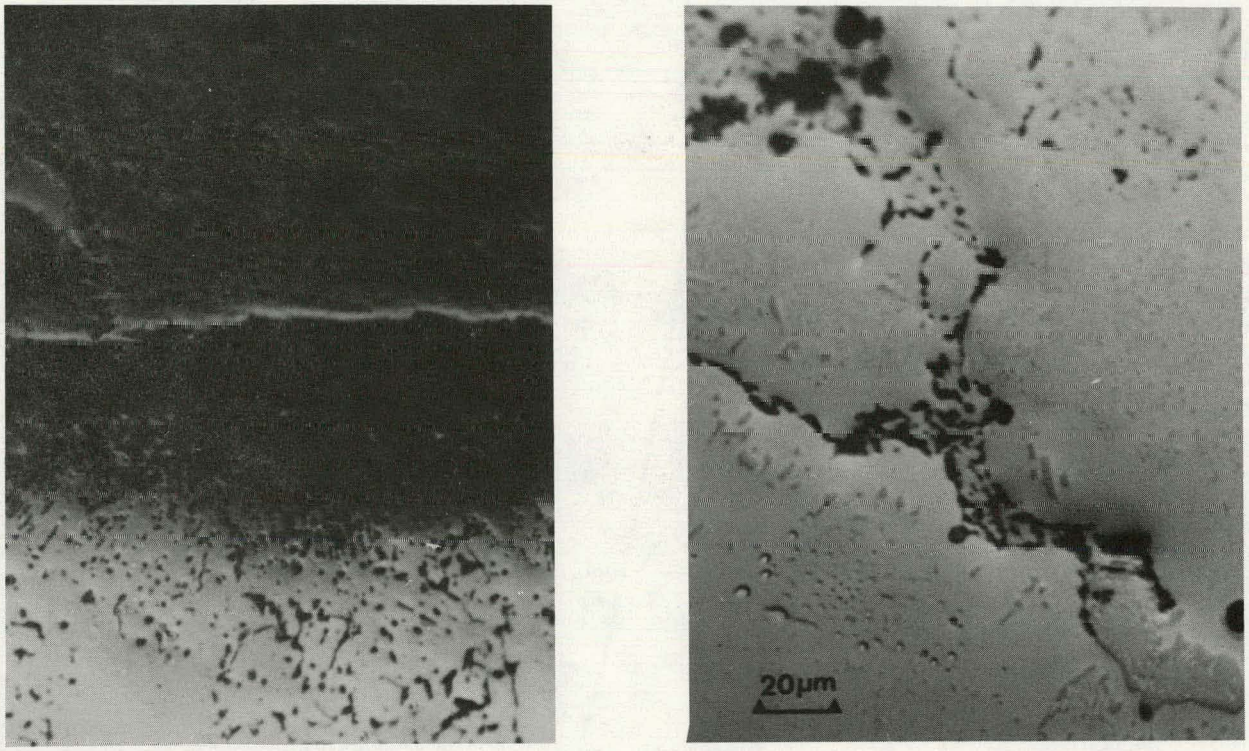

Figure 63 Internal Oxide and Sulfide Penetration into FSX-414 Oxidized at 977°C with a coating of Na_2SO_4 + 20% NaCl.

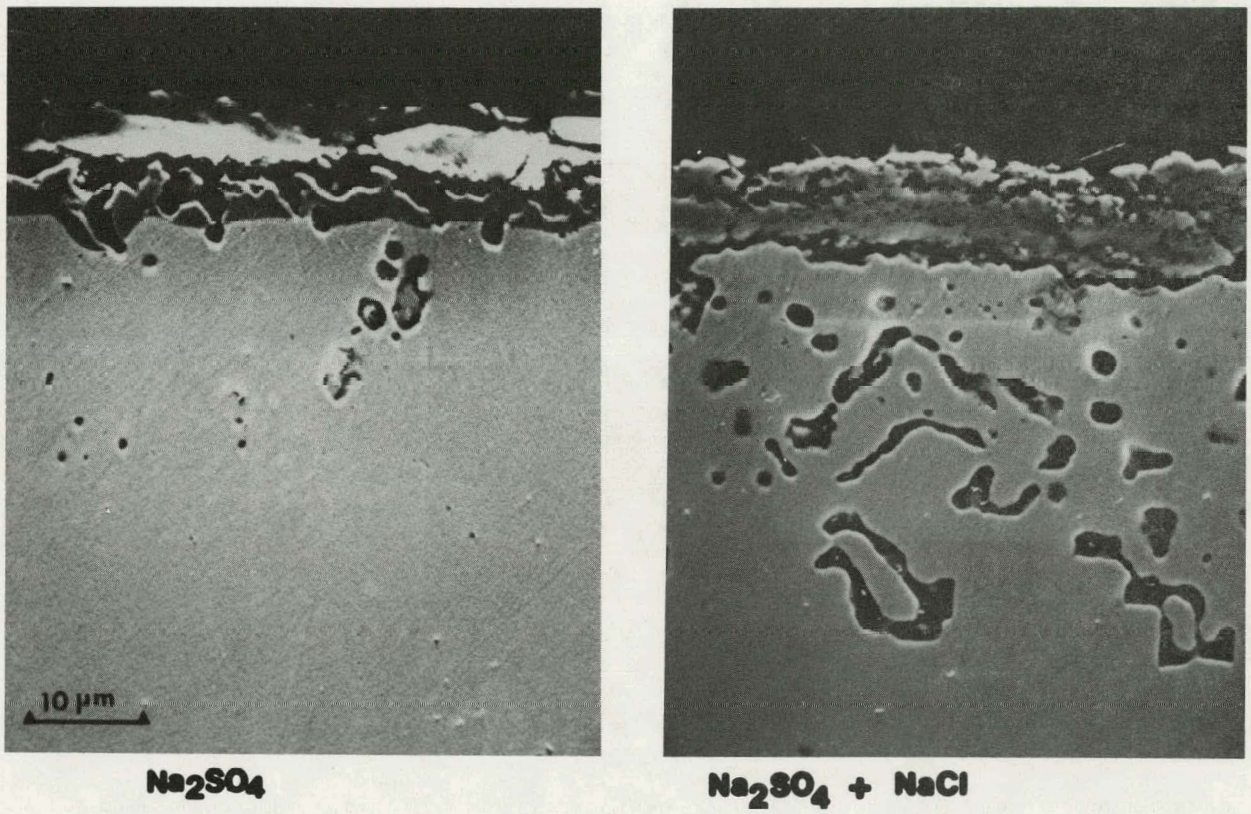

Figure 64 Oxidation Morphology for FSX-414 Reacted at 977°C in 1 atm O_2 with Coatings of Na_2SO_4 (a) and Na_2SO_4 + 20% NaCl (b).

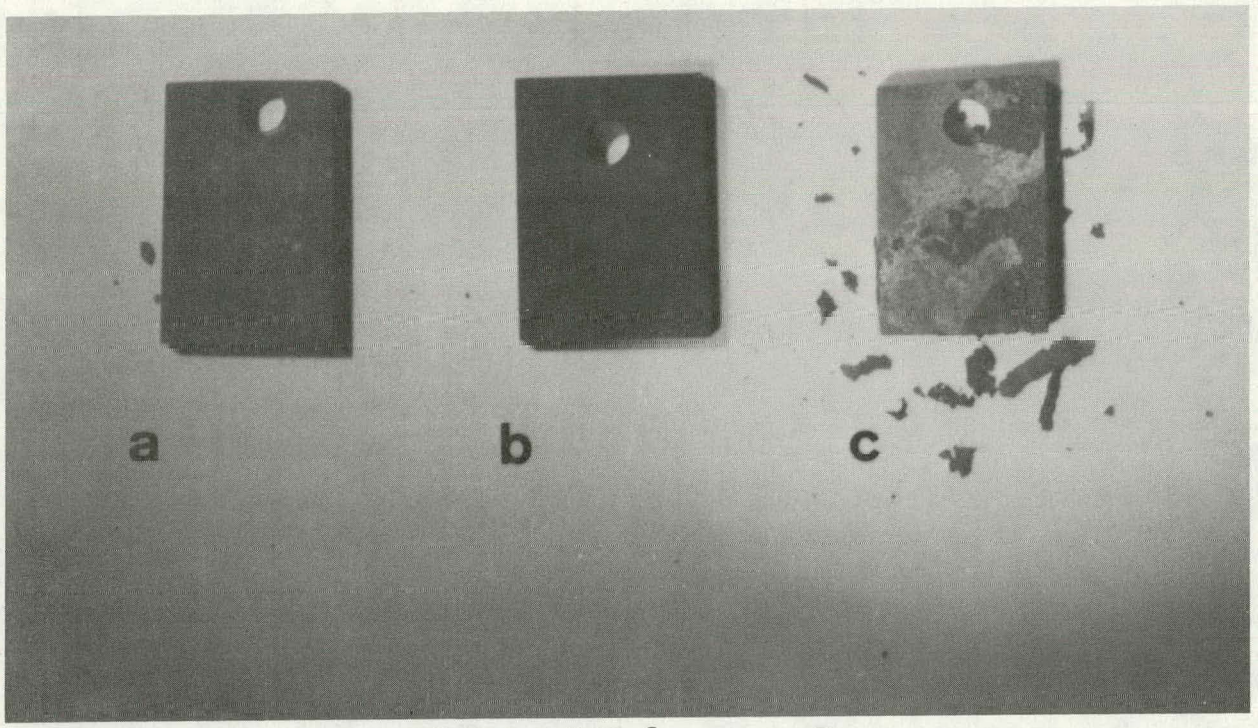

Figure 65 Effect of Na_2SO_4 and NaCl on scale spalling from FSX-414.

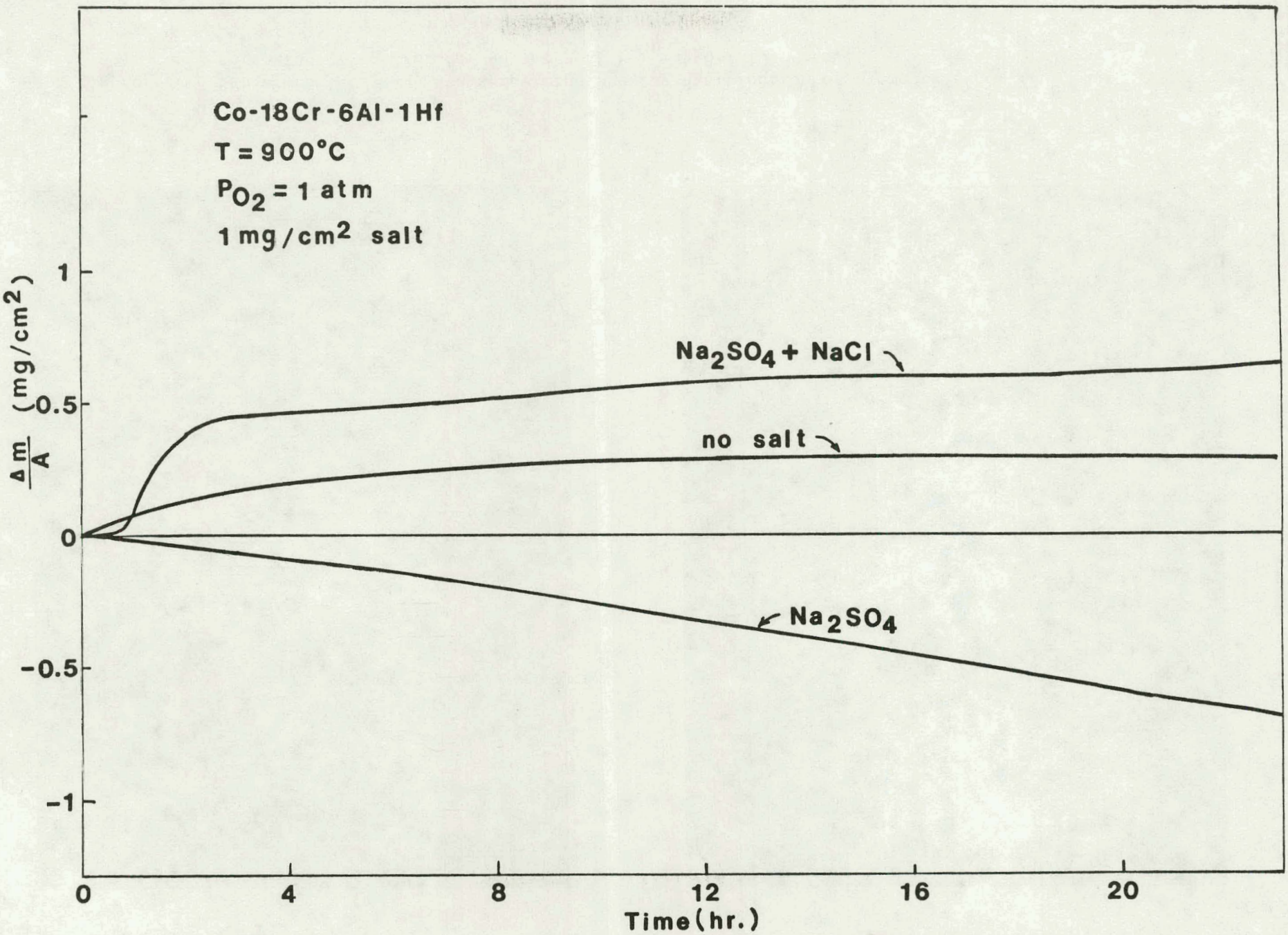

Figure 66 Effect of Na_2SO_4 and NaCl on the Oxidation Rate of Co-18wt%Cr-6wt%Al-1wt%Hf.

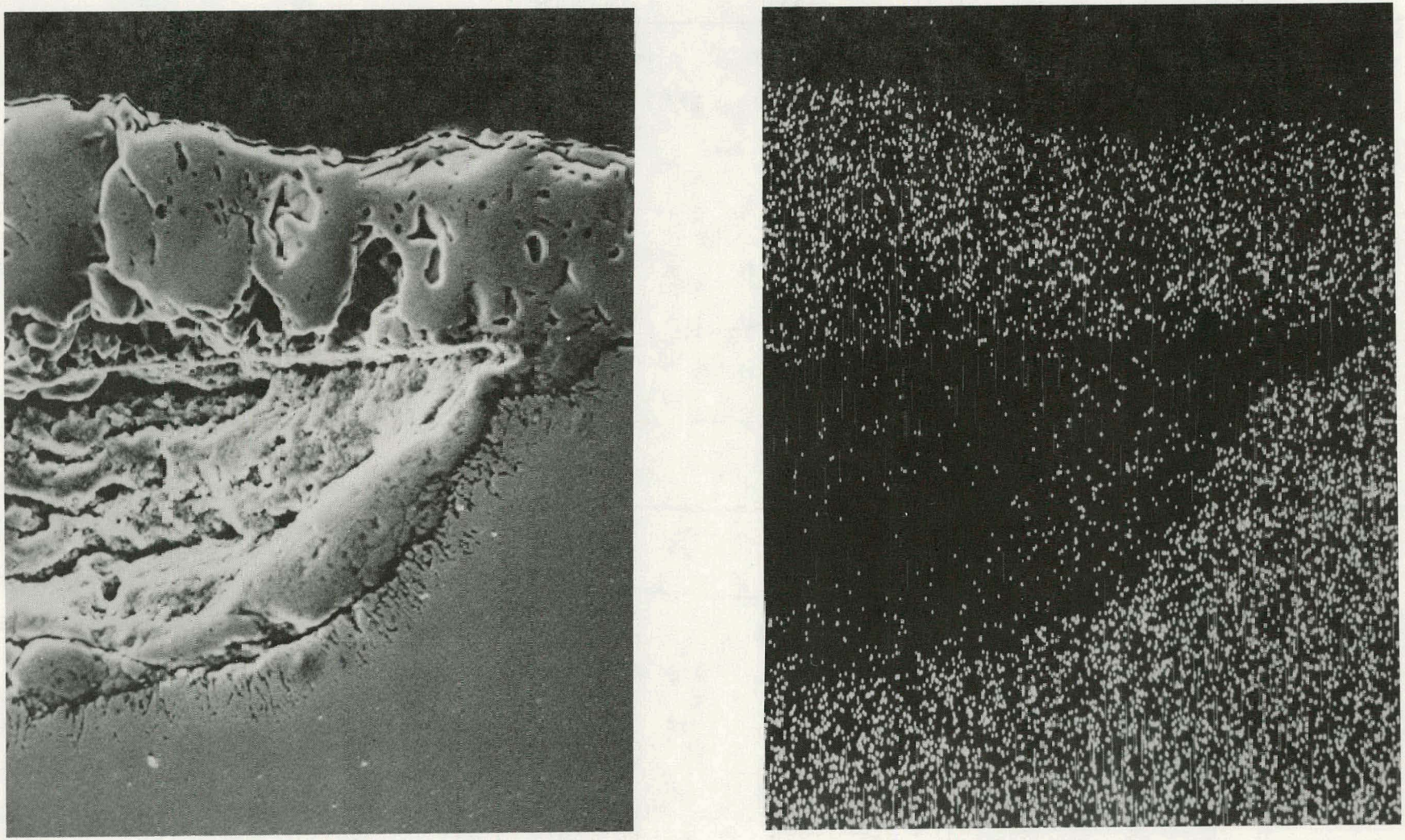

a. 800 x b. Cobalt

Figure 67 SEM photomicrograph and x-ray maps showing distribution of elements after 750°C hot corrosion of Co-27Cr for 48 hours at $P_{SO_3} = 5.8 \times 10^{-3}$ atm.

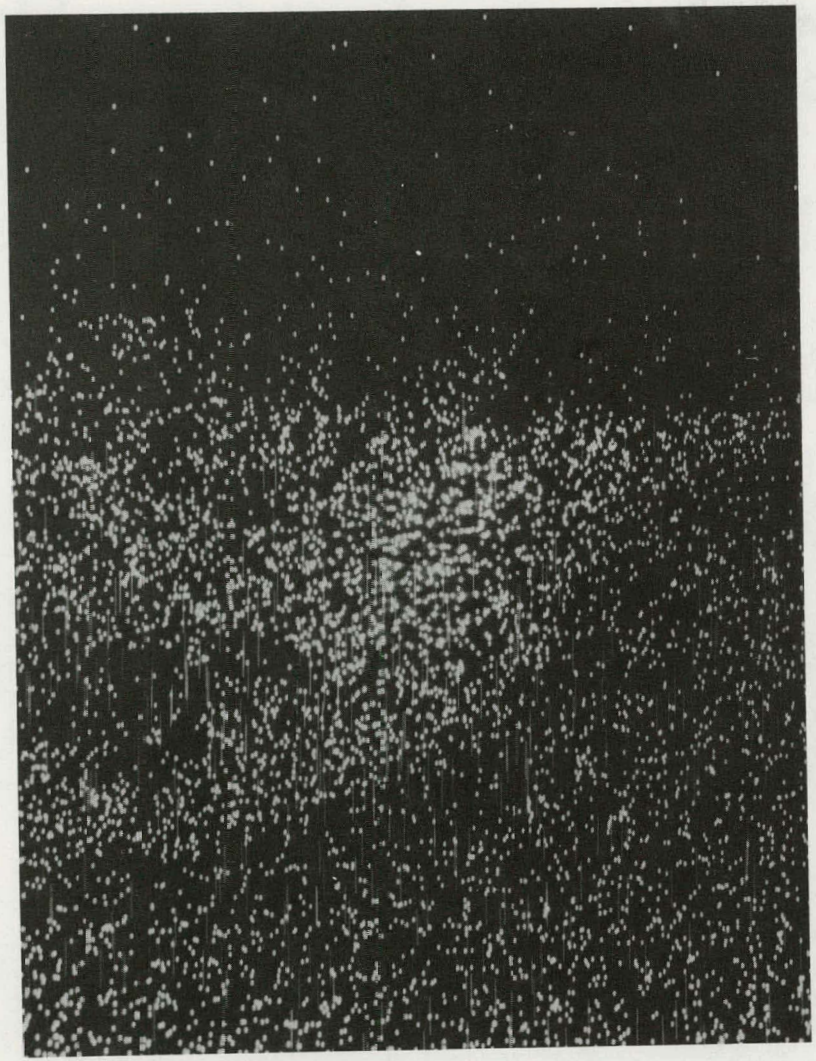

c. Chromium

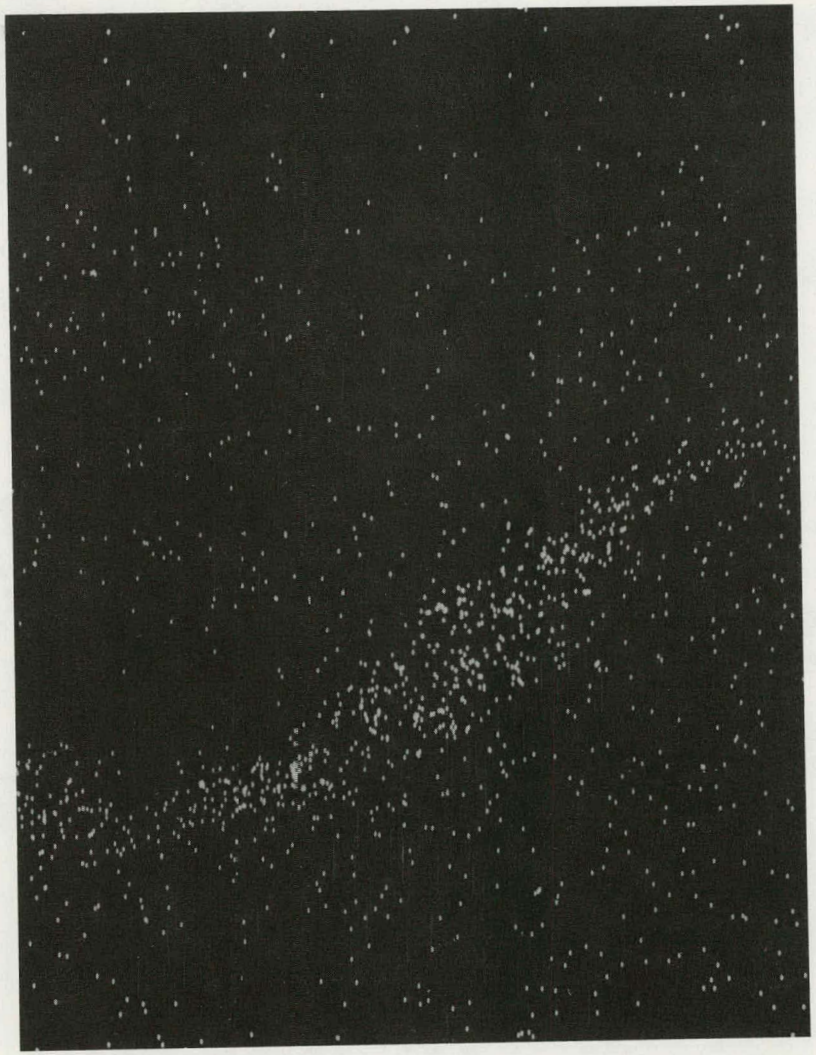

d. Sulfur

Figure 67 continued

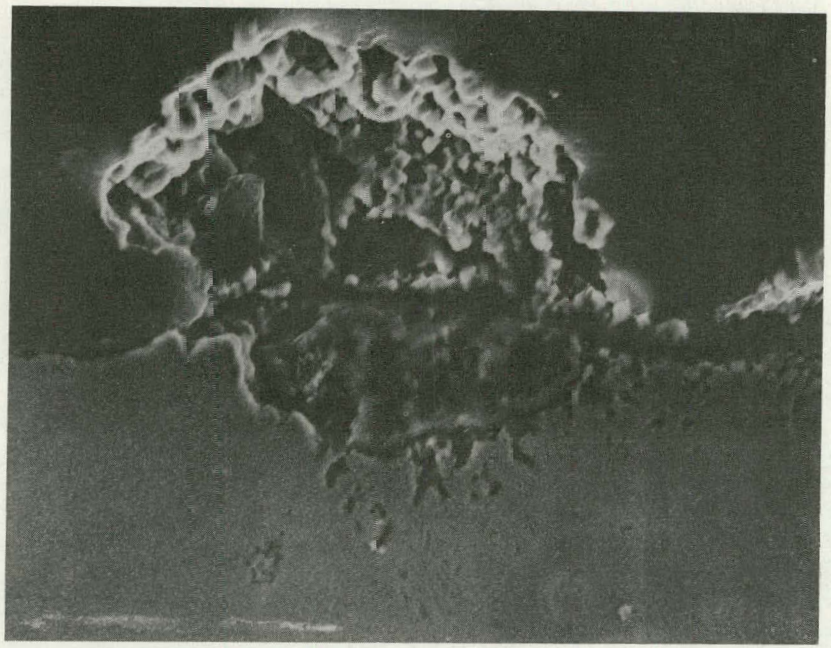

a. 1600 x

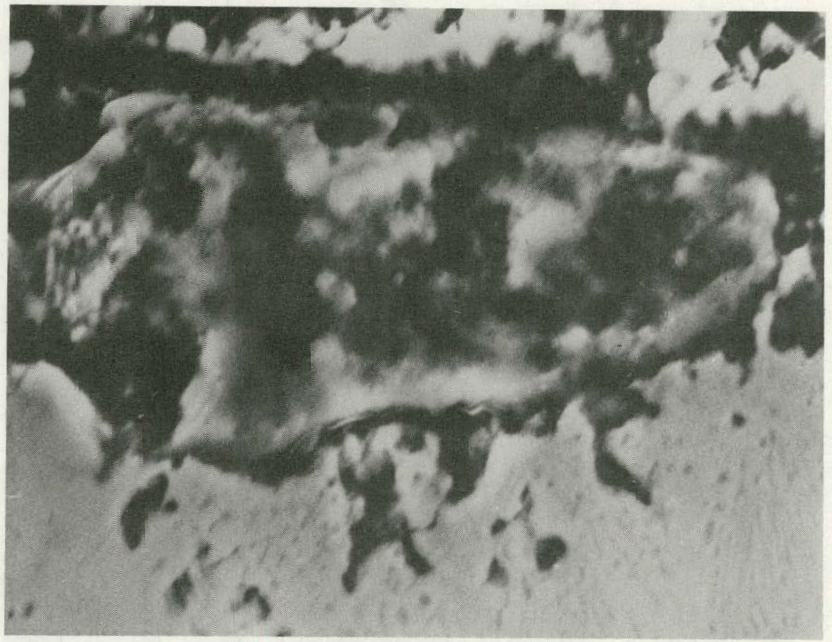

b. 4000 x

Figure 63 SEM photomicrographs and x-ray maps showing element distribution in attack front after 750°C hot corrosion of Co-18Cr-6Al-1Hf for 48 hrs. at $P_{SO_3} = 6 \times 10^{-4}$ atm.

c. Cobalt

d. Chromium

e. Aluminum

Ξ. Sulfur

Figure 68 continued

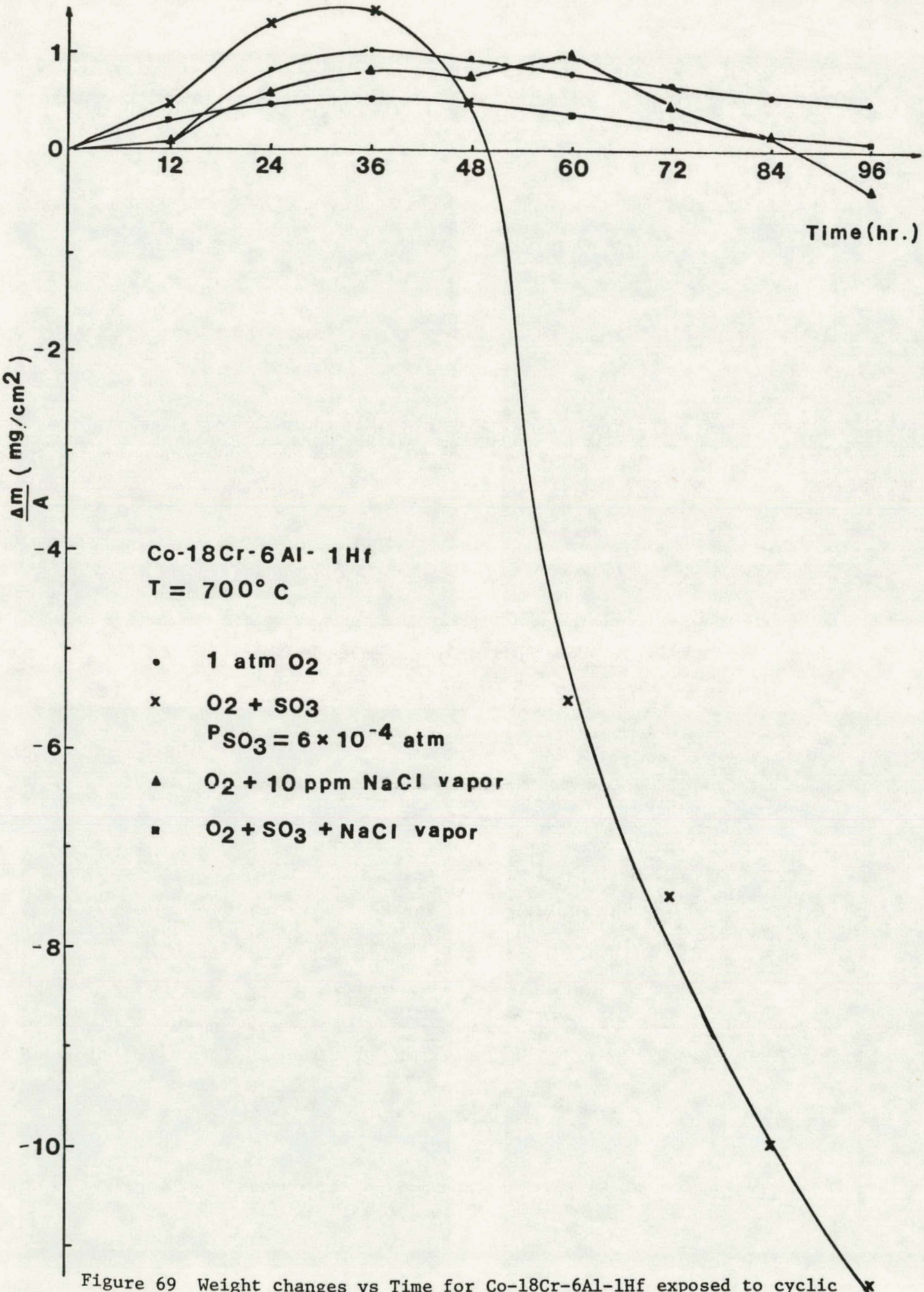

Figure 69 Weight changes vs Time for Co-18Cr-6Al-1Hf exposed to cyclic oxidation and hot corrosion at 700°C.

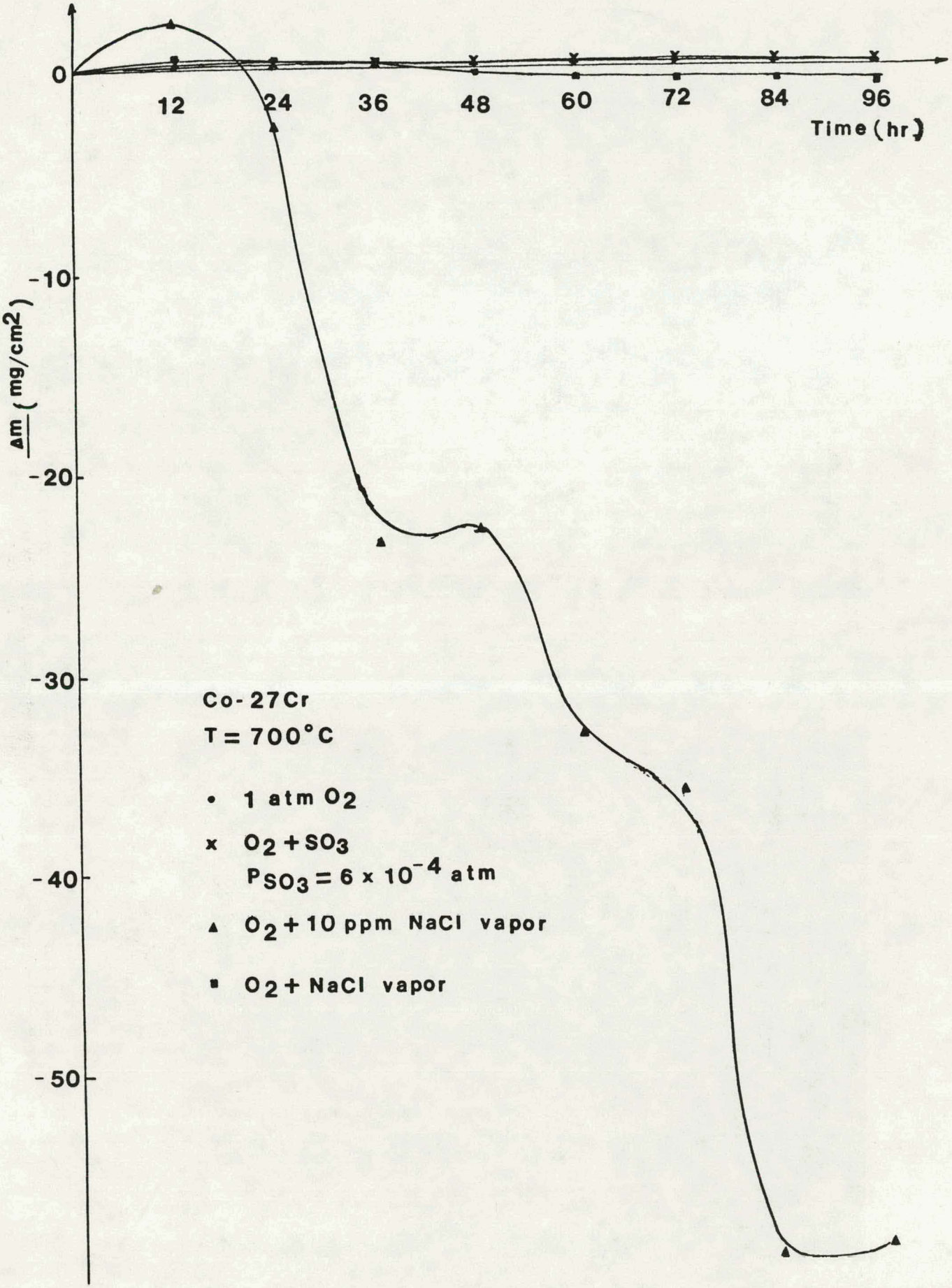

Figure 70 Weight change vs time for Co-27Cr exposed to cyclic oxidation and hot corrosion at 700°C.

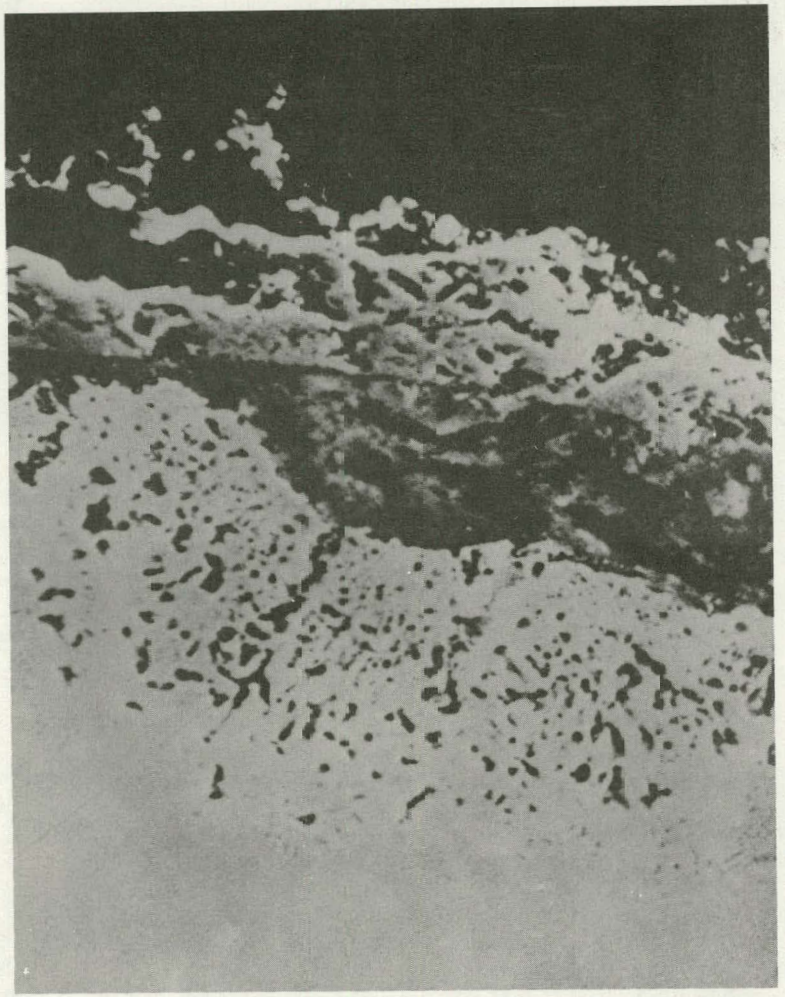

a. 1600 x

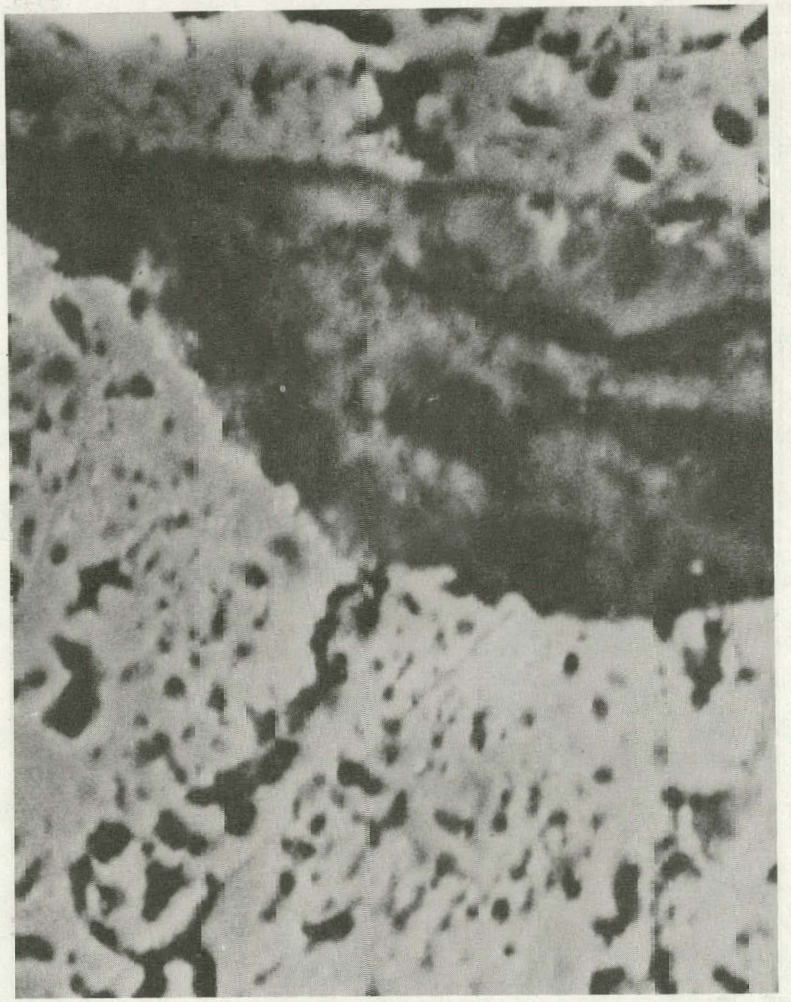

b. 4000 x

Figure 71 SEM photomicrograph and x-ray maps showing element distribution in attack front after 96 hrs. of cyclic hot corrosion testing at 700°C in O_2+10 ppm NaCl (v) 1 mg/cm^2 Na_2SO_4 was applied after every 12 hours.

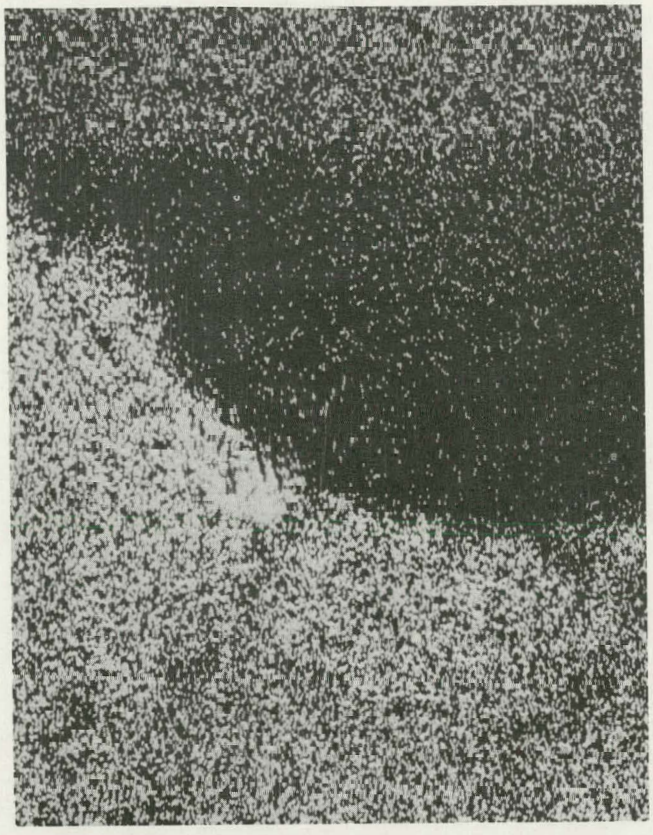

c. Co

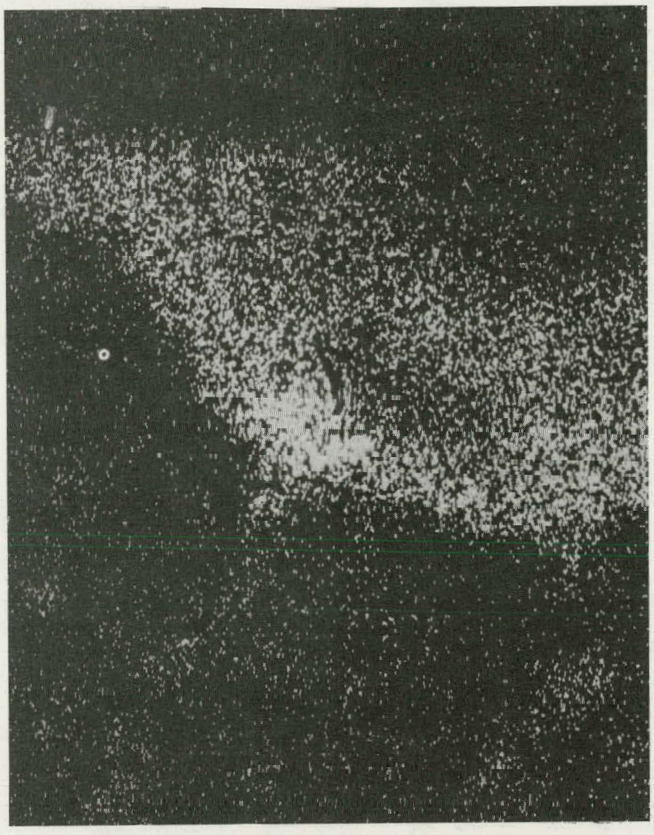

d. Al

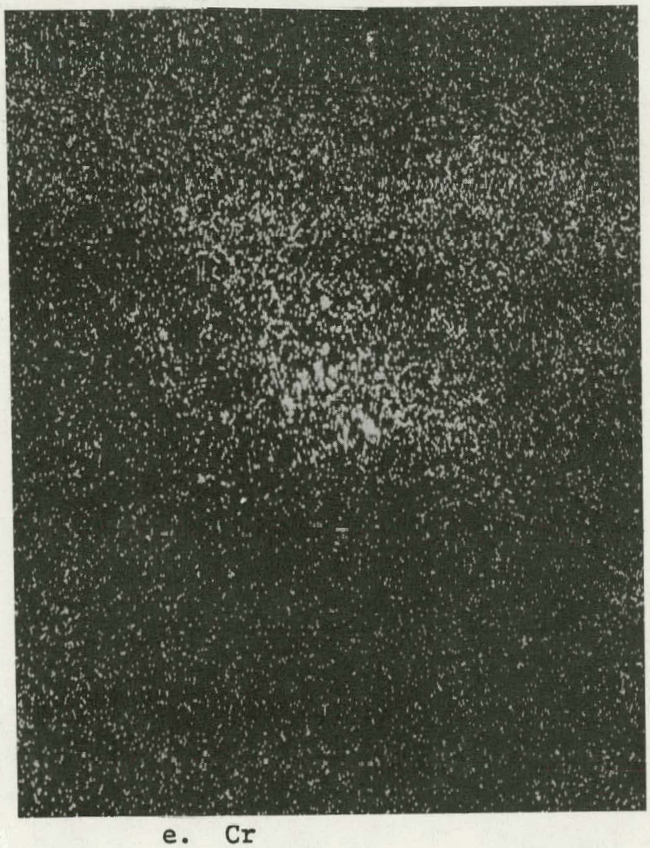

e. Cr

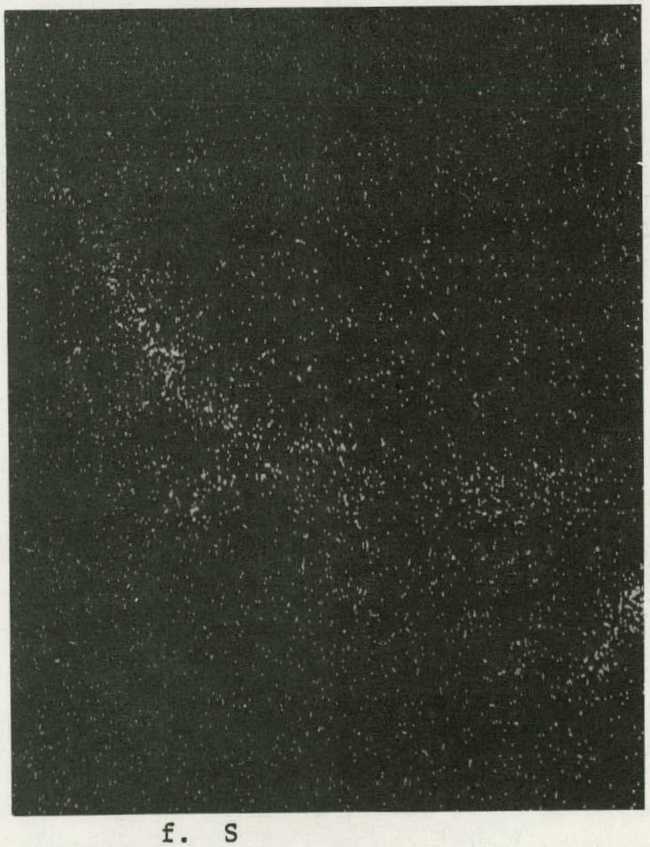

f. S

Figure 71

☆U.S. GOVERNMENT PRINTING OFFICE: 1980-640-258/115